Ph.D Dissertation

Unequal Termination Impedances Microwave Filter Synthesis

비대칭 종단 임피던스 마이크로파 여파기 회로 합성

2017. 02. 22

Graduate School of

Chonbuk National University

Division of Electronics and Information Engineering

Phirun Kim

Unequal Termination Impedances Microwave Filter Synthesis

비대칭 종단 임피던스 마이크로파 여파기 회로 합성

2017. 02. 22

Graduate School of

Chonbuk National University

Division of Electronics and Information Engineering

Phirun Kim

Unequal Termination Impedances Microwave Filter Synthesis

Academic Advisor: Professor Yongchae Jeong

A Dissertation Submitted In Partial Fulfillment of the
Requirements for the Degree of
Doctor of Philosophy

2016. 09. 26

Graduate School of

Chonbuk National University

Division of Electronics and Information Engineering

Phirun Kim

The Ph.D dissertation of Phirun Kim

is approved by

Chair, Professor, Hae-Won Son
Chonbuk National University

Vice Chair, Professor, Jongsik Lim
Soonchunhyang University

Professor, Hee-Yong Hwang
Kangwon National University

Professor, Donggu Im
Chonbuk National University

Advisor, Professor, Yongchae Jeong
Chonbuk National University

2016. 12. 16

Graduate School of

Chonbuk National University

To my beloved wife and families

ACKNOWLEDGEMENTS

First of all, I am great honor to thank God for his impact to my study and life. Moreover, I would like to show a gratitude to my academic advisor Prof. Yongchae Jeong who I regard and respect him as my father. This is not an accident that I studied under him throughout master and PhD program. With his support and profession, I can know the world and share my knowledge through international conferences and Journal publications. I gratefully acknowledge Prof. Hae-Won Son, Prof. Jongsik Lim, Prof. Hee-Yong Hwang, and Prof. Donggu Im for serving on my defense committee. Moreover, I would like to appreciate to all the people who have been involved and helped me finishing this dissertation. I also thank the current and previous members of Microwave Circuits Design Laboratory, Dr. G. Chaudhary, Dr. N. Ryu, J. Jeong, J. Park, J. Kim, Q. Wang, S. Lee, S. Jeong, J. Koo, and B. An, for their assistance, cooperation and encouragement.

I appreciate Prof. Dae-Hwan Bae for his support and driven my education go higher and lead me to know God. I thanks to God that introduces to me a kindness people such as elder Hosoo Haan and his family for helping me while I stay in this country. I also thank to BK21+ for support me throughout Master and PhD program. Also thanks to brother T. Tharoeun and other WE&C members who is my good family in Christ and always encourage and give me a hope.

Moreover, I would like to thank to my lovely wife (Leanghorn Ky) who means to my life with her sweet and pure love. Thank for your understanding of my busy time in laboratory. I do love you with no end.

Finally, I would like to give thanks to my warm family that they always provided me a strong support and encouragement. I am indebted to my parent for providing me a good attitude and support me from the childhood. I do love all of you in my heart.

TABLE OF CONTENTS

CHAPTER 3

DESIGN OF ULTRA-HIGH TRANSFORMING RATIOS COUPLED LINE IMPEDANCE TRANSFORMER WITH BANDPASS RESPONSES

CHAPTER 4

DESIGN OF LUMPED ELEMENTS BANDPASS FILTER WITH AIRBITRARY TERMINATION IMPEDANCE

CHAPTER 5

DISTRIBUTED UNEQUAL TERMINATION IMPEDANCE λ/4 COUPLED LINE BANDPASS FILTER

CHAPTER 6

DISTRIBUTED UNEQUAL TERMINATION COUPLED LINE STEPPED IMPEDANCE RESONATOR BANDPASS FILTER

CHAPTER 7

CONCLUSION AND FUTURE WORKS

LIST OF FIGURES

LIST OF TABLES

ABSTRACT

Phirun Kim
Division of Electronics and Information Engineering
The Graduate School
Chonbuk National University

Conventional power amplifiers and filters are independently designed based on 50 Ω system impedance. Therefore, matching networks are required in order to match the amplifier and filters. The additional matching network may cause the non-negligible insertion loss and efficiency degradation. Therefore, the matching network or bandpass filter should be considered in order to reduce the insertion loss.

The dissertation mainly discusses the general design of unequal termination impedance bandpass filter. Moreover, the new synthesis of parallel coupled line stepped impedance resonator was presented with controllable spurious frequencies. The filter might be designed with multi-stage and arbitrary image impedance by using low-pass prototype elements. It can be design for Chebyshev or Butterworth responses. The new unequal termination impedances microwave filter synthesis equations are significant in the modern communications system design. The proposed filter can be used directly match the input/output termination impedance of the amplifier in order to reduce a circuit size, cost, non-negligible insertion loss of matching network or filter, and complexity network.

Keywords: Bandpass filters, image impedance, parallel coupled lines, step impedance resonators, unequal termination.

ABBREVIATIONS

ADS	advanced design system
BPF	band pass filter
DC	direct current
DGS	defected ground structure
FBW	fractional bandwidth
EM	electromagnetic
HFSS	high frequency structure simulator
IT	impedance transformer
LPF	low pass filter
LTE	long term evolution
MM	millimeter
NA	not available
PA	power amplifier
PCB	print circuit board
RF	radio frequency
RL	return loss
SIR	stepped impedance resonator
TL	transmission line
UHITR	ultra-high impedance transforming ratio

CHAPTER 1

DISSERTATION OVERVIEW

1.1 Introduction

The RF/microwave filter is a key circuit which play an important role in mobile and satellite communications, radar, and remote sensing systems operating at high frequencies. In general, the performances of the filter are described in terms of insertion loss, return loss, frequency-selectivity (or attenuation at rejection band), group-delay variation in the passband, and so on. Filters are required to have small insertion loss, high return loss, good out-of-band suppression, and high frequency-selectivity to prevent an interference of signals in the passband.

As well known, the direct-coupled microwave filter can be obtained from Butterworth (or maximally flat magnitude filter) and Chebyshev (or equal ripple magnitude filter) frequency responses. Since Chebyshev response filter has better frequency selectivity than Butterworth response filter, it has been widely used in the filter design.

1.2 Literature Review

The bandpass filter (BPF) with arbitrary termination impedances have been analyzed in order to reduce circuit size, loss, complex circuit, and provide an out-of-band suppression. Typically, the general BPFs were started to analyze and design with equal termination impedances (50-to-50 Ω) [1]-[5]. In [1], the general equations of parallel coupled line BPF were derived for Chebyshev and

Butterworth responses. After that, a new analysis of parallel coupled line BPF was introduced in [2] with arbitrary image impedance, and the new analysis were able to control the coupling coefficient of coupled lines. Moreover, a modified coupled line BPF using defected ground structure (DGS) and additional stubs were introduced in [3] and [4] with wide stopband characteristics. In [5], a new design equations of parallel coupled line BPF were derived up to nine stages (n = 9) base on the composite *ABCD* matrices with wide passband characteristics. An impedance transformer is one of the arbitrary termination impedance circuits that can transform one termination impedance to the specific impedance. Actually, a quarter wavelength transmission line (TL) is well known the impedance transformer and widely used. However, this network has some limitations such as difficulty in realization for very high impedance transforming ratio [6] and poor out-of-band suppression [7]. In order to overcome these limitations, various types coupled line transformers were presented in [8]-[16].

In [8], a coupled three-line was used to get a wide passband response for an impedance transforming ratio (r) of 3.4. However, the out-of-band suppression is poor with the restricted in r. In [9], a single open-circuit coupled line was introduced as the impedance transformer, and it was able to control the coupling coefficient of coupled line. In [10]-[12], a coupled line with a shunt TL and its application with power divider and high efficiency power amplifier were demonstrated. The shunt open stub TL was used to produce transmission zeros at the stopband and enhance r. As well, the impedance transformer analyzed in [13] was able to obtain sharper and higher r compared to [10], but it was limited by a number of stages (n) as two. On the other hand, a short-ended coupled-line impedance transformer with higher r was designed with a suitable for large load impedance (50-1000 Ω) [14]. In [15], a design of multi-section parallel coupled line BPF was presented as an impedance matching network using an optimizing process.

Typically, microwave circuits are independently designed with 50 Ω termination impedance and then operate together. It is quite a challenge to design the BPF with arbitrary termination impedances and apply as the matching network of other microwave circuits to reduce the non-negligible insertion loss of normal matching networks. In [16]-[18], the input and output matching networks of amplifier were designed by optimization from the ladder network of arbitrary termination low-pass filter by using a design technique of [19]. However, the stopband of the low frequencies (close to DC) were poor characteristics and the attenuation at center frequency is varied according to r. Moreover, the BPF with one [20], two [21], and three [22] poles were analyzed using coupling matrix to directly match with the output impedance of amplifier. The co-design method might reduce the circuit size and provide a higher overall efficiency. The general synthesis approach of coupling matrix was briefly explained in [23] without any fabrication for validations.

A new design techniques have been subjects of requirements for circuit size, cost, ease of fabrication, and multi-functions to use in modern wireless communication systems. Although, an arbitrary image impedance of parallel coupled line BPF was introduced a new design equation in [2] with a controllable coupling of coupled line, however, the spurious responses are produced at higher frequencies such as $2f_0$ and $3f_0$. In order to improve the harmonic suppression characteristic, there are many methods by using such as modified coupled line structure, DGS, and shunt stub TL were analyzed and introduced with wide stopband characteristics. Besides the additional DGS and shunt stub TL, parallel coupled line stepped impedance resonators (SIRs) were proposed in [24]-[31] and its characteristic impedances of coupled line can be calculated by using a low-pass prototype values. Typically, the general SIR BPFs were analyzed and designed with equal termination impedances (50-to-50 Ω) with an image impedance of 50 Ω. The SIR structure is able to control the spurious frequency by varying an impedance ratios and it can also obtain more compact size with multistage structure. However, the image impedance (Z_2) of a coupled line must be chosen equal to the termination impedance to avoid mismatched.

1.3 Dissertation Overview

The main object of the dissertation is focused on the derivation of new synthesis of unequal termination impedances BPF. A new design equations are able to design the BPF with n-resonators, arbitrary termination impedance, arbitrary image impedance of coupled line, and controllable a spurious frequency. The design equations were derived base on a multistage coupled lines theory. These new equations can make a significant impact on the advanced wireless systems.

The dissertation is organized as follows. Chapter 2 describes a relevant fundamental theories of microwave filters. The purpose of this chapter is to give a brief basic transmission line theory, two-port microwave network, and other relevant theories that would be useful in the design of microwave filters.

Chapter 3 describes the design of two stages coupled line impedance transformer with BPF response. In this chapter, the design equations are explained with the simulation and measurement to show validity.

Chapter 4 presents the design of unequal termination impedance BPF with lumped elements. In this chapter, the design formulas are all explicitly derived step-by-step to clearly describe a design procedure. Moreover, the ideal simulations are done with arbitrary termination impedance.

Chapter 5 describes new design equations for unequal termination impedances parallel coupled line BPF. With new design formulas, the parallel coupled line BPFs might be calculated and design with *n*-resonators, arbitrary termination impedance, and arbitrary image impedance of coupled line by using low-pass prototype elements values.

In Chapter 6, the general design formulas of arbitrary termination impedances SIR BPF are analyzed in detail with simulation and measurement validation. Similar to Chapter 5, the new design equations are applicable on *n*-resonators, arbitrary termination impedance, and arbitrary image impedance of coupled line. However, in this chapter the spurious frequencies are able to control variously in the higher stopband.

Finally, Chapter 7 of the dissertation presents the conclusion and future work. The significance and contributions of the dissertation is summarized in this chapter.

CHAPTER 2

FUNDAMENTAL THEORIES OF MICROWAVE FILTER

2.1 Lossless Transmission Lines

A forward travelling wave from the source to the load along TL guide is reflected by a mismatched termination load. Fig. 2.1 shows a lossless TL terminated in an arbitrary load impedance Z_L.

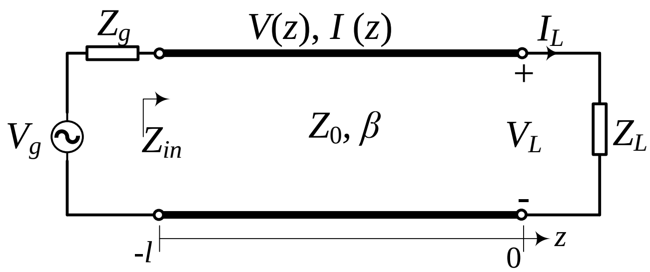

Fig. 2.1. A transmission line terminated with a load impedance Z_L.

The total voltage on the TL is a sum of incident and reflected waves [32] due to $Z_L \neq Z_0$ and given as:

$$V(z) = V_0^+ e^{-j\beta z} + V_0^- e^{j\beta z} . \tag{2.1}$$

Similarly, the total current on the TL is written as:

$$I(z) = \frac{V_0^+}{Z_0} e^{-j\beta z} - \frac{V_0^-}{Z_0} e^{j\beta z} . \tag{2.2}$$

The load impedance Z_L can be expressed as a ratio of the terminal voltage to current at $z = 0$ as

$$Z_L = \frac{V(0)}{I(0)} = \frac{V_0^+ + V_0^-}{V_0^+ - V_0^-} Z_0 \,. \tag{2.3}$$

From (2.3), the ratio of the reflected voltage wave to the incident voltage wave is defined as the voltage reflection coefficient, Γ:

$$\Gamma = \frac{V_0^-}{V_0^+} = \frac{Z_L - Z_0}{Z_L + Z_0} \,. \tag{2.4}$$

The total voltage and current waves on the TL can be written as

$$V(z) = V_0^+ \left(e^{-j\beta z} + \Gamma e^{j\beta z} \right), \tag{2.5}$$

$$I(z) = \frac{V_0^+}{Z_0} \left(e^{-j\beta z} - \Gamma e^{j\beta z} \right). \tag{2.6}$$

To obtain Γ = 0, the load impedance must be equal (matched) to the characteristic impedance Z_0 of the TL. At a distance $l = -z$ from the load, the input impedance seen looking toward the load is defined as

$$Z_{\text{in}} = \frac{V(-l)}{I(-l)} = Z_0 \frac{V_0^+ \left(e^{j\beta l} + \Gamma e^{-j\beta l} \right)}{V_0^+ \left(e^{j\beta l} - \Gamma e^{-j\beta l} \right)} = Z_0 \frac{1 + \Gamma e^{-2j\beta l}}{1 - \Gamma e^{-2j\beta l}} \,. \tag{2.7}$$

From (2.4) and (2.7), the general form of the input impedance may be obtained as

$$\begin{aligned} Z_{\text{in}} &= Z_0 \frac{\left(Z_L + Z_0 \right) e^{j\beta l} + \left(Z_L - Z_0 \right) e^{-j\beta l}}{\left(Z_L + Z_0 \right) e^{j\beta l} - \left(Z_L - Z_0 \right) e^{-j\beta l}} \\ &= Z_0 \frac{Z_L \left(e^{j\beta l} + e^{-j\beta l} \right) + Z_0 \left(e^{j\beta l} - e^{-j\beta l} \right)}{Z_L \left(e^{j\beta l} - e^{-j\beta l} \right) + Z_0 \left(e^{j\beta l} + e^{-j\beta l} \right)} \end{aligned}$$

$$= Z_0 \frac{Z_L \cos\beta l + jZ_0 \sin\beta l}{Z_0 \cos\beta l + jZ_L \sin\beta l} = Z_0 \frac{Z_L + jZ_0 \tan\beta l}{Z_0 + jZ_L \tan\beta l}. \tag{2.8}$$

There are two special cases that often appear in the analysis of microwave circuit design. Fig. 2.2 (a), (b) show two special cases that the TL is terminated in a short and an open circuit, respectively. For the short-circuit, the voltage is zero at the load (Z_L = 0), while the current is a maximum there. The following input impedance is

$$Z_{\text{in}} = jZ_0 \tan\beta l \ . \tag{2.9}$$

For the open-circuit line, the current is zero at the load (Z_L = ∞), while the voltage is a maximum. The input impedance is

$$Z_{\text{in}} = -jZ_0 \cot\beta l \ . \tag{2.10}$$

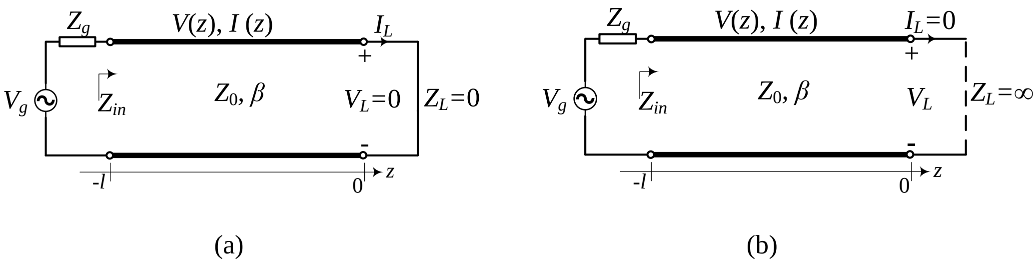

Fig. 2.2. A transmission line terminated with (a) short and (b) open circuits.

2.2 Two-Port Network Parameters

2.2.1 Scattering Parameters

The scattering (or *S*-parameters) of a two-port network are defined in terms of reflection or transmission waves [32]-[33]. Fig. 2.3 shows a two-port network with real characteristic impedance at each port (Z_{01} and Z_{02}). The relationship between the reflected and incident waves and the S-parameter matrix of two-port network is given by

$$\begin{bmatrix} b_1 \\ b_2 \end{bmatrix} = \begin{bmatrix} S_{11} & S_{12} \\ S_{21} & S_{22} \end{bmatrix} \begin{bmatrix} a_1 \\ a_2 \end{bmatrix}. \tag{2.11}$$

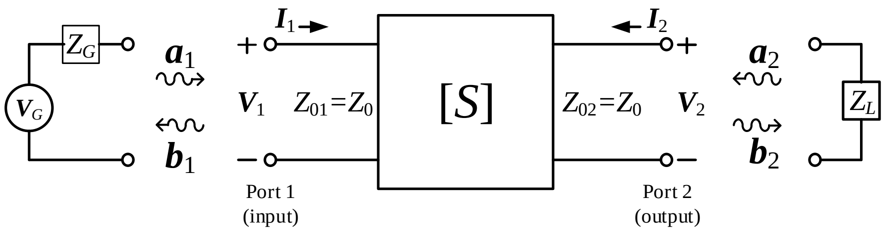

Fig. 2.3. A two-port network.

The S-parameters of two-port network are defined as

$$\begin{aligned} S_{11} &= \left.\frac{b_1}{a_1}\right|_{a_2=0} = \frac{\text{reflected power wave at port 1}}{\text{incident power wave at port 1}} \\ S_{12} &= \left.\frac{b_1}{a_2}\right|_{a_1=0} = \frac{\text{reflected power wave at port 1}}{\text{incident power wave at port 2}} \\ S_{21} &= \left.\frac{b_2}{a_1}\right|_{a_2=0} = \frac{\text{reflected power wave at port 2}}{\text{incident power wave at port 1}} \\ S_{22} &= \left.\frac{b_2}{a_2}\right|_{a_1=0} = \frac{\text{reflected power wave at port 2}}{\text{incident power wave at port 2}} \end{aligned} \tag{2.12}$$

The parameters S_{11} and S_{22} are called the reflection coefficients, the S_{12} and S_{21} are called the transmission coefficient. These are the parameters measurable at microwave frequencies. Some special cases, the S-parameters have following relation as

$$S_{12} = S_{21} \quad \text{(For reciprocal network)} \tag{2.13a}$$

$$S_{11} = S_{22} \quad \text{(For symmetrical network)} \tag{2.13b}$$

$$|S_{21}|^2 + |S_{11}|^2 = 1, \ |S_{12}|^2 + |S_{22}|^2 = 1 \ \text{(For lossless passive network).} \tag{2.13c}$$

2.2.2 Impedance and Admittance Parameters

The impedance parameters (*Z*-parameters) and its matrix for two-port network is probably the most common [32]-[34]. The relationship between the current, voltage at each port and the *Z* matrix is given by

$$\begin{bmatrix} V_1 \\ V_2 \end{bmatrix} = \begin{bmatrix} Z_{11} & Z_{12} \\ Z_{21} & Z_{22} \end{bmatrix} \begin{bmatrix} I_1 \\ I_2 \end{bmatrix}. \tag{2.14}$$

From (2.14), the *Z*-parameters of two-port network are defined as

$$Z_{11} = \left.\frac{V_1}{I_1}\right|_{I_2=0} \quad (2.15\text{a}) \qquad Z_{12} = \left.\frac{V_1}{I_2}\right|_{I_1=0} \quad (2.15\text{b})$$

$$Z_{21} = \left.\frac{V_2}{I_1}\right|_{I_2=0} \quad (2.15\text{c}) \qquad Z_{22} = \left.\frac{V_2}{I_2}\right|_{I_1=0}. \quad (2.15\text{d})$$

The *Z*-parameters are known as the open-circuit impedance parameters [35], and [*Z*] is called an open-circuit impedance matrix. The [*Z*] is often employed in the calculation of series network connection [32-33]. In case of $Z_{12} = Z_{21}$, the network is reciprocal network. If network are symmetrical, then $Z_{12} = Z_{21}$ and $Z_{11} = Z_{22}$. For a lossless network, the *Z*-parameter are all purely imaginary.

For the parallel network connection, the admittance matrix [*Y*] has to be adopted for the convenience, which is known as a short-circuit admittance matrix

[Y]. The relationship between the voltage and current at each port and Y-parameter matrix is given by

$$\begin{bmatrix} I_1 \\ I_2 \end{bmatrix} = \begin{bmatrix} Y_{11} & Y_{12} \\ Y_{21} & Y_{22} \end{bmatrix} \begin{bmatrix} V_1 \\ V_2 \end{bmatrix}. \tag{2.16}$$

From (2.16), the Z-parameters of two-port network are defined as

$$Y_{11} = \left.\frac{I_1}{V_1}\right|_{V_2=0} \quad (2.17a) \qquad Y_{12} = \left.\frac{I_1}{V_2}\right|_{V_1=0} \quad (2.17b)$$

$$Y_{21} = \left.\frac{I_2}{V_1}\right|_{V_2=0} \quad (2.17c) \qquad Y_{22} = \left.\frac{I_2}{V_2}\right|_{V_1=0}. \quad (2.17d)$$

Similarly, in case of $Y_{12} = Y_{21}$, the network is reciprocal network. Moreover, if the network is symmetrical, then $Y_{11} = Y_{22}$. For a lossless network, the Y-parameters are all purely imaginary. The relation of impedance and admittance matrix can be written as

$$[Y] = [Z]^{-1}. \tag{2.18}$$

2.2.3 The Transmission (*ABCD*) Parameters

The advantage of the *ABCD* matrix is that the cascaded two-port networks can be characterized by simply multiplying their *ABCD* matrices. The *ABCD* matrix is defined for a two-port network in terms of the port voltages and currents [32] as shown in Fig. 2.4(a) and can be defined as

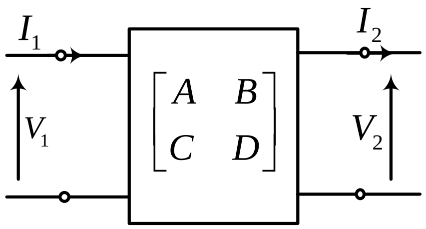

(a)

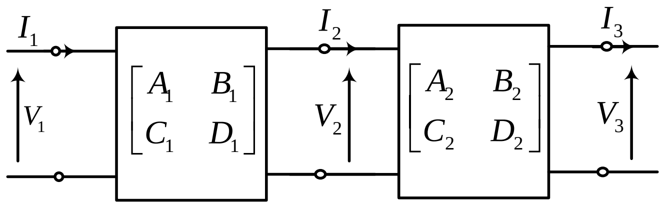

(b)

Fig. 2.4. (a) A two-port network and (b) a cascade connection of two-port networks.

$$\begin{aligned} V_1 &= AV_2 + BI_2 \\ I_1 &= CV_2 + DI_2 \end{aligned} \tag{2.19a}$$

or in matrix form as

$$\begin{bmatrix} V_1 \\ I_1 \end{bmatrix} = \begin{bmatrix} A & B \\ C & D \end{bmatrix} \begin{bmatrix} V_2 \\ I_2 \end{bmatrix}. \tag{2.19b}$$

Fig. 2.4(b) show a cascade connection of two-port networks. The *ABCD* matrixes of two networks are defined as

$$\begin{bmatrix} V_1 \\ I_1 \end{bmatrix} = \begin{bmatrix} A_1 & B_1 \\ C_1 & D_1 \end{bmatrix} \begin{bmatrix} V_2 \\ I_2 \end{bmatrix}, \tag{2.20a}$$

$$\begin{bmatrix} V_2 \\ I_2 \end{bmatrix} = \begin{bmatrix} A_2 & B_2 \\ C_2 & D_2 \end{bmatrix} \begin{bmatrix} V_3 \\ I_3 \end{bmatrix}. \tag{2.20b}$$

The overall *ABCD* matrix of the cascaded two-port networks in Fig. 2.4(b) is defined as

$$\begin{bmatrix} V_1 \\ I_1 \end{bmatrix} = \begin{bmatrix} A_1 & B_1 \\ C_1 & D_1 \end{bmatrix} \begin{bmatrix} A_2 & B_2 \\ C_2 & D_2 \end{bmatrix} \begin{bmatrix} V_3 \\ I_3 \end{bmatrix}, \tag{2.21}$$

which shows that a cascaded connection of two-port networks is equivalent to a single two-port network containing a product of the *ABCD* matrices. The properties of the *ABCD* matrix are categorized into the following categories:

$$AD - BC = 1 \quad \text{for a reciprocal network} \tag{2.22a}$$

$$A = D \quad \text{for a symmetrical network} \tag{2.22b}$$

If the network is lossless, then *A* and *D* will be purely real and *B* and *C* will be purely imaginary [34]. Table 2.1 lists useful two-port networks and their *ABCD* matrices.

2.2.4 Even- and Odd-mode Network Analysis

If a network is symmetrical, it is convenient for network analysis using the well-known even- and odd-mode excitation method [36-37]. Suppose the circuit in Fig. 2.5 is a symmetrical circuit. Under even- and odd-mode excitations, the symmetrical plane at the center can be considered as a perfect magnetic wall (open-circuit) and electric wall (short-circuit). Since the symmetrical two-port network can be obtained by a linear combination of the even- and odd-mode excitations. Therefore, the network analysis will be simplified by separately analyzing the one-port even- and odd-mode networks.

TABLE 2.1 SOME USEFUL TWO-PORT NETWORK AND THEIR *ABCD* MATRIX [32].

Name	Circuit	ABCD matrix
Series circuit element	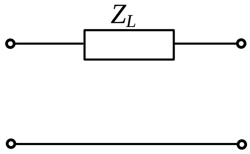	$\begin{bmatrix} 1 & Z \\ 0 & 1 \end{bmatrix}$
Shunt circuit element	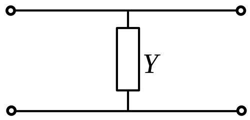	$\begin{bmatrix} 1 & 0 \\ Y & 1 \end{bmatrix}$
T network	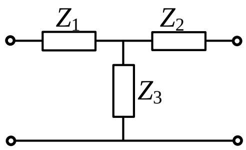	$\begin{bmatrix} 1+\frac{Z_1}{Z_3} & Z_1+Z_2+\frac{Z_1Z_2}{Z_3} \\ \frac{1}{Z_3} & 1+\frac{Z_2}{Z_3} \end{bmatrix}$
π network	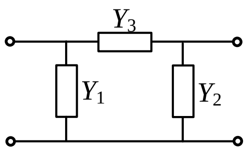	$\begin{bmatrix} 1+\frac{Y_2}{Y_3} & \frac{1}{Y_3} \\ Y_1+Y_2+\frac{Y_1Y_2}{Y_3} & 1+\frac{Y_1}{Y_3} \end{bmatrix}$
Transmission line	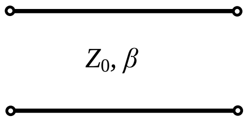	$\begin{bmatrix} \cos\beta l & jZ_0\sin\beta l \\ j\frac{\sin\beta l}{Z_0} & \cos\beta l \end{bmatrix}$
Ideal transformer	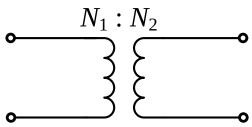	$\begin{bmatrix} \frac{N_1}{N_2} & 0 \\ 0 & \frac{N_2}{N_1} \end{bmatrix}$

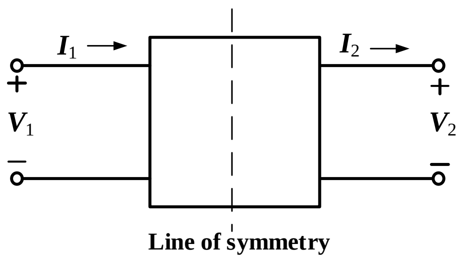

Fig. 2.5. Symmetrical two-port network.

For the one-port even- and odd-mode S-parameters are

$$S_{11e} = \frac{b_e}{a_e} \tag{2.23a}$$

$$S_{11o} = \frac{b_o}{a_o} \tag{2.23b}$$

where the subscripts e and o stand for even- and odd-mode, respectively. For the symmetrical network, the relationships of wave variables are

$$a_1 = a_e + a_o \tag{2.24a}$$

$$a_2 = a_e - a_o \tag{2.24b}$$

$$b_1 = b_e + b_o \qquad \text{(2.24b)}$$

$$b_2 = b_e - b_o\,. \qquad \text{(2.24b)}$$

Letting $a_2 = 0$, the equation (2.23) and (2.24) can be written as

$$a_1 = 2a_e = 2a_o \tag{2.25a}$$

$$b_1 = S_{11e}a_e + S_{11o}a_o \tag{2.25b}$$

$$b_2 = S_{11e}a_e - S_{11o}a_o\,. \tag{2.25c}$$

From (2.12), the two-port S-parameters are

$$S_{11} = \left.\frac{b_1}{a_1}\right|_{a_2=0} = \frac{1}{2}\left(S_{11e} + S_{11o}\right) \tag{2.26a}$$

$$S_{21} = \left.\frac{b_2}{a_1}\right|_{a_2=0} = \frac{1}{2}\left(S_{11e} - S_{11o}\right) \tag{2.26b}$$

For a symmetrical network, $S_{11} = S_{22}$ and $S_{21} = S_{12}$ can be obtained. Suppose $Z_{\mathrm{in}e}$ and $Z_{\mathrm{in}o}$ represent one-port input impedance of even- and odd-mode networks, respectively. The reflection coefficients of one-port can be obtained as

$$S_{11e} = \frac{Z_{\mathrm{in}e} - Z_0}{Z_{\mathrm{in}e} + Z_0} \tag{2.27a}$$

$$S_{11o} = \frac{Z_{\mathrm{in}o} - Z_0}{Z_{\mathrm{in}o} + Z_0}\,. \tag{2.27b}$$

Substituting (2.26) and (2.27) into (2.25), the S-parameters can be obtained as

$$S_{11} = S_{22} = \frac{Z_{\mathrm{in}e} Z_{\mathrm{in}o} - Z_0^2}{\left(Z_{\mathrm{in}e} + Z_0\right)\left(Z_{\mathrm{in}o} + Z_0\right)} \tag{2.28a}$$

$$S_{21} = S_{12} = \frac{Z_{\mathrm{in}e} Z_0 - Z_{\mathrm{in}o} Z_0}{\left(Z_{\mathrm{in}e} + Z_0\right)\left(Z_{\mathrm{in}o} + Z_0\right)} \tag{2.28b}$$

2.2.5 Image Impedance

The image impedance method is commonly used for analysis and design of filter consisting of parallel-coupled TL and building of matching network. For the uniform TL, the characteristic impedance of the TL is also its image impedance. The image parameters can be used not only on symmetrical network, but also on asymmetrical network [33]. The equations for the image impedance can be derived from the circuit shown in Fig. 2.6 with a termination impedance Z_L.

In case Z_L is equal to Z_{I1}, the input impedance Z_{in} of the circuit will also be equal to Z_{I1}. Thus, the network is symmetric with a plane of (S-S'), and the input impedance of Z_{in} is defined as an image impeance Z_{I1} at port 1. Therefore, the total

ABCD parameters of the cascade network are found as

$$\begin{bmatrix} A_T & B_T \\ C_T & D_T \end{bmatrix} = \begin{bmatrix} AD+BC & 2AB \\ 2CD & AD+BC \end{bmatrix},\ AB = BA \text{ and } CD = DC \quad (2.29)$$

From (2.29), the *ABCD* parameters in term of voltage and current can be written as

$$\begin{aligned} V_1 &= A_T V_2 + B_T I_2 \\ I_1 &= C_T V_2 + D_T I_2. \end{aligned} \quad (2.30)$$

So, the input impedance Z_{in} is given as

$$Z_{\text{in}} = \frac{V_1}{I_1} = \frac{A_T V_2 + B_T I_2}{C_T V_2 + D_T I_2} = \frac{A_T Z_L + B_T}{C_T Z_L + D_T}\ , \quad (2.31)$$

Suppose $Z_{I1} = Z_{\text{in}} = Z_L$, the image impedance Z_{I1} can be derived from (2.31) as

$$\begin{aligned}
&Z_{I1} D_T - B_T = Z_{I2}(A_T - Z_{I1} C_T) \\
&Z_{I1} D_T - B_T = \frac{D_T Z_{I1} + B_T}{C_T Z_{I1} + A_T}(A_T - Z_{I1} C_T) \\
&\left(Z_{I1} D_T - B_T\right)\left(C_T Z_{I1} + A_T\right) = \left(D_T Z_{I1} + B_T\right)(A_T - Z_{I1} C_T) \\
&Z_{I1}{}^2 D_T C_T + Z_{I1} D_T A_T - Z_{I1} B_T C_T - B_T A_T = Z_{I1} D_T A_T - Z_{I1}{}^2 D_T C_T + B_T A_T - Z_{I1} C_T B_T \\
&2 Z_{I1}{}^2 D_T C_T = 2 B_T A_T
\end{aligned}$$

$$Z_{I1} = \sqrt{\frac{B_T A_T}{D_T C_T}} \quad (2.32a)$$

Then, the image impedance at port 2 is readily found as

$$Z_{I2} = \sqrt{\frac{B_T D_T}{A_T C_T}}\ . \quad (2.32b)$$

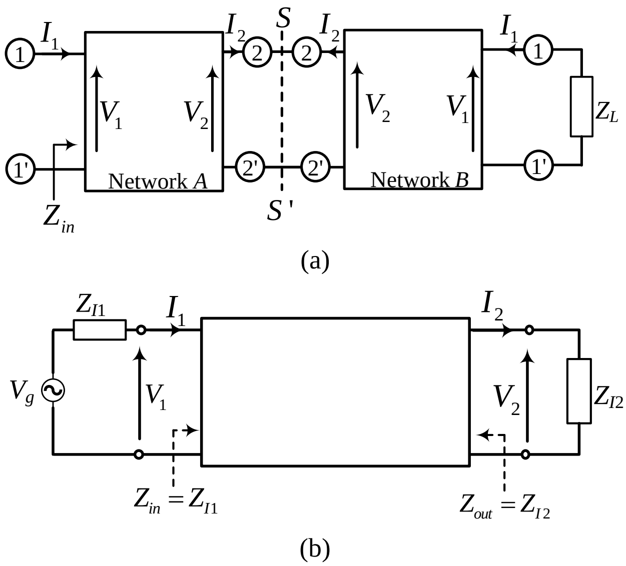

Fig. 2.6. Two-port networks: (a) two networks in cascade and (b) two-port network with perfectly matched.

2.3 Microwave Filters

Fig. 2.7 shows the lumped element low-pass filter prototype and its dual network with identical response [35]. The network might begin with either a shunt element or a series element as shown in Fig. 2.7. The element indicated in Fig. 2.7 are defined as:

$$g_0 = \begin{cases} \text{generator resistance } R_0, \text{ if } g_1 \text{ is shunt (Fig. 2.7(a))} \\ \text{generator resistance } G_0, \text{ if } g_1 \text{ is series (Fig. 2.7(b))} \end{cases}$$

$$\underset{i=1 \text{ to } n}{g_i} = \begin{cases} \text{inductance of series inductors} \\ \text{capacitance of shunt capacitors} \end{cases}$$

$$R_{n+1} = \begin{cases} \text{load resistance } R_{n+1}, \text{ if } g_n \text{ is in shunt} \\ \text{load conductance } G_{n+1}, \text{ if } g_n \text{ is in series} \end{cases}$$

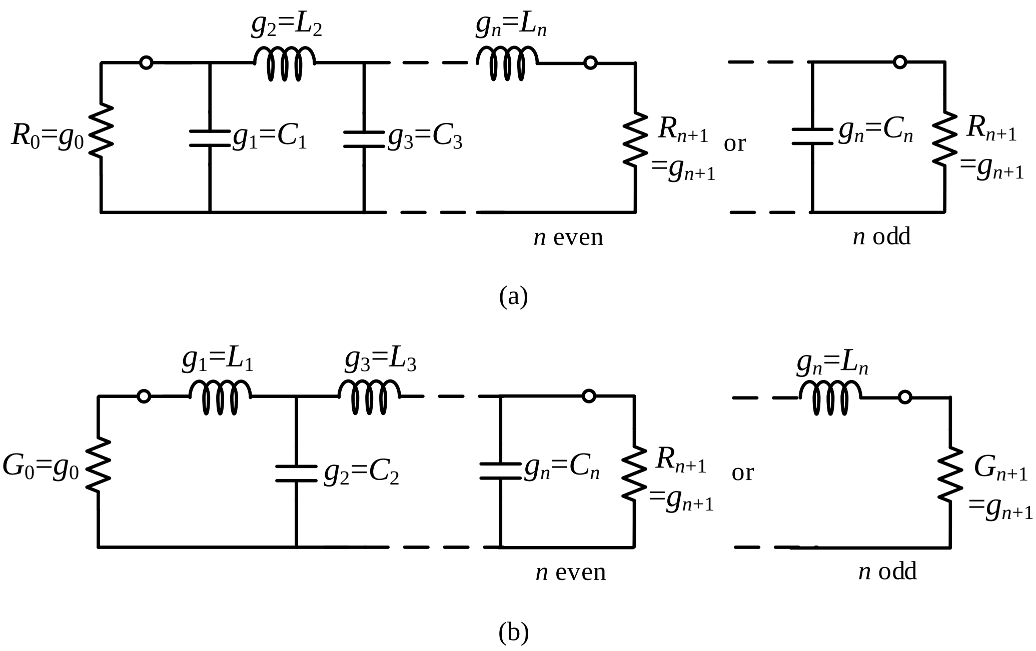

Fig. 2.7. Ladder circuits for low-pass filter prototype and their element: (a) prototype beginning with a shunt element and (b) prototype beginning with a series element.

In order to obtain the exact frequency responses, the element values in the filter network shown in Fig. 2.7 have to be determined.

2.3.1 Maximally Flat Low-pass Prototype

Fig. 2.7 shows the normalized dual circuit of low-pass prototype structure, where the termination source impedance is 1 Ω and the cutoff frequency is 1 rad/sec. The element values for the ladder-type circuits can be defined according to Butterworth (or maximally flat) and Chebyshev (or equal ripple) low-pass filter responses and have been discussed detailedly in [35]. The reactive elements for i = 1 to n represents either the series inductor or shunt capacitor.

The normalized reactive elements of the prototype for a low-pass Butterworth response by using terminations $g_0 = g_{n+1} = 1\ \Omega$ are computed as

$$g_i = 2\sin\frac{(2i-1)\pi}{2n} \quad \text{for } i = 1,2,...,n\,. \tag{2.33}$$

According to number of n, the stop-band attenuation characteristics can be calculated as

$$L_A\left(\omega'\right) = 10\log_{10}\left[1+\varepsilon\left(\frac{\omega'}{\omega_1'}\right)^{2n}\right] \quad \text{dB} \tag{2.34}$$

where

$$\varepsilon = 10^{\frac{L_{Ar}}{10}} - 1. \tag{2.35}$$

In this case, L_{Ar} and ω_1' are the maximum attenuation and the band edge angular frequency (L_{Ar} = 3 dB), respectively.

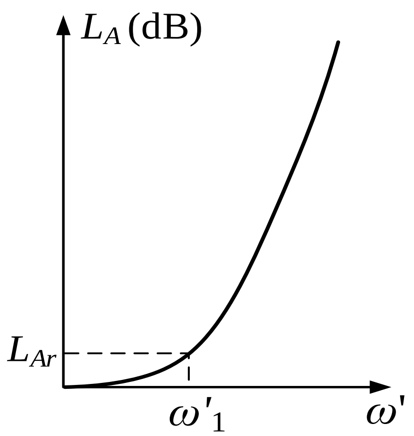

Fig. 2.8. A Maximally flat low-pass attenuation characteristic.

2.3.2 Chebyshev (Equal-ripple) Low-pass Prototype

The elements of the prototype for a low-pass Chebyshev response having pass-band ripple L_{Ar} dB and $g_0 = 1$ are computed as

$$g_1 = \frac{2a_1}{\gamma} \tag{2.36a}$$

$$g_i = \frac{4a_{i-1}a_i}{b_{i-1}g_{i-1}},\ i = 2, 3, \cdots, n \tag{2.36b}$$

$$g_{i+1} = \begin{cases} 1 \quad \text{for } n \text{ odd} \\ \coth^2\left(\dfrac{\beta}{4}\right) \quad \text{for } n \text{ even} \end{cases} \tag{2.36c}$$

where

$$\beta = \ln\left(\coth\frac{L_{Ar}}{17.37}\right), \tag{2.37a}$$

$$a_i = \sin\left[\frac{(2i-1)\pi}{2n}\right],\ \ i = 1, 2, \cdots, n \tag{2.37b}$$

$$b_i = \sinh^2\left(\frac{\beta}{2n}\right) + \sin^2\left(\frac{i\pi}{n}\right). \tag{2.37c}$$

Similar to Butterworth response, the stop-band attenuation characteristics can by calculated according to the number of *n*.

$$L_A\left(\omega'\right) = 10\log_{10}\left\{1 + \varepsilon\cos^2\left[n\cos^{-1}\left(\frac{\omega'}{\omega_1'}\right)\right]\right\},\ \ \left(\text{for } \omega' \le \omega_1'\right) \tag{2.38a}$$

$$L_A\left(\omega'\right)=10\log_{10}\left\{1+\varepsilon\cosh^2\left[n\cosh^{-1}\left(\frac{\omega'}{\omega_1'}\right)\right]\right\},\ \left(\text{for } \omega' \geq \omega_1'\right) \quad (2.38b)$$

where

$$\varepsilon = 10^{\frac{L_{Ar}}{10}} - 1. \quad (2.39)$$

Fig. 2.9 shows Chebyshev low-pass attenuation characteristic.

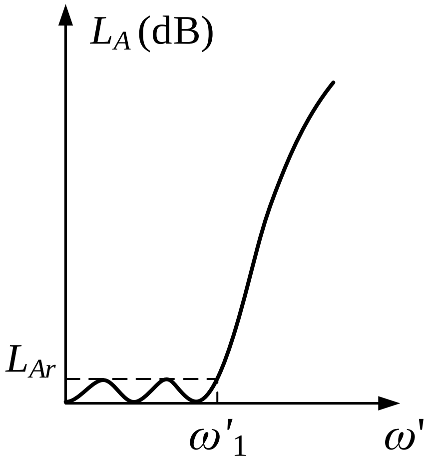

Fig. 2.9. Chebyshev low-pass attenuation characteristic.

The Butterworth and Chebyshev low-pass filter responses have terminated resistors of equal or nearly equal at each termination. In practice, the low-pass filters must be designed with same termination impedance (typically R_0 = R_{n+1} = 50 Ω) and different operating frequency bands. Therefore, the impedance and frequency scalings are required. The transformation from low-pass filter to highpass, bandpass, and bandstop filters are presented in [32]-[34].

2.4 Impedance and Frequency Transformation Filters

The low-pass filter prototypes of the previous section were normalized designs with a termination impedance of 1 Ω and a cutoff frequency of ω_c = 1 rad/sec. In the practical, the frequency characteristics and the element values are applied frequency and impedance transformations of the low-pass prototype. Also, the practical low-pass, highpass, bandpass, and band-stop microwave filters are designed from an initial low-pass prototype filter through the transformation from prototype low-pass filter impedance and frequency scalings. The frequency transformation causes an effect on all the reactive elements accordingly, but no effect on the resistive elements. The termination impedances are chosen arbitrarily with equal (R_S = R_L) or unequal terminations ($R_S \neq R_L$). The impedance transformation can be done by scaling the normalized generator impedance or conductance to a desired impedance, Z_0, or admittance, Y_0. The scalings of frequency and impedance will have no effect on the response shape [38]. Thus, the impedance transformation provide the new filter component values as

$$L'' = R_0 L \qquad (2.40a)$$

$$C'' = \frac{C}{R_0}, \qquad (2.40b)$$

$$R_S'' = R_0, \qquad (2.40c)$$

$$R_L'' = R_0 R_L \,. \qquad (2.40d)$$

2.4.1 Frequency scaling for low-pass filters

To scale the cutoff frequency of a low-pass prototype from unity to ω_c, frequency scaled low-pass response can be obtained. Fig. 2.10 (a) and (b) shows the frequency scaling from a low-pass prototype to a practical low-pass filter having a cutoff frequency ω_c. The frequency scaling is simply given as

$$\omega = \frac{\omega}{\omega_C} \qquad \rightarrow \quad \left|S_{21}^{'}\left(j\omega\right)\right|^2 = \left|S_{21}\left(j\frac{\omega}{\omega_C}\right)\right|^2 . \tag{2.41}$$

So the scaled values are obtained as

$$j\omega L^{''} = j\left(\frac{1}{\omega_C}\right)\omega L \tag{2.42a}$$

$$j\frac{1}{\omega C^{''}} = \frac{1}{j\left(\frac{1}{\omega_C}\right)\omega C} . \tag{2.42b}$$

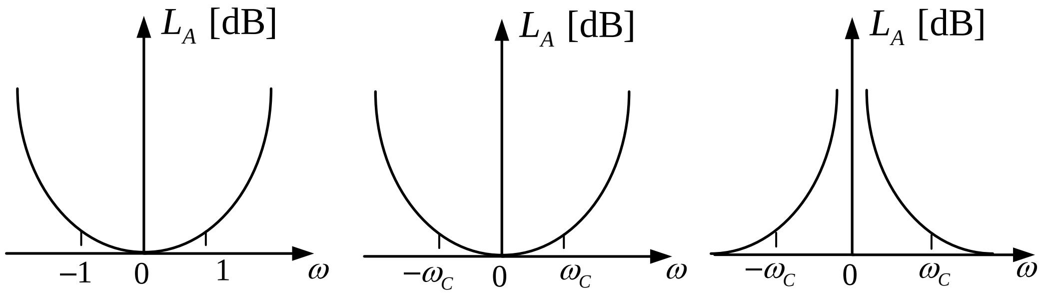

Fig. 2.10. Frequency scaling for low-pass filters and transformation to highpass response: (a) low-pass filter prototype response, (b) frequency scaling for low-pass response, and (c) transformation to highpass response.

Thus, the both impedance and frequency scaling are obtained as

$$L^{''} = \frac{R_0 L}{\omega_C} \tag{2.43a}$$

$$C^{''} = \frac{C}{R_0 \omega_C} . \tag{2.43b}$$

2.4.2 Frequency scaling for low-pass to highpass filters

Fig. 2.10(c) shows a highpass response transformed from the low-pass response. The frequency maps $\omega = 0$ to $\omega = \pm\infty$ and cutoff occurs when $\omega = \pm\omega_C$. The negative sign is needed to convert inductors (and capacitors) to realizable capacitors (and inductors). The frequency scaling is given as

$$\omega = -\left(\frac{\omega_C}{\omega}\right). \tag{2.44}$$

So the scaled values are below.

$$\frac{1}{j\omega C''} = \frac{1}{j\left(-\frac{\omega_C}{\omega}\right)C} \tag{2.45a}$$

$$j\omega L'' = j\left(-\frac{\omega_C}{\omega}\right)L \tag{2.45b}$$

Thus, the both impedance and frequency scaling are obtained as

$$L'' = \frac{R_0}{\omega_C C} \tag{2.46a}$$

$$C'' = \frac{1}{R_0 \omega_C L} . \tag{2.46b}$$

2.4.3 Frequency scaling for low-pass to bandpass filters

Instead of a single cutoff frequency for low-pass and highpass, two frequencies ω_1 and ω_2 can be used to denote the lower and upper passband edges. Then a

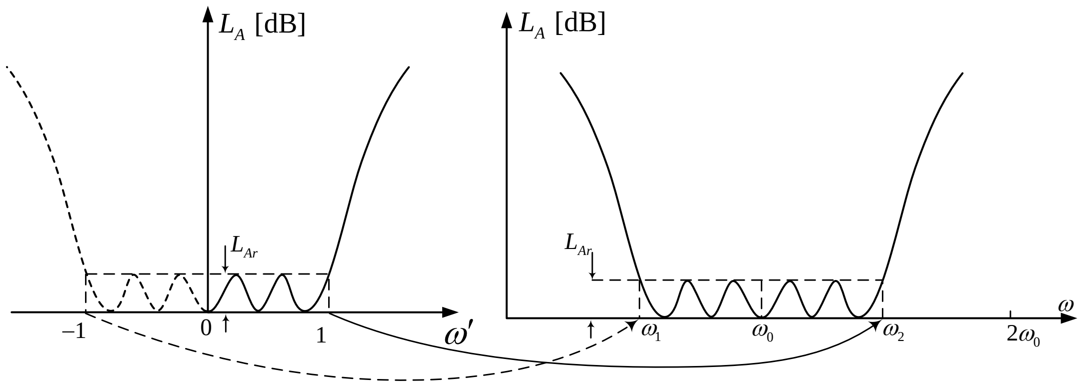

Fig. 2.11. Frequency transformation from low-pass to bandpass filter.

bandpass response can be obtained using the following frequency transformation.

$$\omega = \frac{\omega_0}{\omega_2 - \omega_1}\left(\frac{\omega}{\omega_0} - \frac{\omega_0}{\omega}\right) = \frac{1}{FBW}\left(\frac{\omega}{\omega_0} - \frac{\omega_0}{\omega}\right) \tag{2.47}$$

where

$$FBW = \frac{\omega_2 - \omega_1}{\omega_0} \tag{2.48a}$$

$$\omega_0 = \sqrt{\omega_1 \omega_2}\ . \tag{2.48b}$$

Fig. 2.11 illustrate the low-pass prototype filter transform to the bandpass response. Where ω_0, ω_1, and ω_2 are transformed from 0, -1, 1 [rad/sec], respectively. The detailed explanation can be done as below.

$$\frac{1}{FBW}\left(\frac{\omega}{\omega_0} - \frac{\omega_0}{\omega}\right) = 0 \ @\ \omega = \omega_0 \tag{2.49a}$$

$$\frac{1}{FBW}\left(\frac{\omega}{\omega_0} - \frac{\omega_0}{\omega}\right) = \frac{1}{FBW}\left(\frac{\omega_1^2 - \omega_0^2}{\omega_1\omega_0}\right) = \frac{1}{FBW}\left(\frac{(\omega_1 - \omega_0)(\omega_1 + \omega_0)}{\omega_1\omega_0}\right) \cong \frac{\omega_0}{2\Delta}\left(\frac{-2\Delta\omega_1}{\omega_1\omega_0}\right) = -1 \ @\ \omega = \omega_1 \tag{2.49b}$$

$$\frac{1}{FBW}\left(\frac{\omega}{\omega_0} - \frac{\omega_0}{\omega}\right) = \frac{1}{FBW}\left(\frac{\omega_2^2 - \omega_0^2}{\omega_2\omega_0}\right) = \frac{1}{FBW}\left(\frac{(\omega_2 - \omega_0)(\omega_2 + \omega_0)}{\omega_2\omega_0}\right) \cong \frac{\omega_0}{2\Delta}\left(\frac{2\Delta\omega_2}{\omega_2\omega_0}\right) = 1 \ @\ \omega = \omega_2 \tag{2.49c}$$

where ω_0 and FBW denotes the center angular frequency and the fractional bandwidth, respectively. Using this frequency transformation, the reactive element of the highpass can be obtained

$$j\omega g \rightarrow j\frac{1}{FBW}\left(\frac{\omega}{\omega_0}-\frac{\omega_0}{\omega}\right)g = j\omega\frac{g}{FBW\omega_0}+\frac{1}{j\omega}\frac{\omega_0 g}{FBW}. \tag{2.50}$$

Then

$$\frac{1}{j\omega C}=\frac{1}{j\frac{1}{FBW}\left(\frac{\omega}{\omega_0}-\frac{\omega_0}{\omega}\right)C}=\frac{1}{j\omega\left(\frac{1}{FBW\omega_0}\right)C+\frac{1}{j\omega\left(\frac{FBW}{\omega_0 C}\right)}}\Rightarrow C_P^{"}=\left(\frac{1}{FBW\omega_0}\right)C,\ L_P^{"}=\left(\frac{FBW}{\omega_0 C}\right)$$

$$j\omega L = j\frac{1}{FBW}\left(\frac{\omega}{\omega_0}-\frac{\omega_0}{\omega}\right)L = j\omega\left(\frac{1}{FBW\omega_0}\right)L+\frac{1}{j\omega\left(\frac{FBW}{\omega_0 L}\right)}\Rightarrow C_S^{"}=\left(\frac{FBW}{\omega_0 L}\right),\ L_S^{"}=\left(\frac{L}{FBW\omega_0}\right),$$

which implies that inductive/capacitive elements in the low-pass prototype will be transformed to series/parallel *LC* resonant circuit in the BPF. The elements for the series *LC* resonator in the BPF are

$$L_S^{"}=\left(\frac{1}{FBW\omega_0}\right)L \tag{2.51a}$$

$$C_S^{"}=\left(\frac{FBW}{\omega_0}\right)\frac{1}{L}. \tag{2.51b}$$

with impedance scaling, the elements for the series *LC* resonator in the BPF are

$$L_S^{"}=\left(\frac{R_0 L}{FBW\omega_0}\right) \tag{2.52a}$$

$$C_S^{"}=\left(\frac{FBW}{\omega_0}\right)\frac{1}{R_0 L}. \tag{2.52b}$$

Similarly, the elements for the shunt *LC* resonator in the BPF are

$$L_P'' = \left(\frac{FBW}{\omega_0}\right)\frac{1}{C} \tag{2.53a}$$

$$C_P'' = \left(\frac{1}{FBW\,\omega_0}\right)C\,. \tag{2.53b}$$

with impedance scaling, the elements for the shunt *LC* resonator in the BPF.

$$L_P'' = \frac{FBW}{\omega_0}\frac{R_0}{C} \tag{2.54a}$$

$$C_P'' = \frac{C}{FBW\,\omega_0 R_0} \tag{2.54b}$$

2.4.4 Frequency scaling for low-pass to bandstop filters

Fig. 2.12 shows the transformation of low-pass to bandstop response. The inverse transformation of the bandpass response can be used to obtained a band-stop response.

$$\omega = \frac{FBW}{\frac{\omega_0}{\omega} - \frac{\omega}{\omega_0}}\,. \tag{2.55}$$

The angular frequencies 0, 1, -1 of the low-pass are mapped to $\pm\infty$, ω_1, ω_2, respectively.

$$0 \rightarrow \pm\infty,\ \ 1 \rightarrow \omega_1,\quad -1 \rightarrow \omega_2$$

Then

$$j\omega L = j\frac{FBW}{\frac{\omega_0}{\omega} - \frac{\omega}{\omega_0}}L = \frac{1}{\frac{\omega_0}{j\omega FBWL} + j\frac{\omega}{\Omega_C FBW\,\omega_0 L}}$$

$$\frac{1}{j\omega C} = \frac{1}{j\frac{FBW}{\frac{\omega_0}{\omega} - \frac{\omega}{\omega_0}}C} = \frac{1}{j\omega\left(\frac{FBW}{\omega_0}\right)C} + j\omega\frac{1}{FBW\,\omega_0}\frac{1}{C}$$

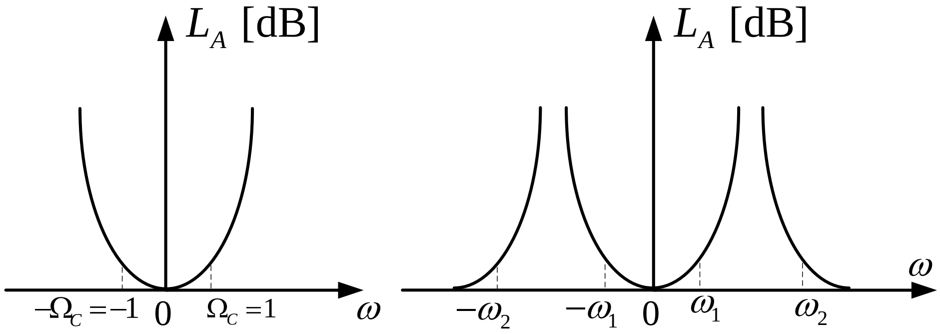

Fig. 2.12. Transformation from low-pass filter prototype response to bandstop response.

Series inductor must be transformed to the series-parallel resonator.

$$C_P'' = \left(\frac{1}{FBW\,\omega_0}\right)\frac{1}{L} \qquad L_P'' = \left(\frac{FBW}{\omega_0}\right)L \qquad \text{for } g \text{ representing series inductance} \tag{2.56}$$

Shunt capacitor must be transformed to the shunt-series resonator.

$$C_S'' = \frac{FBW}{\omega_0}C \qquad L_S'' = \frac{1}{FBW\,\omega_0}\frac{1}{C} \qquad \text{for } g \text{ representing shunt capacitance} \tag{2.57}$$

2.5 Impedance and Admittance Inverters

An impedance inverter is a two-port network that transform the load impedance to an arbitrary impedance. An idealized impedance inverter has an unique property at all frequencies. Fig. 2.13 shows the two-port impedance inverter terminated with load impedance Z_L. The *ABCD* matrix of the ideal impedance inverter is

$$\begin{bmatrix} V_1 \\ I_1 \end{bmatrix} = \begin{bmatrix} 0 & \pm jK \\ \mp \dfrac{j}{K} & 0 \end{bmatrix} \begin{bmatrix} V_2 \\ -I_2 \end{bmatrix}. \tag{2.58}$$

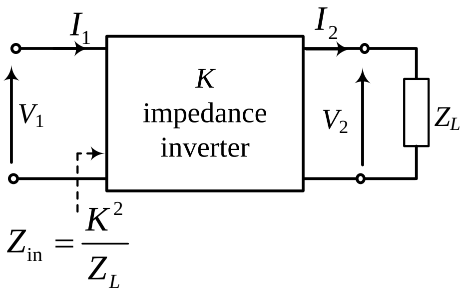

Fig. 2.13. Impedance inverter.

The input impedance of the impedance inverter is given as

$$Z_{\text{in}} = \left.\frac{V_1}{I_1}\right|_{Z_L} = \frac{AZ_L + B}{CZ_L + D} = \frac{K^2}{Z_L}. \tag{2.59}$$

An admittance inverter is a two-port network that transform the load admittance to the arbitrary admittance. Also, the ideal admittance inverter has also the unique property at all frequencies. Fig. 2.14 shows the two-port admittance inverter terminated with load admittance Y_L. The *ABCD* matrix of the ideal impedance inverter is

$$\begin{bmatrix} V_1 \\ I_1 \end{bmatrix} = \begin{bmatrix} 0 & \pm j\frac{1}{J} \\ \mp jJ & 0 \end{bmatrix} \begin{bmatrix} V_2 \\ -I_2 \end{bmatrix}. \tag{2.60}$$

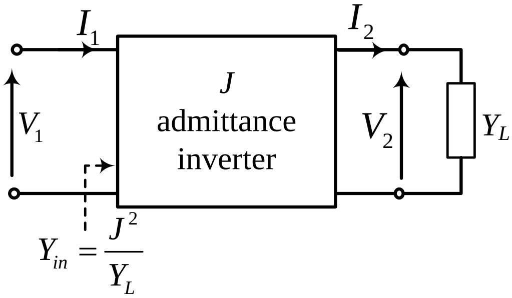

Fig. 2.14. Admittance inverter.

TABLE 2.2 IMPEDANCE AND ADMITTANCE INVERTERS: (A) OPERATION OF IMPEDANCE AND ADMITTANCE INVERTERS, (B) IMPLEMENTATION AS QUARTER-WAVE TRANSFORMERS, (C) IMPLEMENTATION USING TRANSMISSION LINES AND REACTIVE ELEMENTS, AND (D) IMPLEMENTATION USING CAPACITOR NETWORKS.

Impedance inverters	Admittance inverters

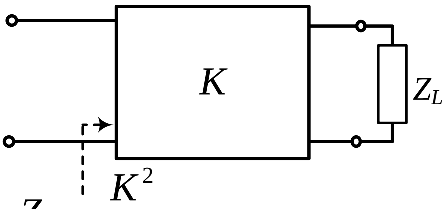

$$Z_{\text{in}} = \frac{K^2}{Z_L}$$

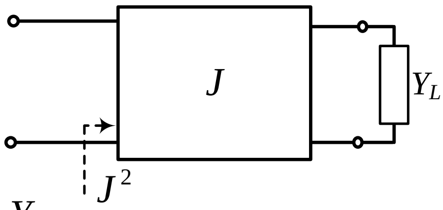

$$Y_{\text{in}} = \frac{J^2}{Y_L}$$

(a)

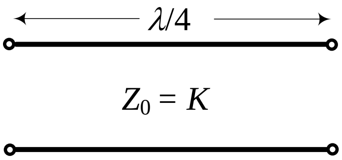

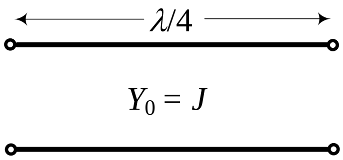

(b)

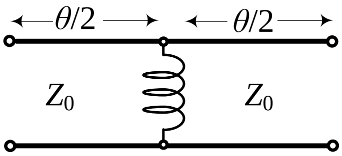

$$K = Z_0 \tan\left|\theta/2\right|$$
$$X = \frac{K}{1-\left(K/Z_0\right)^2}$$
$$\theta = -\tan^{-1}\frac{2X}{Z_0}$$

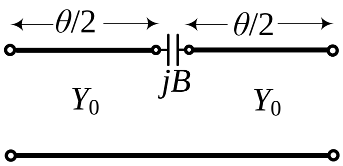

$$J = Y_0 \tan\left|\theta/2\right|$$
$$B = \frac{J}{1-\left(J/Y_0\right)^2}$$
$$\theta = -\tan^{-1}\frac{2B}{Z_0}$$

(c)

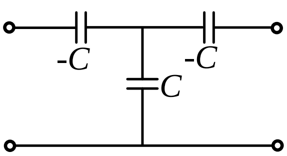

$K=1/\omega C$

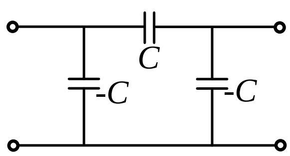

$J=\omega C$

(d)

The input admittance of the admittance inverter is given as

$$Y_{\text{in}} = \left.\frac{I_1}{V_1}\right|_{Y_L} = \frac{CV_2 + DY_L V_2}{AV_2 + BY_L V_2} = \frac{C + DY_L}{A + BY_L} = \frac{J^2}{Y_L} . \tag{2.61}$$

As seen from (2.58) and (2.60), impedance and admittance inverters have the ability to transform the load impedance or admittance to the arbitrary input impedance and admittance.

Table 2.2 shows the conceptual operation of two-port impedance or admittance inverters. The inverter can be used to transform series-connected elements to shunt-connected elements, or vice versa. The impedance or admittance inverter can be constructed using a quarter-wavelength TL of the appropriate characteristic impedance as shown in Fig. 2.15(b). Fig. 2.15 (c) and (d) show the implementations using TL and reactive elements and capacitor networks

CHAPTER 3

DESIGN OF ULTRA-HIGH TRANSFORMING RATIOS COUPLED LINE IMPEDANCE TRANSFORMER WITH BANDPASS RESPONSES

In this section, ultra-high impedance transforming ratio (UHITR) impedance transformer (IT) with a bandpass response is presented by cascading two open-circuited coupled lines. The circuit elements of the proposed IT can be found easily by using analytical design equations. The proposed network can provide two transmission poles in the passband as well as wide out-of-band suppression characteristics and can be fabricated without any difficulty in microstrip technology.

3.1 Design Theory

Fig. 3.1 shows the proposed structure of the UHITR IT. The proposed IT consists of a cascading of two sections of open-circuited coupled lines with even-mode impedances (Z_{0e1}, Z_{0e2}) and odd-mode impedance (Z_{0o}), respectively. The Z_{0o} of both coupled lines is assumed to be the same for convenience and simplicity in the analysis and fabrication. First, two-port Z-parameters are derived from four-port parallel coupled line by applying an open circuit boundary condition for port 2 and 4. The two-port Z-parameters are derived as (3.1).

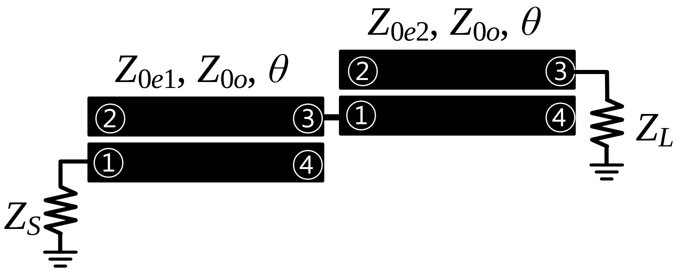

Fig. 3.1. Proposed impedance transformer for ultra-high impedance transforming ratio.

$$Z_{11} = -j\frac{Z_{0ei}+Z_{0o}}{2}\cot\theta = -j\frac{Z_{pi}}{2}\cot\theta, \tag{3.1a}$$

$$Z_{13} = -j\frac{Z_{0ei}-Z_{0o}}{2}\csc\theta = -j\frac{Z_{mi}}{2}\csc\theta, \tag{3.1b}$$

$$Z_{31} = -j\frac{Z_{0ei}-Z_{0o}}{2}\csc\theta = -j\frac{Z_{mi}}{2}\csc\theta, \tag{3.1c}$$

$$Z_{33} = -j\frac{Z_{0ei}+Z_{0o}}{2}\cot\theta = -j\frac{Z_{pi}}{2}\cot\theta, \tag{3.1d}$$

where

$$Z_{mi} = Z_{0ei} - Z_{0o},\ \ i = 1 \text{ and } 2 \tag{3.2a}$$

$$Z_{pi} = Z_{0ei} + Z_{0o}\,. \tag{3.2b}$$

Then two-port *Z*-parameters are converted into *ABCD*-parameters and they are given as

$$A_i = \frac{Z_{pi}}{Z_{mi}}\cos\theta \tag{3.3a}$$

$$B_i = j\frac{Z_{mi}^2 - Z_{pi}^2\cos^2\theta}{2Z_{mi}\sin\theta} \tag{3.3b}$$

$$C_i = j\frac{2\sin\theta}{Z_{mi}} \tag{3.3c}$$

$$D_i = \frac{Z_{pi}}{Z_{mi}}\cos\theta\,. \tag{3.3d}$$

The total *ABCD*-parameters of the cascaded coupled lines are given as (3.4)

$$\begin{bmatrix} A & B \\ C & D \end{bmatrix} = \begin{bmatrix} A_1 & B_1 \\ C_1 & D_1 \end{bmatrix}\begin{bmatrix} A_2 & B_2 \\ C_2 & D_2 \end{bmatrix} = \begin{bmatrix} A_1A_2 + B_1C_2 & A_1B_2 + B_1D_2 \\ C_1A_2 + D_1C_2 & C_1B_2 + D_1D_2 \end{bmatrix} \tag{3.4}$$

where

$$A = \frac{\left(Z_{p1} + Z_{p2}\right)Z_{p1}\cos^2\theta - Z_{m1}^2}{Z_{m1}Z_{m2}} \tag{3.5a}$$

$$B = j\cot\theta\left[\frac{Z_{p1}Z_{m2}^2 + Z_{m1}^2Z_{p2} - \left(Z_{p1} + Z_{p2}\right)Z_{p1}Z_{p2}\cos^2\theta}{2Z_{m1}Z_{m2}}\right] \tag{3.5b}$$

$$C = j\frac{2\sin\theta\cos\theta\left(Z_{p1} + Z_{p2}\right)}{Z_{m1}Z_{m2}} \tag{3.5c}$$

$$D = \frac{\left(Z_{p1} + Z_{p2}\right)Z_{p2}\cos^2\theta - Z_{m2}^2}{Z_{m1}Z_{m2}}\,. \tag{3.5d}$$

And the electrical length (θ) is $\pi/2$ at the center frequency (f_0).

3.1.1 *S*-parameters analysis

The *S*-parameters of the proposed circuit can be found as (3.6) from the overall *ABCD*-parameters of cascaded coupled lines [33-34].

$$S_{11t} = \frac{AZ_L + B - CrZ_L^2 - DrZ_L}{AZ_L + B + CrZ_L^2 + DrZ_L} \tag{3.6a}$$

$$S_{21t} = \frac{2Z_L\sqrt{r}}{AZ_L + B + CrZ_L^2 + DrZ_L} \tag{3.6b}$$

where

$$r = \frac{Z_S}{Z_L}. \tag{3.7}$$

At f_0, S_{11t} of the proposed circuit is reduced to (3.8).

$$S_{11t}\Big|_{f=f_0} = \frac{Z_{m1}^2 - rZ_{m2}^2}{Z_{m1}^2 + rZ_{m2}^2}. \tag{3.8}$$

In (3.8), S_{11t} depends on even- and odd-mode impedances of coupled lines. From (3.8), three different matched regions are categorized [7], depending on the values of Z_{m1} and Z_{m2}, which are given as (3.9).

$Z_{m1}^2 > rZ_{m2}^2$: over-matched region (3.9a)

$Z_{m1}^2 < rZ_{m2}^2$: under-matched region (3.9b)

$Z_{m1}^2 = rZ_{m2}^2$: perfectly matched region (3.9c)

For the over-matched region with the specific S_{11t}, the value of Z_{0e2} can be calculated as (3.10) using (3.8).

$$Z_{0e2} = Z_{0e1}M + Z_{0o}\left(1 - M\right) \tag{3.10}$$

where

$$M = \sqrt{\frac{1 - S_{11t}\big|_{f=f_0}}{r\left(1 + S_{11t}\big|_{f=f_0}\right)}}\,. \tag{3.11}$$

The value of Z_{0e1} can be derived as (3.12) using (3.6a), (3.9a), and (3.10) for the assumed Z_{0o} by designer.

$$Z_{0e1}^3 X_{o1} + Z_{0e1}^2 X_{o2} + Z_{0e1} X_{o3} + X_{o4} = 0 \tag{3.12}$$

where

$$X_{o1} = M\left(1 + M\right) \tag{3.13a}$$

$$X_{o2} = Z_{0o}\left(2 - M^2 - 3M\right) \tag{3.13b}$$

$$X_{o3} = \left(3M - M^2 - 4\right)Z_{0o}^2 - 4rZ_L^2\left(M + 1\right) \tag{3.13c}$$

$$X_{o4} = Z_{0o}^3\left(M^2 - M + 2\right) + 4rZ_L^2 Z_{0o}\left(M - 3\right). \tag{3.13d}$$

The negative and minimum positive root of (3.12) are not realizable for coupled line application ($Z_{0e1} < Z_{0o}$). So the proper Z_{0e1} is the maximum real positive root of (3.12).

Similarly, for the under-matched region with the specific S_{11t}, the value of Z_{0e2} can be found as (3.14).

$$Z_{0e2} = Z_{0e1}N + Z_{0o}\left(1 - N\right) \tag{3.14}$$

where

$$N = \sqrt{\frac{1 + S_{11t}\big|_{f=f_0}}{r\left(1 - S_{11t}\big|_{f=f_0}\right)}} \tag{3.15}$$

From (3.6a), (3.9b), and (3.14), the value of Z_{0e1} for the under-matched region is derived as (3.16).

$$Z_{0e1}^{3}Y_{u1} + Z_{0e1}^{2}Y_{u2} + Z_{0e1}Y_{u3} + Y_{u4} = 0 \tag{3.16}$$

where

$$Y_{u1} = N\left(1+N\right) \tag{3.17a}$$

$$Y_{u2} = Z_{0o}\left(2-N^{2}-3N\right) \tag{3.17b}$$

$$Y_{u3} = \left(3N-N^{2}-4\right)Z_{0o}^{2} - 4rZ_{L}^{2}\left(N+1\right) \tag{3.17c}$$

$$Y_{u4} = Z_{0o}^{3}\left(N^{2}-N+2\right) + 4rZ_{L}^{2}Z_{0o}\left(N-3\right). \tag{3.17d}$$

Similar to over-matched region, the proper Z_{0e1} among the three Z_{0e1} values is the maximum real positive root of (3.16).

For the perfectly matched region, S_{11t} becomes zero, such that the value of Z_{0e2} can be found as (3.18).

$$Z_{0e2} = \frac{Z_{0e1}}{\sqrt{r}} + Z_{0o}\left(1-\frac{1}{\sqrt{r}}\right) \tag{3.18}$$

From (3.6a), (3.9c), and (3.18), the value of Z_{0e1} for the perfectly matched region can be derived as (3.19).

$$Z_{0e1}^{3}W_{p1} + Z_{0e1}^{2}W_{p2} + Z_{0e1}W_{p3} + W_{p4} = 0 \tag{3.19}$$

where

$$W_{p1} = \frac{1}{r} + \frac{1}{\sqrt{r}} \tag{3.20a}$$

$$W_{p2} = Z_{0o}\left(2 - \frac{1}{r} - \frac{3}{\sqrt{r}}\right) \tag{3.20b}$$

$$W_{p3} = \left(\frac{3}{\sqrt{r}} - \frac{1}{r} - 4\right)Z_{0o}^2 - 4rZ_L^2\left(\frac{1}{\sqrt{r}} + 1\right) \tag{3.20c}$$

$$W_{p4} = Z_{0o}^3\left(\frac{1}{r} - \frac{1}{\sqrt{r}} + 2\right) + 4rZ_L^2 Z_{0o}\left(\frac{1}{\sqrt{r}} - 3\right). \tag{3.20d}$$

Also, the proper Z_{0e1} is the maximum real positive root of (3.19).

The coupling coefficients (C_i) of coupled lines can be determined as (3.21).

$$C_i = \frac{Z_{0ei} - Z_{0o}}{Z_{0ei} + Z_{0o}} \tag{3.21}$$

where i is 1 and 2 for the coupled line 1 and 2, respectively.

To illustrate the design equations (3.10)-(3.21) of the UHITR IT, the required Z_{0e1} and Z_{0e2} are calculated by specifying $S_{11t}|_{f_0}$ = -20 dB, Z_{0o} = 40 Ω, r = 10, and Z_S = 50 Ω at f_0. The calculated values are given in Table 3.1. Using the calculated

TABLE 3.1. CALCULATED VALUES OF IMPEDANCE TRANSFORMER

Match regions	Z_{0o}=40 Ω $S_{11t}\|_{f=f_0}$=-20 dB, Z_S=50 Ω, r=10					
	Z_{0e1} (Ω)	Z_{0e2} (Ω)	C_1 (dB)	C_2 (dB)	f_{p1}/f_0	f_{p2}/f_0
Under	84.57	55.58	-8.9	-15.7	0.9687	1.0313
Over	86.02	53.16	-8.7	-17		
Perfect	85.34	54.34	-8.8	-16.4		

values, the frequency responses are plotted in Fig. 3.2 for different matched regions. As seen in Fig. 3.2, a bandpass filtering response is obtained. The magnitude of return loss ($S_{11t}|_{f0}$) is exactly 20 dB at the f_0 in case of under- and over-matched regions. While two transmission poles are observed in the passband for the under-matched region, only one transmission pole at f_0 is observed in the cases of over- and perfectly matched regions. Thus, the under-matched region is preferable for its wide return loss bandwidth characteristic. The normalized transmission pole frequencies observed in the under-matched region can be found as (3.22) using (3.6a).

$$f_{p1,p2}/f_0 = 1 \mp \left[1 - \frac{2}{\pi} \cos^{-1} \sqrt{\frac{Z_{m1}^2 - rZ_{m2}^2}{\left(Z_{p2} + Z_{p1}\right)\left(Z_{p1} - rZ_{p2}\right)}} \right] \tag{3.22}$$

where f_{p1} and f_{p2} are the lower and upper transmission pole frequencies, respectively.

To illustrate the relation between 20 dB return loss (RL) fractional bandwidth (*FBW*) and C_i according to Z_{0o} with different r, the calculated values are plotted in Fig. 3.3 for all matched regions. As shown in Fig. 3.3(a)-(c), loose coupling coefficients are obtained with high Z_{0o}. However, a wide *FBW* can be obtained with low Z_{0o} which increase C_i as shown in Fig. 3.3(b)-(d). The 20 dB RL *FBW* of the under-matched region is wider than perfectly and over-matched regions. On the other hand, the *FBW*s of under-matched and perfectly matched regions are proportional to r. The 20 dB RL *FBW* of the over-matched region is only one point at f_0, which is not presented on the graph. Thus, the tradeoff between *FBW* and C_i

should be considered.

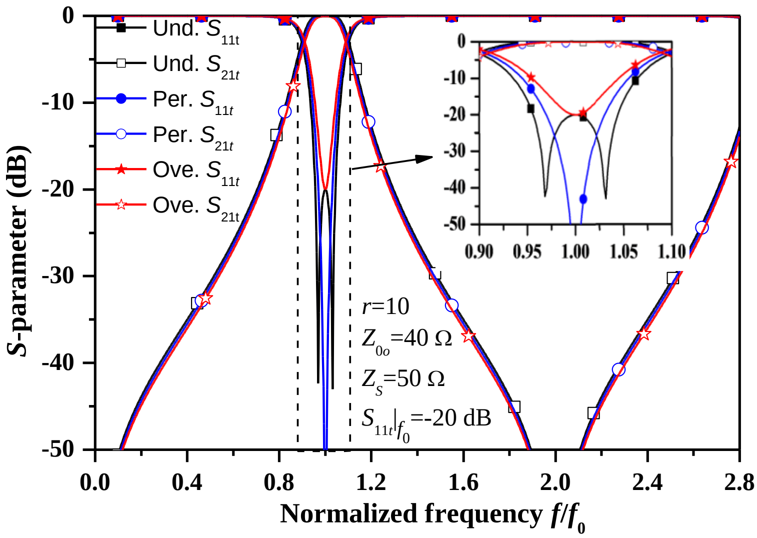

Fig. 3.2. Frequency responses of transformer for three different matched regions.

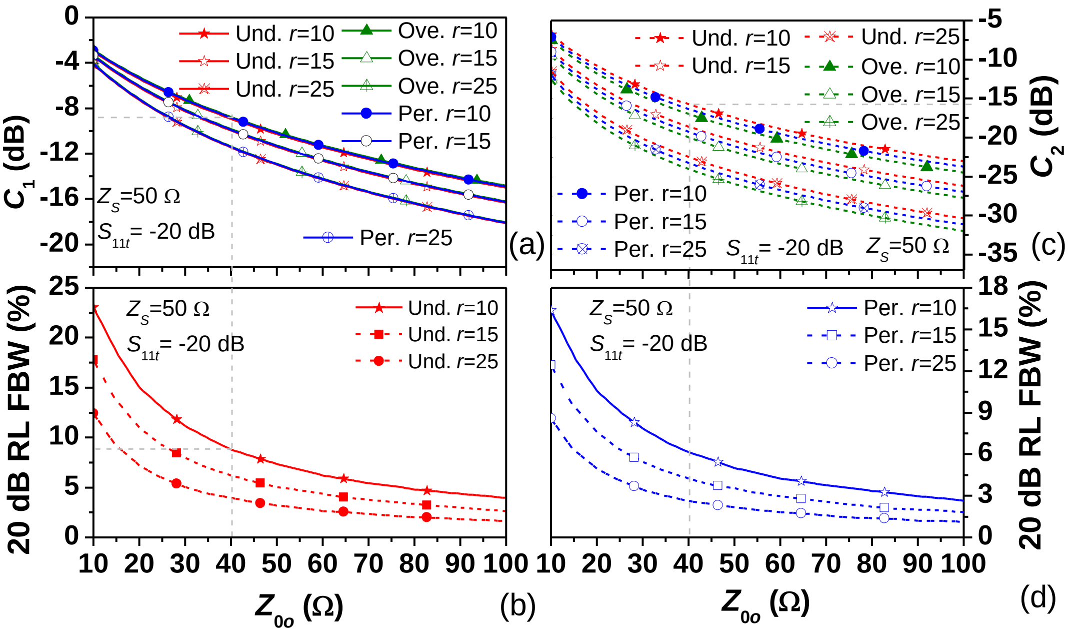

Fig. 3.3. Design graph according to Z_{0o} and different r: (a) C_1, (b) 20 dB return loss FBW of under-matched region, (c) C_2, and (d) 20 dB return loss FBW of perfectly matched region.

3.1.2 Design procedure of IT network

The design procedure of IT is summarized as follows.

a) First, specify the Z_S, Z_L, Z_{0o}, f_0, and $|S_{11t}|$ at f_0 for all matched regions.

b) For the over-matched region, calculate Z_{0e1} using (3.11), (3.12), and (3.13). After obtaining Z_{0e1}, calculate Z_{0e2} using (3.10).

c) For the under-matched region, calculate Z_{0e1} using (3.15), (3.16), and (3.17). Then calculate Z_{0e2} using (3.14).

d) For the perfectly matched region, calculate Z_{0e1} using (3.19) and (3.20). Then Z_{0e2} is obtained by (3.18).

e) Finally, obtain the physical dimensions of coupled lines according to PCB substrate from the LineCalc of Advanced Design System (ADS) and optimize using EM simulator.

3.2 The Simulation and Experimental Results

For the verification, a 5-to-50 Ω (r = 10, Z_S = 50 Ω) UHITR IT was designed, simulated, and fabricated at f_0 = 2.6 GHz. The MATLAB tool was used to calculate the elements values (see appendix A). For this purpose, the values of S_{11t} and Z_{0o} are chosen as -20 dB and 40 Ω at f_0, respectively. In this design, the under-matched region was chosen. The calculated values are shown in Table 3.1. The EM simulation was performed using Ansoft's HFSS v13.

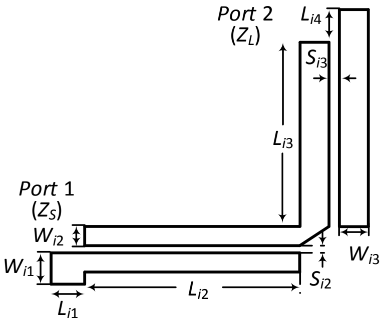

(a)

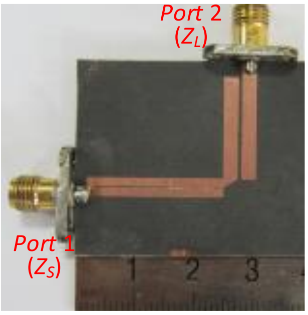

(b)

Fig. 3.4. (a) EM simulation layout and (b) photograph of fabricated PCB. (W_{i1} = 2.4, L_{i1} = 2, W_{i2} = 1.35, L_{i2} = 22.7, S_{i2} = 0.3, W_{i3} = 2.4, L_{i3} = 17.2, S_{i3} = 0.65, and L_{i4} = 3) (unit: mm).

The proposed circuit was fabricated on a substrate with ε_r = 2.2 and h = 31 mils. Fig. 3.4 shows the layout and a photograph of the fabricated UHITR IT. The overall circuit size of fabricated network is 30 × 25 mm^2. The ADS simulator and network analyzer were co-used to measure the proposed UHITR IT. Fig. 3.5 shows the simulation and measurement results of the proposed UHITR IT. The measured results showed good agreement with the simulation results. The measured S_{21t} and S_{11t} at f_0 = 2.6 GHz were -0.55 dB and -21.47 dB, respectively. The 18 dB return loss frequency band is from 2.515 to 2.73 GHz (*FBW* = 8.27%). The maximum S_{11} and S_{22} in frequency band are -19.92 dB and -18.18 dB, respectively. Two transmission poles are located at 2.54 GHz and 2.67 GHz. The bandpass characteristic is obtained with wide out-of-band suppression. However, a spurious response was occurred at around 2f_0 due to the different even- and odd-modes of the coupled lines on the microstrip line [39]. The out-of-band suppression characteristics are higher than 20 dB from DC to 1.92 GHz and better than 18 dB from 3.28 to 7.2 GHz. The performance comparisons are summarized in Table 3.2.

Although reference [15] provides wider *FBW* and bandpass response, however, *r* is too small.

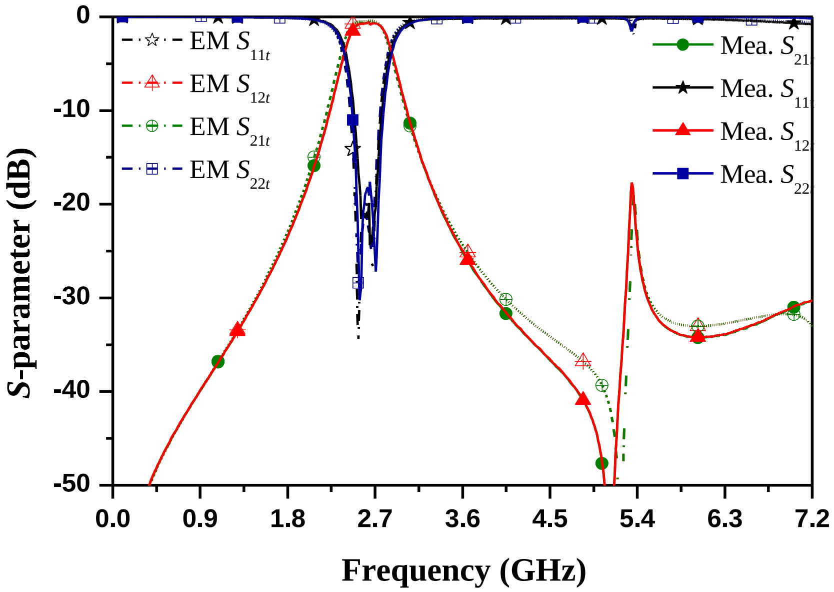

Fig. 3.5. EM simulation and measurement results.

TABLE 3.2. PERFORMANCE COMPARISON WITH PREVIOUS WORKS.

Ref.	f_0 (GHz)	FBW (%)	Impedance ratio (r)	>18 dB Out-of-band suppression	PCB Technology
[2]	1.5	*85	3.4	NA	Strip Line
[3]	2	≈*7	2	NA	Microstrip Line
[4]	2.6	*35	2	DC-1.42 / 3.8-6.65 GHz	Microstrip Line
[5]	3	**20	1.5	*** 2.4-2.56 / 3.5-4.32 GHz	Microstrip Line
This work	**2.6**	**8.27 (-18 dB S_{11})**	**10**	DC-2 / 3.28-7.2 GHz	**Microstrip Line**

*: -20 dB S_{11} FBW, **: -12 dB S_{11} FBW, ***: estimated from Fig. 5 of [5]

3.3 Summary and Discussion

An impedance transformer with UHITR is proposed, investigated, and fabricated in this chapter. The UHITR can be obtained by controlling coupling coefficients of coupled lines. The proposed circuit is fabricated without difficulty with microstrip line technology. By choosing the properly matched region of coupled lines, two transmission poles are obtained in the passband. A low insertion loss is obtained with high impedance transforming ratio and provide a bandpass response.

CHAPTER 4

DESIGN OF LUMPED ELEMENTS BANDPASS FILTER WITH AIRBITRARY TERMINATION IMPEDANCE

In this chapter, the general design equations of unequal termination impedance bandpass filters (BPFs) using lumped elements is presented. The design equations for specific filters are derived step-by-step in detail and validated with simulations.

4.1 Coupled-Resonator Filter

Fig. 4.1 shows the capacitive coupled-resonator BPF using lumped element [35]. The termination impedances may have any values, and may be equal or unequal of pure resistance or complex impedance, as the desired. The inductors L_{ri} of resonators may be selected any values. The formulas for the individual elements utilize the values g_1, g_2, g_3, $\cdots$, g_n of the low-pass prototype filter, which are computed from the formulas in Section 2.3 for Chebyshev or Butterworth responses. The bandpass response is obtained from the prototype elements by transforming the frequency scaling that already discuss in Section 2.4.

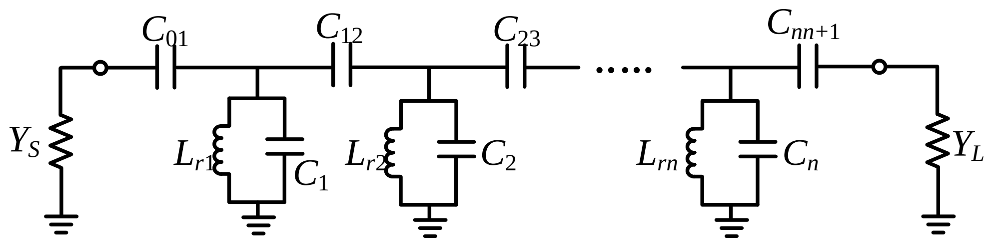

Fig. 4.1. Capacitive coupled lumped elements filter.

Fig. 4.2 depicts the low-pass prototype lumped-element circuit. The input admittance is determined as (4.1).

$$Y_{\text{in}}' = \frac{1}{j\omega g_1 + \frac{1}{Y_1'}} \tag{4.1}$$

where

$$Y_1' = j\omega g_2 + Y_2' \tag{4.2a}$$

$$Y_2' = \frac{1}{j\omega g_3 + \frac{1}{Y_3'}} \tag{4.2b}$$

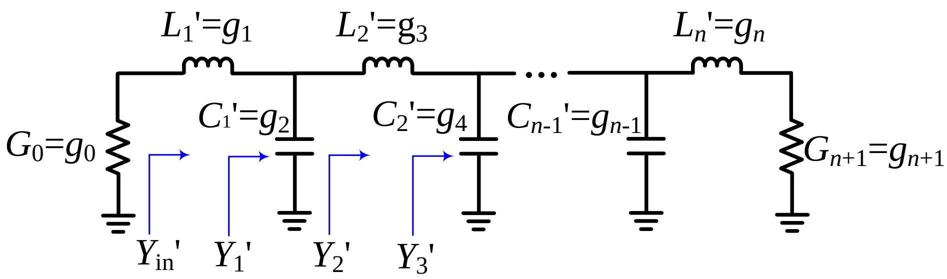

Fig. 4.2. Lumped elements ladder netowrk for low-pass prototype.

The derivation starts by expanding the input admittance of the network as the first Cauer form:

$$Y_{\text{in}}'(\omega') = \cfrac{1}{j\omega' g_1 + \cfrac{1}{j\omega' g_2 + \cfrac{1}{\dots + \cfrac{1}{j\omega' g_n + \cfrac{1}{g_{n+1}}}}}} \tag{4.3}$$

Then, the transformation is done by replacing *ω'* as

$$\frac{Y_{\text{in}}(\omega)}{Y_0} = \left.\frac{Y_{\text{in}}'(\omega')}{g_0}\right|_{\omega' = \frac{\omega_1'}{FBW}\left(\frac{\omega}{\omega_0} - \frac{\omega_0}{\omega}\right)} \tag{4.4}$$

where

$$\omega' = \frac{\omega_1'}{FBW}\left(\frac{\omega}{\omega_0} - \frac{\omega_0}{\omega}\right) \text{ with typically } \omega_1' = 1, \tag{4.5b}$$

$$FBW = \frac{\omega_2 - \omega_1}{\omega_0}, \quad \omega_0 = \sqrt{\omega_1 \omega_2}\,. \tag{4.5b}$$

Therefore, the final input admittance of lumped elements low-pass prototype become as

$$\frac{Y_{\text{in}}(\omega)}{g_0} = \cfrac{\cfrac{FBW}{g_0 g_1}}{j\left(\cfrac{\omega}{\omega_0} - \cfrac{\omega_0}{\omega}\right) + \cfrac{\cfrac{FBW}{g_1} \cdot \cfrac{FBW}{g_2}}{j\left(\cfrac{\omega}{\omega_0} - \cfrac{\omega_0}{\omega}\right) + \dots + \cfrac{\cfrac{FBW}{g_{n-1}} \cdot \cfrac{FBW}{g_n}}{j\left(\cfrac{\omega}{\omega_0} - \cfrac{\omega_0}{\omega}\right) + \cfrac{FBW}{g_n} \cdot \cfrac{1}{g_{n+1}}}}}. \tag{4.6}$$

Fig. 4.3 illustrates BPF using admittance inverters with termination admittance Y_S and Y_L. Similarly, the input admittance is determined as (4.7).

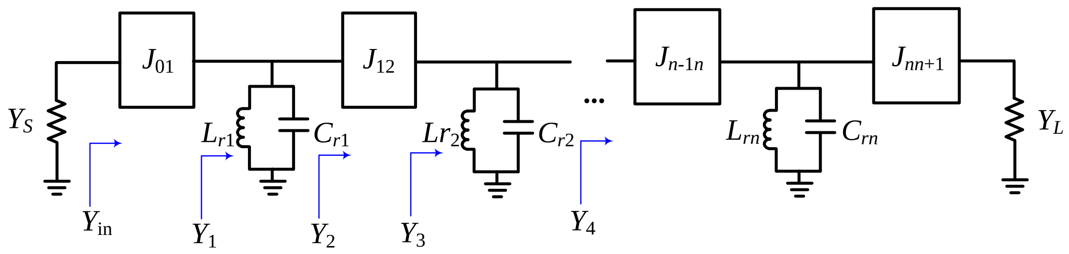

Fig. 4.3. Bandpass filter with admittance inverters.

$$Y_{\mathrm{in}} = \frac{J_{01}^{\;2}}{Y_1} \tag{4.7}$$

where

$$Y_1 = jB_1(\omega) + Y_2 \tag{4.8a}$$

$$Y_2 = \frac{J_{12}^{\;2}}{Y_3} \tag{4.8b}$$

$$Y_3 = jB_2(\omega) + Y_4 \tag{4.8c}$$

B_m (m=1, 2, ⋯, n) is the susceptance of resonators. By expanding the input admittance with a frequency transformation, the final input admittance is derived as (4.9).

$$\frac{Y_{\mathrm{in}}(\omega)}{Y_S} = \cfrac{\dfrac{J_{01}^{\;2}}{\omega_0 C_{r1} Y_S}}{j\left(\dfrac{\omega}{\omega_0} - \dfrac{\omega_0}{\omega}\right) + \cfrac{\dfrac{J_{12}^{\;2}}{(\omega_0 C_{r1})(\omega_0 C_{r2})}}{j\left(\dfrac{\omega}{\omega_0} - \dfrac{\omega_0}{\omega}\right) + \cfrac{\dfrac{J_{23}^{\;2}}{(\omega_0 C_{r2})(\omega_0 C_{r3})}}{j\left(\dfrac{\omega}{\omega_0} - \dfrac{\omega_0}{\omega}\right) + \dots + \cfrac{\dfrac{J_{n-1n}^{\;2}}{(\omega_0 C_{rn-1})(\omega_0 C_{rn})}}{j\left(\dfrac{\omega}{\omega_0} - \dfrac{\omega_0}{\omega}\right) + \cfrac{\dfrac{J_{nn+1}^{\;2}}{\omega_0 C_{rn}}}{Y_L}}}}} \tag{4.9}$$

By equating equations (4.6) and (4.9), the *J*-inverter are derived as (4.10).

$$J_{01} = \sqrt{\frac{Y_S FBW}{g_0 g_1 \omega_0 L_r}} \tag{4.10a}$$

$$J_{ii+1} = FBW \sqrt{\frac{1}{g_i g_{i+1} \left(\omega_0 L_r\right)^2}} \tag{4.10b}$$

$$J_{nn+1} = \sqrt{\frac{Y_L FBW}{g_n g_{n+1} \left(\omega_0 L_r\right)}} \tag{4.10c}$$

where

$$\omega_0{}^2 = \frac{1}{C_{rn} L_r} \rightarrow \omega_0 C_{rn} = \frac{1}{\omega_0 L_r} \tag{4.11a}$$

$$L_r = L_{r1} = L_{r2} = \cdots = L_{rn} \tag{4.11b}$$

4.1.1 Capacitive of Coupled Resonators

In application, the *J*-inverter can be realized with capacitors. Fig. 4.4 shows a section of *J*-inverter and its *π*-type equivalent circuit. The *ABCD* parameters is used to derived the design equations. As mention in Section 2.5, the *ABCD* matrix of *J*-inverter is obtained as (4.12).

$$\begin{pmatrix} A & B \\ C & D \end{pmatrix} = \begin{pmatrix} 0 & \pm \dfrac{j}{J} \\ \pm jJ & 0 \end{pmatrix} \tag{4.12}$$

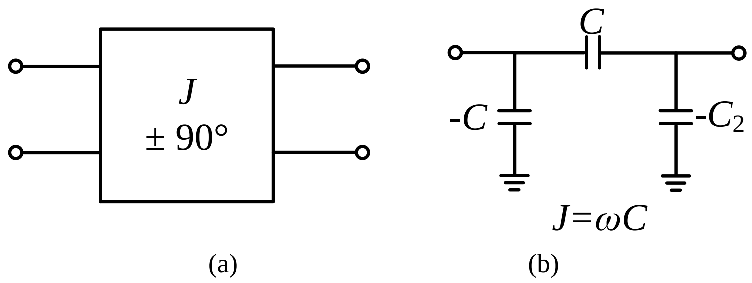

Fig. 4.4. (a) *J*-inverter and (b) Implementation using capacitor networks.

Similarly, the *ABCD* matrix of π-type equivalent circuit is determined as

$$\begin{pmatrix} A & B \\ C & D \end{pmatrix} = \begin{pmatrix} 1 & 0 \\ -j\omega C & 1 \end{pmatrix} \begin{pmatrix} 1 & \dfrac{1}{j\omega C} \\ 0 & 1 \end{pmatrix} \begin{pmatrix} 1 & 0 \\ -j\omega C & 1 \end{pmatrix} = \begin{pmatrix} 0 & \dfrac{-j}{\omega C} \\ -j\omega C & 0 \end{pmatrix}. \quad (4.13)$$

By equating (4.12) and (4.13), the series capacitors can be derived as (4.14).

$$C_{ii+1}\Big|_{i=1 \text{ to } n-1} = \frac{J_{ii+1}}{\omega_0} \quad (4.14)$$

Figure 4.5 (a) shows an equivalent circuit of series capacitor with π-type network and its equivalent *J*-inverter circuit. Then, the new equivalent network of Fig. 4.1 is transformed as Fig. 4.5(b) by replacing intermediate series capacitors as π-type network. From Fig. 4.5(a), the new equivalent circuit of Fig. 4.5 (b) is transformed as Fig. 4.6(a). Fig. 4.6(b) shows the final equivalent circuit of Fig. 4.5 (b) by summation the shunt capacitors between inverters.

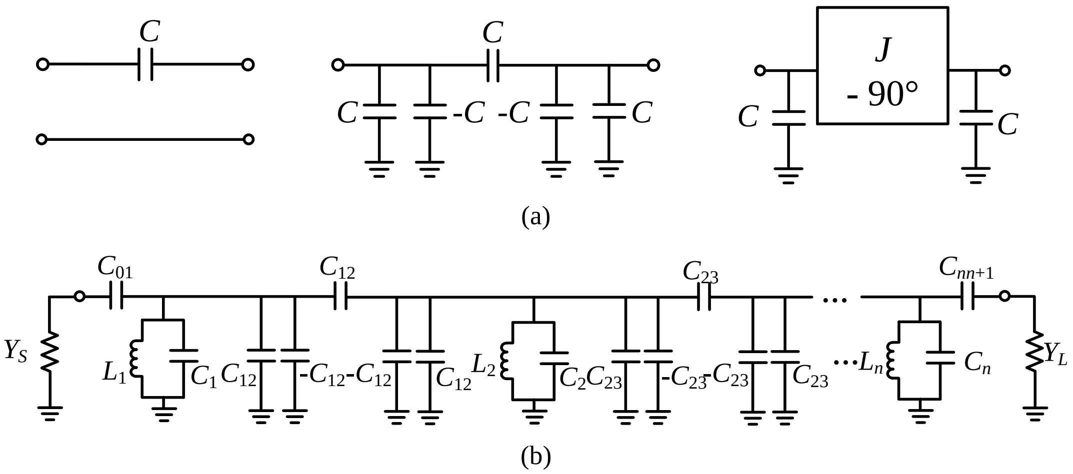

Fig. 4.5. (a) transformed J-inverter from coupling capacitor and (b) equivalent circuit of coupled resonator bandpass filter.

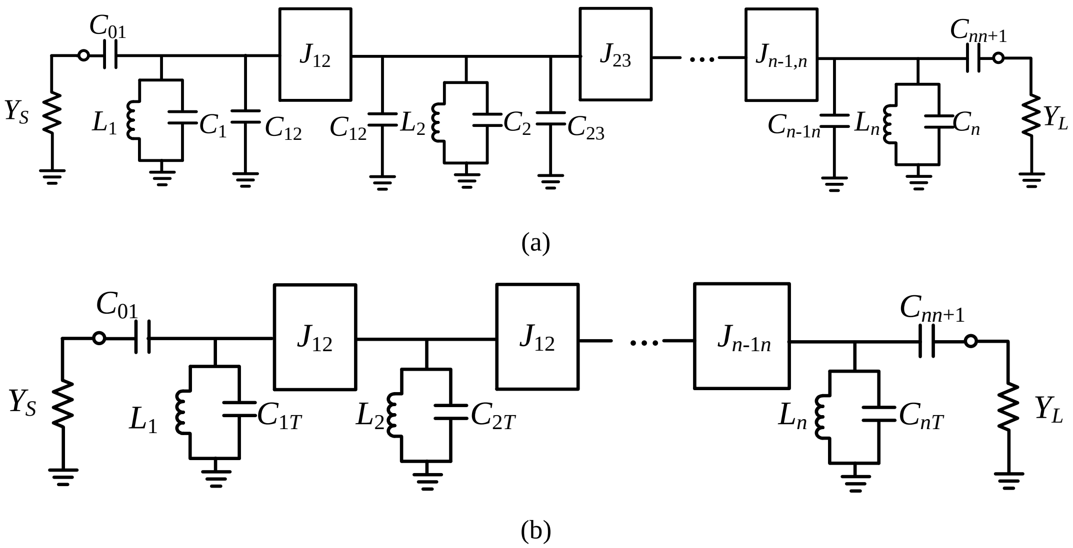

Fig. 4.6. (a) Capacitive coupled BPF with equivalent J-inverter and (b) its equivalent circuit.

Hence, the total shunt capacitors of the resonator are become as (4.15).

$$C_{1T} = C_1 + C_{12} \tag{4.15a}$$

$$C_{2T} = C_{12} + C_2 + C_{23} \tag{4.15b}$$

$$C_{n-1T} = C_{n-2n-1} + C_{n-1} + C_{n-1n} \tag{4.15c}$$

$$C_{nT} = C_{n-1n} + C_n \tag{4.15d}$$

4.1.2 Compensation of Complex Termination

Fig. 4.7 shows a series capacitor with a source termination impedance and its equivalent circuit using *J*-inverter. From Fig. 4.7 (a), the input impedance and admittance are determined as (4.16).

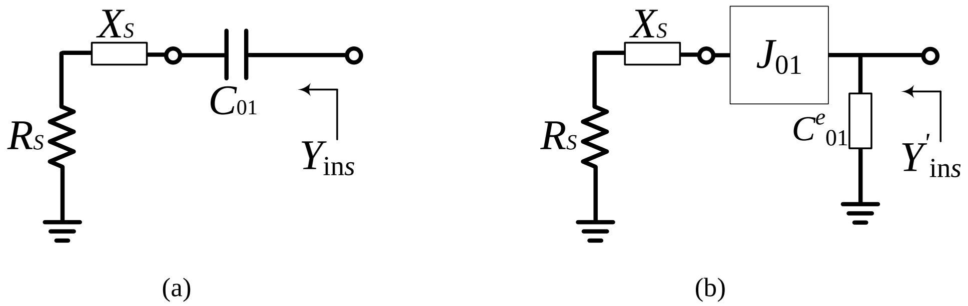

Fig. 4.7. (a) Source termination with a series capacitor and (b) equivalent source termination with *J*-inverter.

$$Z_{\text{in}S} = R_S - j\left(\frac{1}{\omega C_{01}} - X_S\right) \tag{4.16a}$$

$$Y_{\text{in}S} = \frac{1}{Z_{\text{in}S}} = \frac{R_S}{R_S{}^2 + \left(\frac{1}{\omega C_{01}} - X_S\right)^2} + j\frac{\frac{1}{\omega C_{01}} - X_S}{R_S{}^2 + \left(\frac{1}{\omega C_{01}} - X_S\right)^2} \tag{4.16b}$$

Similarly, from Fig. 4.7 (b) the input admittance of its equivalent circuit can be derived as

$$Z_S = R_S + jX_S \tag{4.17a}$$

$$Y_{\text{in}S}{}' = \frac{J_{01}{}^2}{Y_S} + j\omega C^e_{01} = J_{01}{}^2 R_S + j\left(J_{01}{}^2 X_S + \omega C^e_{01}\right). \tag{4.17b}$$

By comparing the real part of (4.16b) and (4.17b), the series capacitance of C_{01} is derived as (4.18b).

$$J_{01}{}^{2}R_S = \frac{R_S}{R_S{}^{2} + \left(\dfrac{1}{\omega C_{01}} - X_S\right)^{2}} \tag{4.18a}$$

$$C_{01} = \frac{J_{01}}{\omega\sqrt{1 - J_{01}{}^{2}R_S^{2}} + J_{01}X_S} \tag{4.18b}$$

Then, the capacitor C_{01}^{e} of the equivalent circuit is derived by equating the imaginary part of (4.16b) and (4.17b).

$$J_{01}^{2}X_S + \omega C_{01}^{e} = \frac{\dfrac{1}{\omega C_{01}} - X_S}{R_S{}^{2} + \left(\dfrac{1}{\omega C_{01}} - X_S\right)^{2}} \tag{4.19a}$$

$$C_{01}^{e} = \frac{C_{01}\left(1 - \omega C_{01}X_S\right)}{R_S{}^{2}\omega^{2}C_{01}{}^{2} + \left(X_S\omega C_{01} - 1\right)^{2}} - \frac{J_{01}^{2}X_S}{\omega} \tag{4.19b}$$

Similar to the source part, the input admittance of the load as shown in Fig. 4.8 is derived as (4.20a) and (4.20b), respectively.

$$Y_{\text{in}L} = \frac{1}{Z_{\text{in}L}} = \frac{R_L}{R_L{}^{2} + \left(\dfrac{1}{\omega C_{nn+1}} - X_L\right)^{2}} - j\frac{\dfrac{1}{\omega C_{nn+1}} - X_L}{R_L{}^{2} + \left(\dfrac{1}{\omega C_{nn+1}} - X_L\right)^{2}} \tag{4.20a}$$

$$Y_{\text{in}L}{}' = J_{nn+1}^{2}R_L + j\left(J_{nn+1}^{2}X_L + \omega C_{nn+1}^{e}\right) \tag{4.20b}$$

From the real-part of (4.20a) and (4.20b), the series capacitance of C_{nn+1} is derived as (4.21).

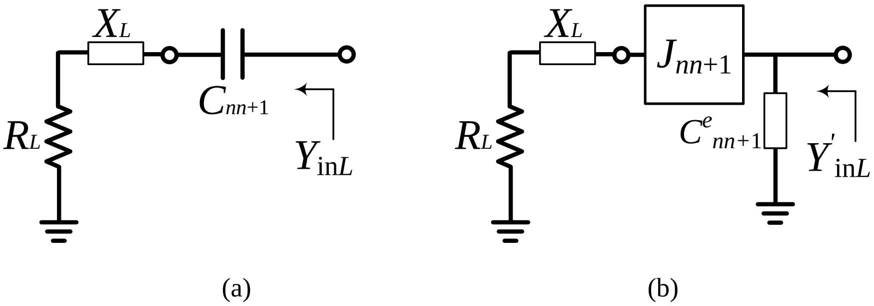

Fig. 4.8. (a) Load termination with a series capacitor and (b) load termination with J-inverter.

$$C_{nn+1} = \frac{J_{nn+1}}{\omega\left(J_{nn+1}X_L + \sqrt{1 - J_{nn+1}^2 R_L^2}\right)} \tag{4.21}$$

Similarly, the capacitor $C^e{}_{nn+1}$ is derived from the imaginary part of (4.20) and it is given by

$$C^e_{nn+1} = \frac{C_{nn+1}\left(1 - \omega C_{nn+1} X_L\right)}{\omega^2 C^2{}_{nn+1} R_L{}^2 + \left(1 - \omega C_{nn+1} X_L\right)^2} - \frac{J_{nn+1}^2 X_L}{\omega}. \tag{4.22}$$

Fig. 4.9 (a) shows an equivalent circuit of Fig. 4.6 (b) with capacitors C^e_{01} and C^e_{nn+1}. In this case the complex impedances of source and load are compensated with first and last resonators, respectively. Thus, the termination impedances of the equivalent circuit become any real termination impedance. Therefore, the total capacitors of resonators are become as

$$C_{r1} = C^e_{01} + C_1 + C_{12} \tag{4.23a}$$

$$C_{r2} = C_{12} + C_2 + C_{23} \tag{4.23b}$$

$$C_{rn-1} = C_{n-2n-1} + C_{n-1} + C_{n-1n} \tag{4.23c}$$

$$C_{rn} = C_{n-1n} + C_n + C^e_{nn+1}. \tag{4.23d}$$

So now the new capacitors of resonators are become as

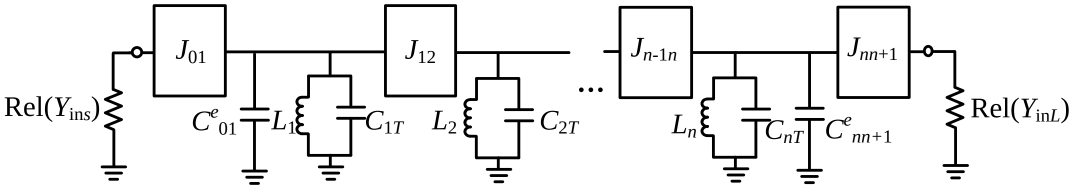

(a)

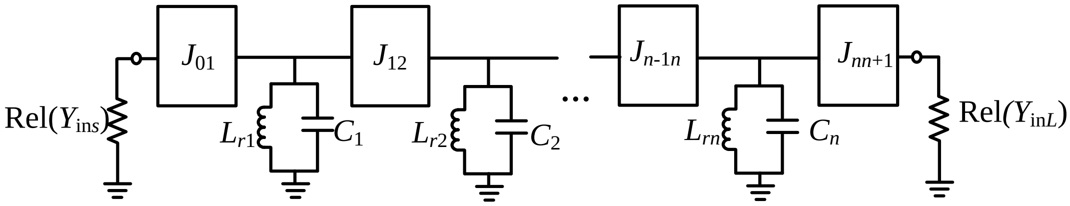

(b)

Fig. 4.9. Equivalent circuit of (a) coupled resonator with new termination and (b) new elements of first and last resonators.

$$C_1 = C_{r1} - C_{01}^e - C_{12} \tag{4.24a}$$

$$C_2 = C_{r2} - C_{12} - C_{23} \tag{4.24b}$$

$$C_{n-1} = C_{rn-1} - C_{n-2n-1} - C_{n-1n} \tag{4.24c}$$

$$C_n = C_{rn} - C_{n-1n} - C_{nn+1}^e \tag{4.24d}$$

Fig. 4.9 (b) shows an equivalent circuit of coupled resonator BPF with a new capacitors of resonators. With a new capacitance, the first and last resonant frequencies are shift to other frequencies depend on the complex termination impedance. Therefore, it can be observed that the detuned resonant frequency causes the slope parameter of their resonator change. So the new resonant frequency of the first and last resonators given by (4.25) based on [40]-[41].

$$f_{1,2} = f_0 \left[\sqrt{1 + \left(\frac{X_{(S,L)}}{2R_S g_{(1,n)}} FBW \right)^2} + \frac{X_{(S,L)} FBW}{2R_S g_{(1,n)}} \right] \tag{4.25}$$

Where f_0 and $X_{(S,L)}$ are the operating frequency and reactants of source and load impedance, respectively. The g_1 or g_n are the lumped element values of the low-pass prototype.

The design formulas for capacitively coupled lumped element filters are summarize as follows.

$$J_{01} = \sqrt{\frac{Y_S FBW}{g_0 g_1 \omega_0 L_r}} \, , J_{ii+1} = FBW \sqrt{\frac{1}{g_i g_{i+1} \left(\omega_0 L_r\right)^2}} \, , J_{nn+1} = \sqrt{\frac{Y_L FBW}{g_n g_{n+1} \left(\omega_0 L_r\right)}}$$

$$C_{01} = \frac{J_{01}}{\omega_1 \sqrt{1 - J_{01}{}^2 R_S^2} + J_{01} X_S} \, , \qquad C_{ii+1}\Big|_{j=1 \text{ to } n-1} = \frac{J_{ii+1}}{\omega_0}$$

$$C_{nn+1} = \frac{J_{nn+1}}{\omega_2 \left(J_{nn+1} X_L + \sqrt{1 - J_{nn+1}^2 R_L^2} \right)}$$

$$C_1 = C_{r1} - C_{01}^e - C_{12}, \qquad C_2 = C_{r2} - C_{12} - C_{23}$$

$$C_{n-1} = C_{rn-1} - C_{n-2n-1} - C_{n-1n}, \qquad C_n = C_{rn} - C_{n-1n} - C_{nn+1}^e$$

where

$$C_{r1} = \frac{1}{\omega_1 L_{r1}}, \quad C_{ri} = \frac{1}{\omega_0 L_{ri}}, \; i = 2, 3, \cdots, n, \quad C_{rn} = \frac{1}{\omega_2 L_{rn}}$$

$$C_{01}^e = \frac{C_{01}\left(1 - \omega_1 C_{01} X_S\right)}{R_S{}^2 \omega_1^2 C_{01}{}^2 + \left(X_S \omega_1 C_{01} - 1\right)^2} - \frac{J_{01}^2 X_S}{\omega_1}$$

$$C^{e}_{nn+1} = \frac{C_{nn+1}\left(1-\omega_2 C_{nn+1} X_L\right)}{\omega_2^2 C^2{}_{nn+1} R_L{}^2 + \left(1-\omega_2 C_{nn+1} X_L\right)^2} - \frac{J^2_{nn+1} X_L}{\omega_2}$$

$$f_{1,2} = f_0\left[\sqrt{1+\left(\frac{X_{(S,L)}}{2R_S g_{(1,n+1)}} FBW\right)^2} + \frac{X_{(S,L)} FBW}{2R_S g_{(1,n+1)}}\right]$$

4.2 Simulation

To verify the analytical analysis of the proposed BPF, the real and complex unequal termination impedance BPFs were designed with a Chebyshev and Butterworth responses. The calculations have been done using Matlab R2016a (see appendix B). The Advanced Design System 2016.1 was used to simulate the proposed circuit. Table 4.1 and 4.2 are shown the calculated values of coupled resonator BPF with Chebyshev and Butterworth responses, respectively. The specification of the proposed are shown in the tables. The inductors of shunt resonators are chosen to be 4 nH for all resonators. The *S*-parameter characteristic of the Chebyshev response in Fig. 4.10 (a) and (b) are shown the narrow and broad-band characteristic responses, respectively. Thus, as is indicated in Fig. 4.10(a), the *S*-parameter characteristics of real and complex impedance are good agreement. Three transmission poles are occurred in the passband. The fractional bandwidth of the passband edge is obtained 5% for equal ripple response. Fig. 4.10(b) shows a broad-band *S*-parameter characteristic with a wide stopband. Fig. 4.11 is shown *S*-parameter comparison of different termination BPF with Butterworth response. Similar to the equal ripple response, the characteristics of equal and unequal termination BPF are good agreement. The 3 dB bandwidth of the whole passband is obtained 5%. Moreover, the return loss of complex termination impedance is slightly more narrow than the real termination impedance.

TABLE 4.1. CALCULATED VALUE OF CHEBYSHEV RESPONSE OF COUPLED RESONATOR BPF.

f_0 = 1 GHz, n = 3, FBW = 5%, L_{Ar} = 0.043 dB				
C_i (pF)/L_i(nH)			$C_{01}/C_{12}/C_{23}/C_{34}$ (pF)	Z_S/Z_L (Ω)
4.985/4	5.68/4	4.985/4	1.16/0.33/0.33/1.16	50/50
3.6/4	5.68/4	4.985/4	2.46/0.33/0.33/1.16	10/50
4.014/4	5.67/4	4.985/4	2.78/0.33/0.33/1.16	15-j20/50

TABLE 4.2. CALCULATED VALUE OF BUTTERWORTH RESPONSE OF COUPLED RESONATOR BPF.

f_0 = 1 GHz, n = 3, FBW = 5%				
C_i (pF)/L_i(nH)			$C_{01}/C_{12}/C_{23}/C_{34}$ (pF)	Z_S/Z_L (Ω)
5.156/4	5.885/4	5.156/4	1.06/0.22/0.22/1.06	50/50
3.886/4	5.885/4	5.156/4	2.27/0.22/0.22/1.06	10/50
4.27/4	5.88/4	5.156/4	2.48/0.23/0.22/1.06	15-j20/50

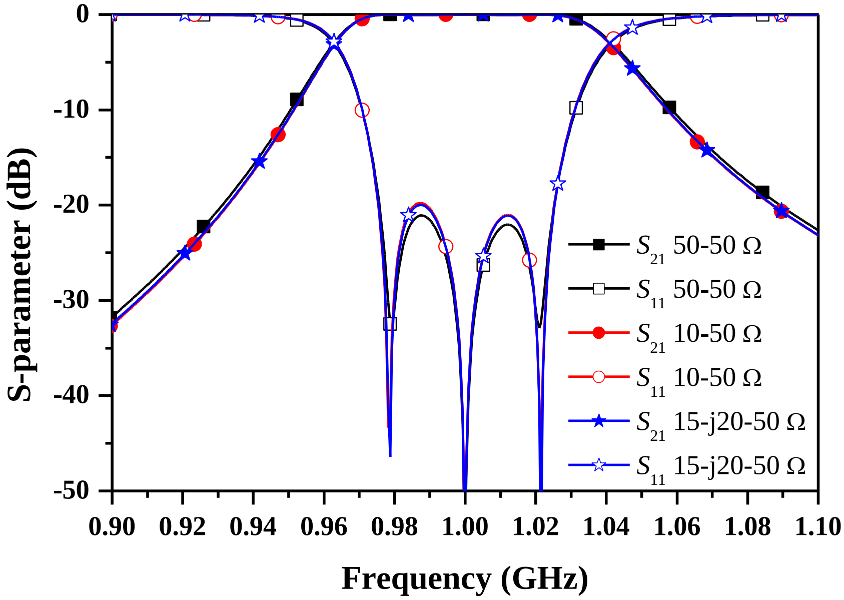

(a)

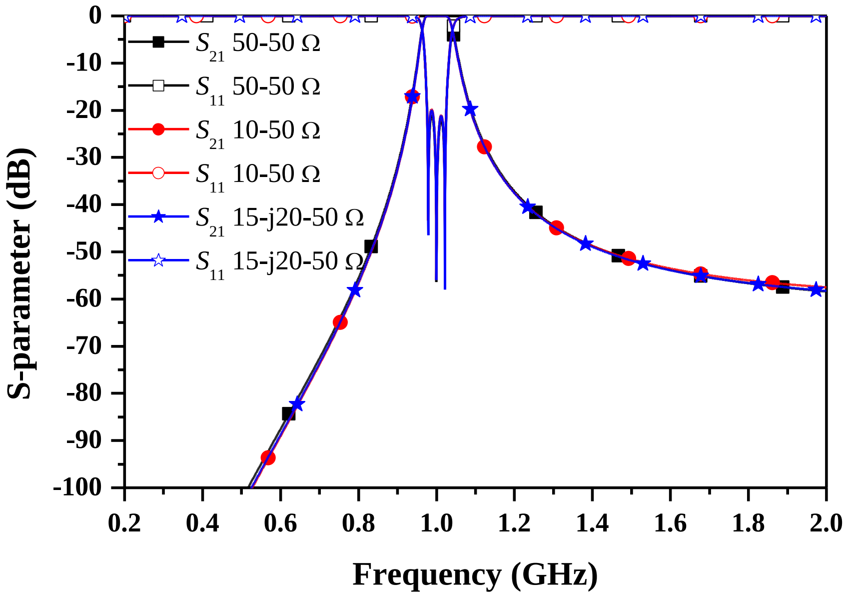

(b)

Fig. 4.10. *S*-parameter characteristic of coupled resonator bandpass filter with Chebyshev response: (a) narrow and (b) broad bands.

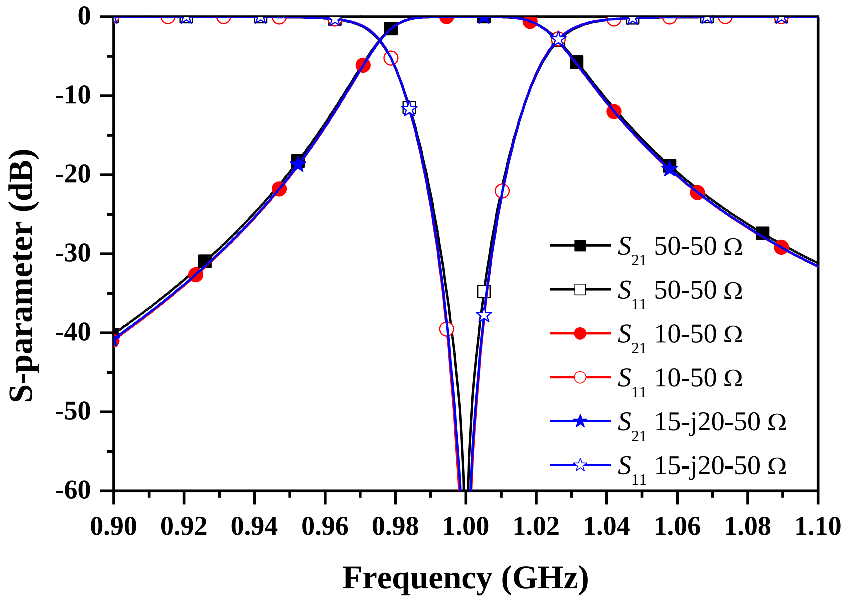

(a)

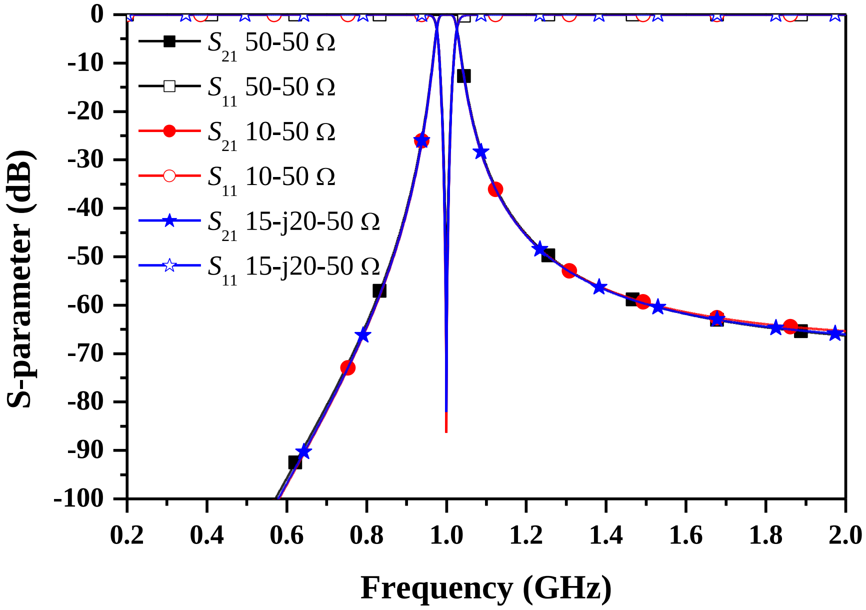

(b)

Fig. 4.11. *S*-parameter characteristic of coupled resonator bandpass filter with Butterworth response (a) narrow and (b) broad bands.

4.3 Summary and Discussion

In this chapter, the new design equations of unequal termination impedance coupled resonators bandpass filter were demonstrated. The theoretical analysis and simulations were presented to validate the proposed design equations. The new analysis is able to design coupled resonator bandpass filter with real or complex termination impedance using lumped elements resonators.

CHAPTER 5

DISTRIBUTED UNEQUAL TERMINATION IMPEDANCE λ/4 COUPLED LINE BANDPASS FILTER

In this section, the general design equations of arbitrary termination impedance BPFs are analyzed and realized using a parallel coupled line structure. The new design equations are able to calculate with *n*-resonators, arbitrary termination impedance, and arbitrary image impedance of coupled line by using low-pass prototype elements value. The coupling coefficients of coupled lines can be controlled by the image impedance (Z_1) without any effect on the filter response.

5.1 Theory and Design Equations

5.1.1 Low-pass Prototype Ladder Network

Fig. 5.1 shows the normalized dual circuits of low-pass prototype structure, where the termination source impedance is 1 Ω and the cutoff frequency is 1 rad/sec. The element values for the ladder-type circuits can be defined for Butterworth (or maximally flat) and Chebyshev (or equal ripple) low-pass filter responses and have been discussed detail in [35]. The reactive elements for i = 1 to n represent either the series inductor or shunt capacitor. Butterworth and Chebyshev low-pass filter responses have terminated with load resistor of equal or nearly equal 1 Ω. For the low-pass filters to be designed with other termination impedances (typically $R_0 = R_{n+1} = 50$ Ω) and other cutoff frequency, the impedance

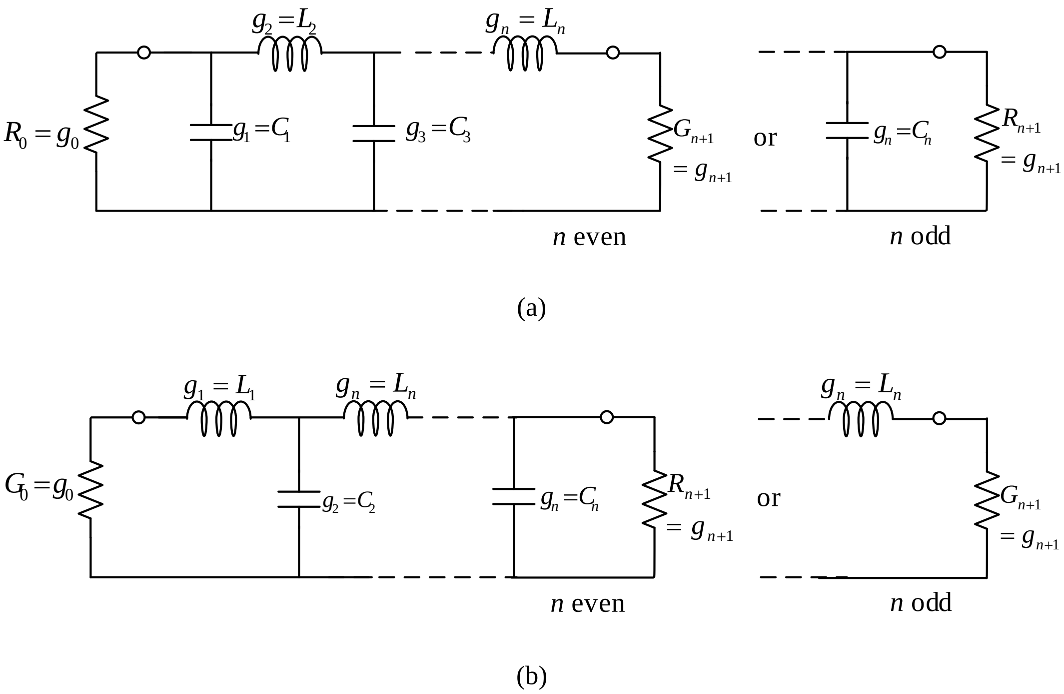

Fig. 5.1. Ladder circuits for low-pass filter prototype and their element: (a) prototype beginning with a shunt element and (b) prototype beginning with a series element.

and frequency scalings are required. Also, the conversion from low-pass filter to highpass, bandpass, or bandstop filters are also presented in [32]-[34].

In the case of the ladder network discussed in [19] and [42], the terminating resistors may be chosen arbitrary ($R_0 \neq R_{n+1}$). However, the transmission characteristics of both Chebyshev [19] and Butterworth [42] filters in the passband are deteriorated around zero frequency. The deterioration at zero frequency is varied according to the impedance transformation ratio (r). The main difference between a new low-pass filter and conventional low-pass filter is that new low-pass filter can be designed with arbitrary termination impedance. However, the deterioration at zero frequency in low-pass filter will cause the center frequency performance of BPF transformed from low-pass filter.

Fig. 5.2 shows the frequency transformation from the arbitrary termination impedance low-pass filter [19] to the BPF with r of 2 and 3. The simulation is done by using the values of Table 6 in [19]. As can seem in Fig. 5.2, the return and insertion losses are poor at center frequency and more deteriorated with higher r.

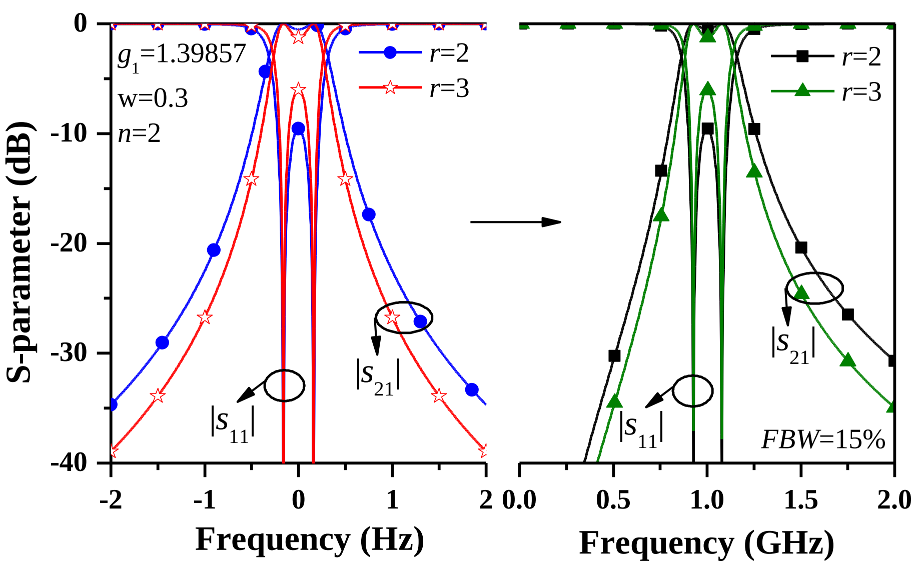

Fig. 5.2. Arbitrary termination impedance low-pass [19-42] and frequency transformed arbitrary termination impedance bandpass filters.

5.1.2 Inverter Coupled Arbitrary Termination Impedance BPF

The ladder type low-pass prototype structures in Fig. 5.1 can transform into inverter coupled low-pass prototype filter using the impedance and admittance inverters (K- or J-inverters). The detail design equations are present in [35]. Ideally, K- or J-inverters are assumed frequency independent so that the low-pass filter easily be transformed to other filter types (such as highpass, bandpass, and band-stop filters) by applying frequency and impedance transformations [34]-[35]. Generally, the slope parameters are used to characterize resonators regardless of their types. Therefore, the generalized structures of arbitrary termination impedance BPFs using *J*- and *K*-inverters are shown in Fig. 5.3. Even though the BPFs in Fig. 5.3 are terminated arbitrarily unlike the conventional BPFs terminated with 50-to-50 Ω, the arbitrary termination impedance BPF can show filter performances of the conventional BPF [38].

From the frequency transformation, two design equation sets from Fig. 5.3 can be derived from series and shunt resonators [35]. The general design equations with specified reactance and susceptance slope parameter are defined as (5.1) and (5.2), respectively.

$$K_{0,1} = \sqrt{\frac{R_S FBW x_1}{g_0 g_1}} \tag{5.1a}$$

$$K_{i,i+1} = FBW\sqrt{\frac{x_i x_{i+1}}{g_i g_{i+1}}} \quad i = 1,\ 2,\ \cdots,\ n\text{-}1 \tag{5.1b}$$

$$K_{n,n+1} = \sqrt{\frac{R_L FBW x_n}{g_n g_{n+1}}} \tag{5.1c}$$

And

$$J_{0,1} = \sqrt{\frac{G_S FBW b_1}{g_0 g_1}} \tag{5.2a}$$

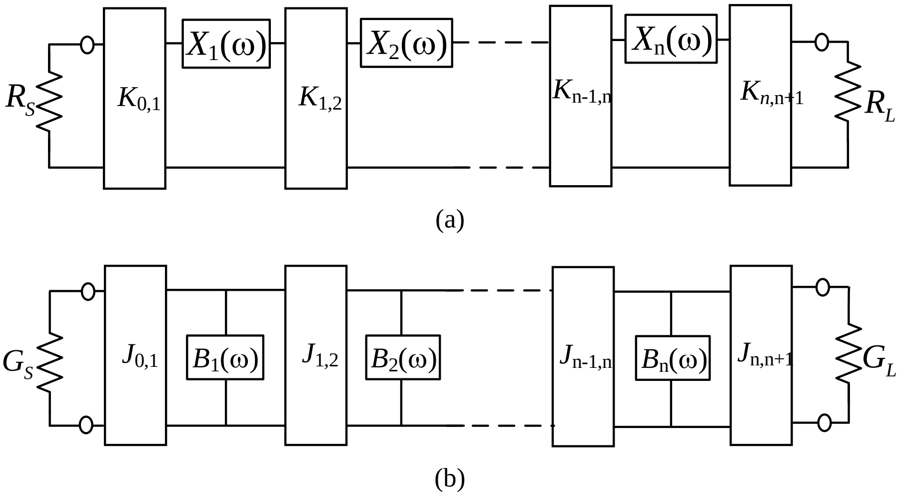

Fig. 5.3. Generalized arbitrary termination impedance bandpass filters with (a) impedance and (b) admittance inverters.

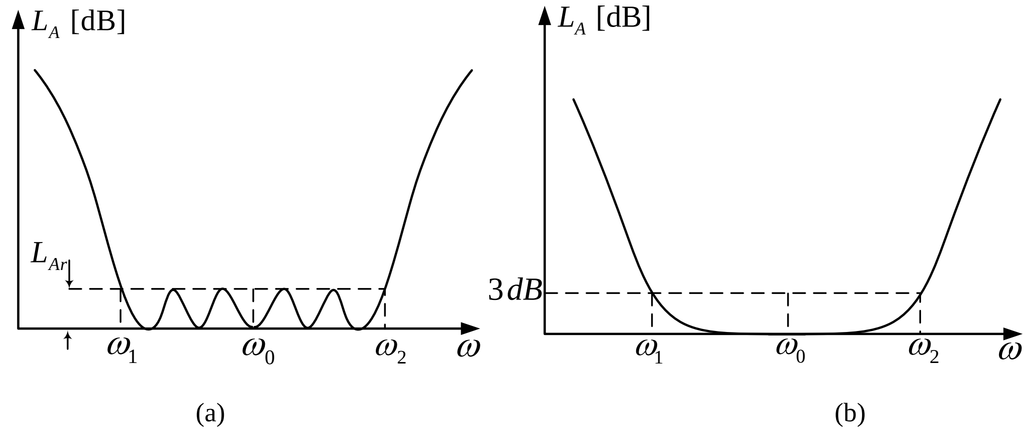

Fig. 5.4. Frequency response of a bandpass filter with (a) Chebyshev (or equal-ripple) and (b) Butterworth (or maximally flat) responses.

$$J_{i,i+1} = FBW\sqrt{\frac{b_i b_{i+1}}{g_i g_{i+1}}} \quad i = 1,\ 2,\ \cdots,\ n-1 \tag{5.2b}$$

$$J_{n,n+1} = \sqrt{\frac{G_L FBW b_n}{g_n g_{n+1}}} \tag{5.2c}$$

where g_i represents the low-pass prototype values, $G_S = 1 / R_S$ and $G_L = 1 / R_L$. The fractional bandwidth (FBW) is defined as

$$FBW = \frac{\omega_2 - \omega_1}{\omega_0}. \tag{5.3}$$

The angular frequencies ω_1 and ω_2 denote the lower and upper passband edge frequencies in case of Chebyshev response and 3-dB cut-off frequencies in case of Butterworth response [33], respectively, as shown in Fig. 5.4.

For series resonators with reactance $X_i(\omega)$, the reactance slope parameters are defined in [33] and [35] as

$$x_i = \frac{\omega_0}{2} \frac{dX_i(\omega)}{d\omega}\bigg|_{\omega=\omega_0}, \ i = 1,\ 2,\ \cdots,\ n. \tag{5.4}$$

For shunt resonators with susceptance $B_i(\omega)$, the susceptance slope parameters are defined as

$$b_i = \frac{\omega_0}{2} \frac{dB_i(\omega)}{d\omega}\bigg|_{\omega=\omega_0}, \ i = 1,\ 2,\ \cdots,\ n. \tag{5.5}$$

To validate the theory, the BPFs are designed with arbitrary termination impedances and different responses. The designed BPF is composed of shunt parallel and series LC resonators for J- and K-inverters, respectively. From [33], the reactance slope parameters of series resonators are defined as $x_i = \omega_0 L''_{si}$ and suceptance slop parameters of shunt resonators are defined as $b_i = \omega_0 C''_{pi}$. The subscript s and p stand for series and parallel, respectively. Under the resonant condition, the series or shunt LC resonators between J- and K-inverters must have zero reactance or susceptance at a center angular frequency (ω_0).

In the design example, all J- and K-inverters in Fig. 5.3 can be calculated using (5.1) and (5.2), respectively. Moreover, the parallel capacitors and series inductors are chosen as 5 pF and 5 nH, respectively. Following the resonance frequency ($\omega_0 = 1 / \sqrt{LC}$), the parallel inductors and series capacitors are calculated. The calculated variables and J-/K-inverters are listed in Table 5.1 and Table 5.2 with

TABLE 5.1 CALCULATED VALUES OF J-INVERTER WITH ARBITRARY TERMINATION IMPEDANCE.

f_c = 1 GHz, FBW = 5%, C''_{pi} = 5 pF								
	R_S/R_L (Ω)	$J_{0,1}$	$J_{1,2}$	$J_{2,3}$	$J_{3,4}$	$J_{4,5}$	n	L''_{pi} (nH)
Butt.	10/50	0.01054	0.00111	0.00471			2	5.066
	80/20	0.00443	0.00111	0.00111	0.00886		3	
	10/500	0.01433	0.00132	0.00085	0.00132	0.00203	4	
Chev. (0.043 dB)	10/50	0.01535	0.0026	0.00686			2	
	80/20	0.00479	0.00162	0.00162	0.00959		3	
	10/500	0.01297	0.00143	0.0011	0.00143	0.00183	4	

TABLE 5.2 CALCULATED VALUES OF K-INVERTER WITH ARBITRARY TERMINATION IMPEDANCE.

f_c = 1 GHz, FBW = 5%, $L''si$ = 5 nH								
	R_S/R_L (Ω)	$K_{0,1}$	$K_{1,2}$	$K_{2,3}$	$K_{3,4}$	$K_{4,5}$	n	C''_{si} (pF)
Butt.	10/50	3.33275	1.11072	7.45225			2	5.066
	80/20	11.2099	1.11072	1.11072	5.60499		3	
	10/500	4.53028	1.32087	0.85011	1.32087	32.0339	4	
Chev. (0.043 dB)	10/50	4.85399	2.60481	10.8538			2	
	80/20	12.1342	1.61832	1.61832	6.06711		3	
	10/500	4.10261	1.43032	1.09943	1.43032	29.0098	4	

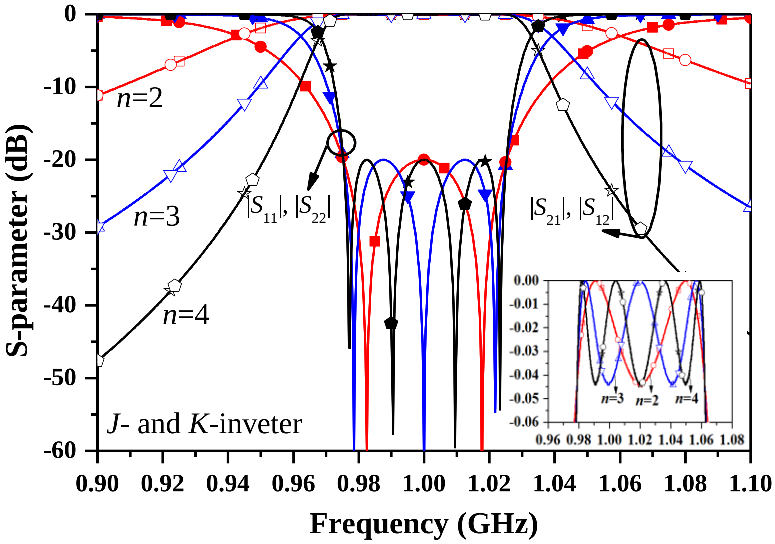

(a)

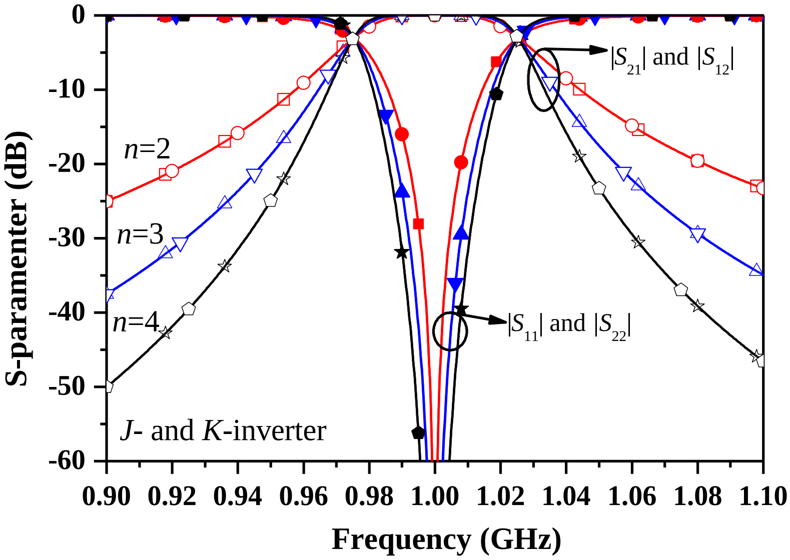

(b)

Fig. 5.5. *S*-parameter characteristics of arbitrary termination impedance BPF using *J*- and *K*-inverters according to order of filter: (a) Chebyshev and (b) Butterworth responses.

Butterworth and Chebyshev responses, respectively. The termination impedances are chosen randomly. The ripple of 0.043 dB in Chebyshev response is chosen to get 20-dB return loss in the passband. The ideal simulation of arbitrary termination

BPF with different n are compared in Fig. 5.5 (a) and (b) for Chebyshev and Butterworth responses for different termination impedance ratios (r), respectively. Obviously, the transmission poles of Chebyshev response in the passband are proportional to n. As n increases, the transmission poles in the passband are increased. Also, it is observed that the higher n has sharper roll-off at the stop frequency bands as compared with a lower n. However, the *FBW* in the passband are maintained. For Butterworth response, the *S*-parameter characteristics are compared with different n shown in Fig. 5.5(b). In this case, the 3 dB cut-off frequencies are maintained but the bandwidths of return loss are narrow as n decreases. The filter characteristics is the same although the termination impedances are different. However, Chebyshev response can obtain wider return loss bandwidth than Butterworth response. With the specification above, especially ripple of 0.043 dB, the stopband attenuation of the Butterworth response is better than the Chebyshev response. The benefit property of Chebyshev and Butterworth response were discussed detail in [35]. The termination impedance and other specifications can be chosen arbitrary. The simulation was done using circuit simulation of Advanced Design System (ADS).

5.1.3 Arbitrary Termination Impedance Coupled Line BPF

Fig. 5.6 shows the proposed structure of arbitrary termination impedance parallel coupled line BPF with n stages. The proposed structure is composed of the cascading parallel coupled lines terminated with source and load conductance, G_S and G_L, respectively. The electrical lengths of each coupled lines are θ. Fig. 5.7

shows the parallel coupled line section and its equivalent circuit. By equating *ABCD* matrix of parallel coupled line and its equivalent circuit, the even- and odd-mode impedances of coupled line can be determined [38]. For more general, the even- and odd-mode impedances are written as

$$\left(Z_{0e}\right)_{i+1}\Big|_{i=0 \text{ to } n} = Z_1\left(1 + J_{i,i+1}Z_1 + J_{i,i+1}^2 Z_1^2\right) \tag{5.6a}$$

$$\left(Z_{0o}\right)_{i+1}\Big|_{i=0 \text{ to } n} = Z_1\left(1 - J_{i,i+1}Z_1 + J_{i,i+1}^2 Z_1^2\right). \tag{5.6b}$$

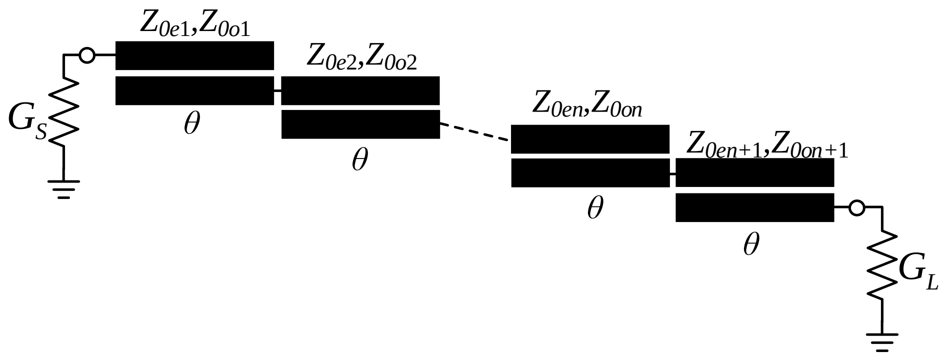

Fig. 5.6. Parallel coupled line bandpass filter.

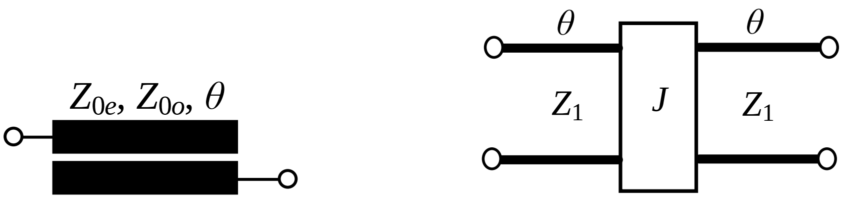

(a) (b)

Fig. 5.7. (a) Single parallel coupled line and (b) its equivalent circuit.

From (5.6), the coupling coefficients (C) of coupled lines are determined as

$$C_{i+1}\Big|_{i=0 \text{ to } n} = \frac{\left(Z_{0e}\right)_{i+1} - \left(Z_{0o}\right)_{i+1}}{\left(Z_{0e}\right)_{i+1} + \left(Z_{0o}\right)_{i+1}}. \tag{5.7}$$

In order to derive the J-inverter values, the susceptance for each equivalent resonator should be derived [43]. Fig. 5.8 shows the equivalent circuit of parallel coupled line BPF. As can seem in Fig. 5.8(a), the termination impedances can be equal or unequal to the image admittance of coupled line Y_1 ($Y_1 = 1 / Z_1$).

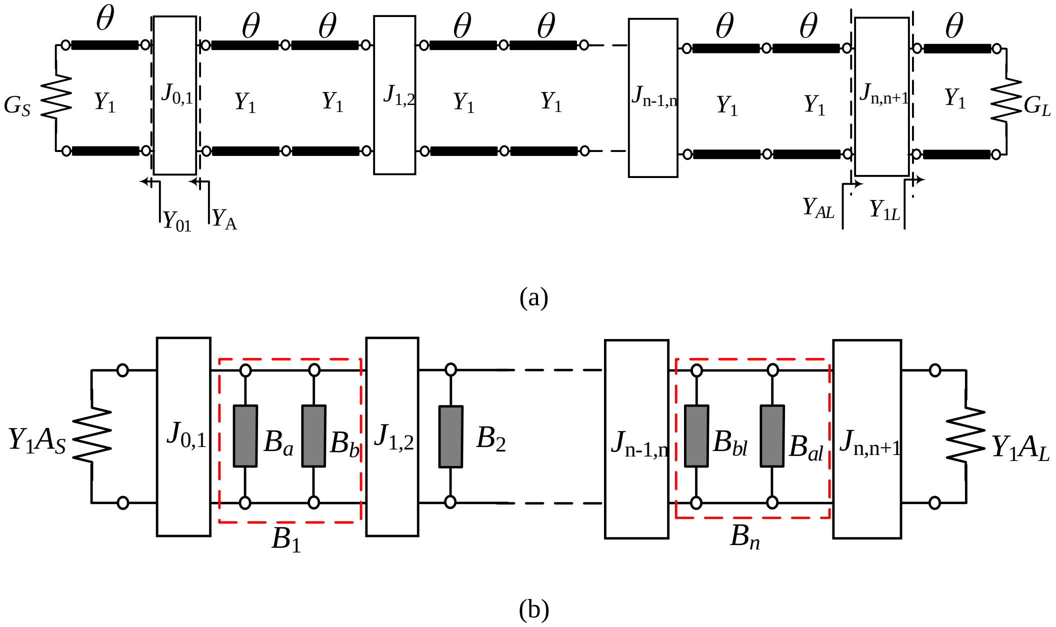

Fig. 5.8. (a) Equivalent circuit of the parallel coupled line bandpass filter and (b) equivalent circuit model of (a).

From Fig. 5.8(a), the input admittance Y_{01} looking into the source is obtained as (5.8) in case G_S is not equal to Y_1.

$$Y_{01} = Y_1 \frac{G_S + jY_1 \tan\theta}{Y_1 + jG_S \tan\theta} \approx Y_1 \left[A_S + j\left(1 - A_S^2\right) a \right] \tag{5.8}$$

where

$$A_S = \frac{Y_1}{G_S} \tag{5.9a}$$

$$a = \frac{\pi}{2}\frac{\left(\omega - \omega_0\right)}{\omega_0} \tag{5.9b}$$

It is assumed that the angular frequency ω is closed to ω_0. Similarly, the input admittance of Y_A in Fig. 5.8(a) is obtained as

$$Y_A = \frac{J_{0,1}^2}{Y_1 A_S} + jB_a \tag{5.10}$$

where

$$B_a = \frac{J_{0,1}^2}{Y_1 A_S}\left(A_S - \frac{1}{A_S} \right) a \,. \tag{5.11}$$

So the equivalent circuit is shown in Fig. 5.8(b). The total susceptance of the first resonator B_1 is shown as

$$B_1\left(\omega\right) = B_a(\omega) + B_b\left(\omega\right) \tag{5.12}$$

where

$$B_b\left(\omega\right) = 2Y_1 a \,. \tag{5.13}$$

From (5.5), the slope parameter of the first resonator is found as

$$b_1 = \frac{\pi}{2}\left[\frac{J_{0,1}^2}{2Y_1}\left(1 - \frac{1}{A_S^2} \right) + Y_1 \right]. \tag{5.14}$$

On the other hand, the input admittance Y_{1L} looking into the load is obtained as

$$Y_{1L} = Y_1 \frac{G_L + jY_1 \tan\theta}{Y_1 + jG_L \tan\theta} \approx Y_1\left[A_L + j\left(1 - A_L^2\right) a \right] \tag{5.15}$$

where

$$A_L = \frac{Y_1}{G_L}. \tag{5.16}$$

Similarly, the input admittance Y_{AL} in Fig. 5.8(a) is obtained as

$$Y_{AL} = \frac{J_{0,1}^2}{Y_1 A_L} + jB_{al} \tag{5.17}$$

where

$$B_{al} = \frac{J_{n,n+1}^2}{Y_1 A_L}\left(A_L - \frac{1}{A_L}\right)a. \tag{5.18}$$

Similarly, the total susceptance of the last resonator B_n is shown as

$$B_n(\omega) = B_{al}(\omega) + B_{bl}(\omega) \tag{5.19}$$

where

$$B_{bl}(\omega) = B_b(\omega) \tag{5.20}$$

Also, the slope parameter of the last resonator is found as

$$b_n = \frac{\pi}{2}\left[\frac{J_{n,n+1}^2}{2Y_1}\left(1 - \frac{1}{A_L^2}\right) + Y_1\right]. \tag{5.21}$$

Beside the first and last susceptance resonators, the susceptances of the intermediate resonators are equal to B_b and the slope parameters are obtained as

$$b_m = \frac{\pi}{2} Y_1 \quad @\ m = 2,\ 3,\ \cdots,\ n-1. \tag{5.22}$$

From (5.2a)-(5.2c), the J-inverters of arbitrary termination impedance and image admittance (Y_1) are derived as

$$J_{0,1} = Y_1 \sqrt{\frac{A_S \dfrac{\pi}{2} FBW}{g_0 g_1 - \dfrac{\pi}{4}\left(A_S - \dfrac{1}{A_S}\right) FBW}} \tag{5.23a}$$

$$J_{1,2} = Y_1 FBW \frac{\pi}{2} \sqrt{\frac{N_1}{g_1 g_2}} \tag{5.23b}$$

$$J_{i,i+1} = Y_1 FBW \frac{\pi}{2} \sqrt{\frac{1}{g_i g_{i+1}}}, \; i = 2,\; 3,\; \cdots,\; n-2 \tag{5.23c}$$

$$J_{n-1,n} = Y_1 FBW \frac{\pi}{2} \sqrt{\frac{N_L}{g_{n-1} g_n}} \tag{5.23d}$$

$$J_{n,n+1} = Y_1 \sqrt{\frac{A_L \dfrac{\pi}{2} FBW}{g_n g_{n+1} - \dfrac{\pi}{4}\left(A_L - \dfrac{1}{A_L}\right) FBW}} \tag{5.23e}$$

where

$$N_1 = \frac{J_{0,1}^2}{2Y_1}\left(1 - \frac{1}{A_S^2}\right) + 1 \tag{5.24a}$$

$$N_L = \frac{J_{n,n+1}^2}{2Y_1}\left(1 - \frac{1}{A_L^2}\right) + 1 . \tag{5.24b}$$

In case of n = 2, the first and the last J-inverters are the same to (5.23a) and (5.23e), respectively. However, the $J_{1,2}$ is found as (5.25).

$$J_{1,2} = FBW Y_1 \frac{\pi}{2} \sqrt{\frac{N_1 N_L}{g_1 g_2}} \tag{5.25}$$

As seem in (5.23) and (5.25), the J-inverters between the first and the last slope parameters of resonators are changed when the termination impedance is not equal to the image impedance of parallel coupled lines. According to (5.23)-(5.25), the J-inverters can be calculated with arbitrary termination impedances and image impedance of parallel coupled lines by using MatLab (see appendix C and D). Therefore, from (5.6) and (5.7) the coupling coefficient of coupled line can be controlled by the image impedance (Z_1) of coupled line. In order to demonstrate the analysis, a parallel coupled line BPFs were designed and simulated. Using (5.23)-(5.25), an ideal circuit parameters of arbitrary termination impedance coupled line BPF are calculated with n = 2, 3, and 4, passband ripple L_{Ar} = 0.0434 dB, and FBW = 5% for Chebyshev and Butterworth responses. The terminations are choosing randomly. Fig. 5.9(a) shows the S-parameter characteristics and equal ripples of Chebyshev response coupled line BPF with different n. As seem in the figure, the number of transmission poles are proportional to n. Also, the stopband attenuation

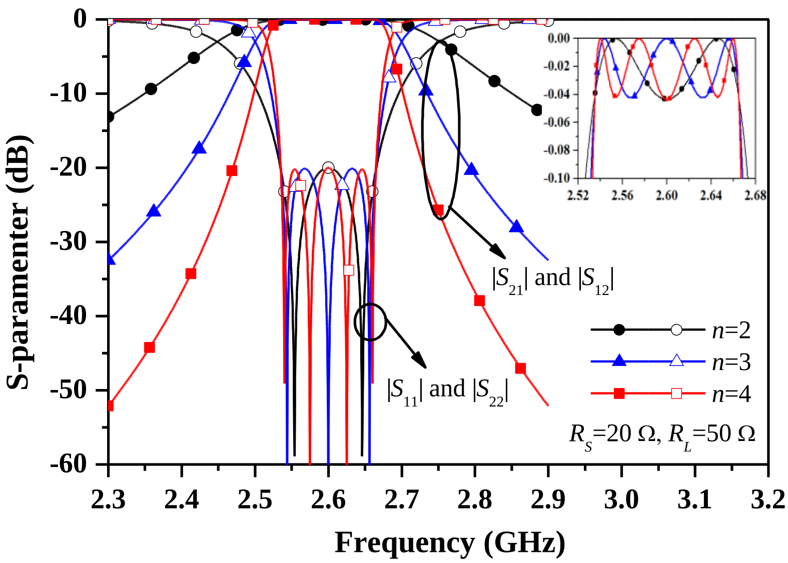

(a)

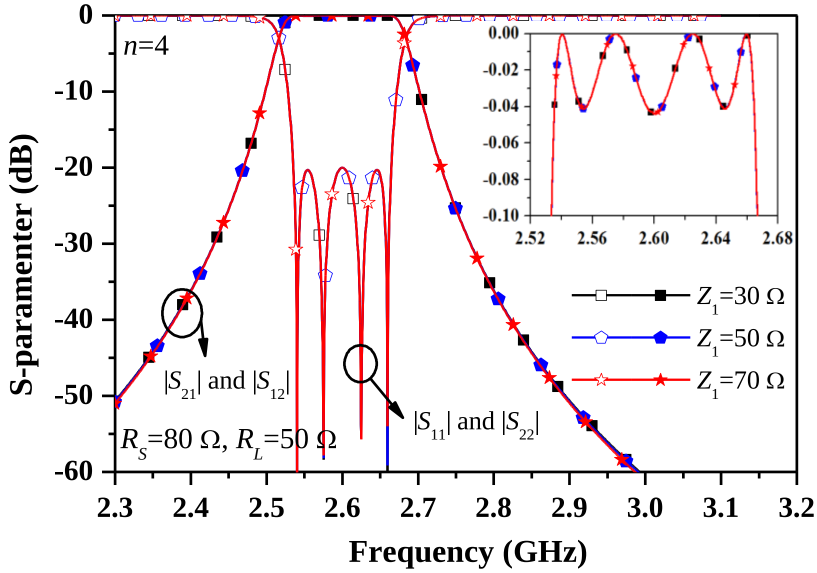

(b)

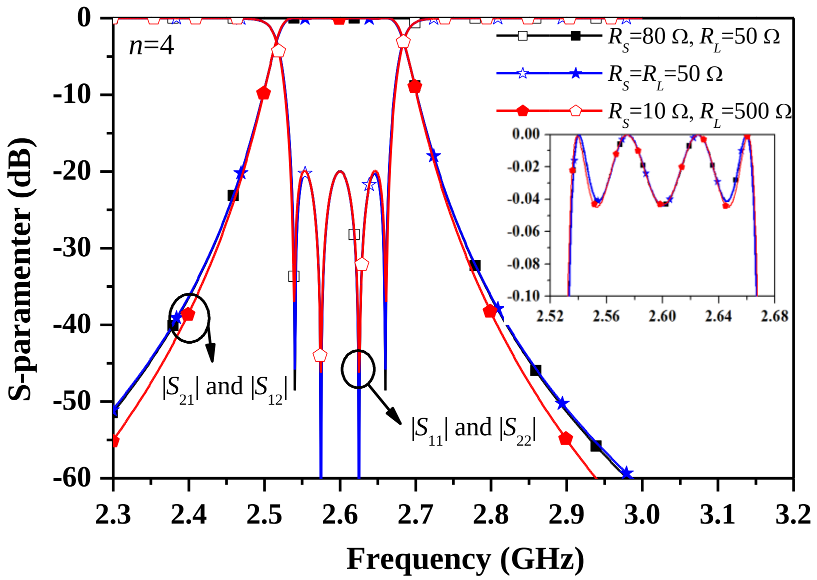

(c)

Fig. 5.9. S-parameters of Chebyshev coupled line BPF with different (a) n, (b) Z_1, and (c) r.

characteristics become steeper as n increases. The simulation is done using R_S = 20 Ω, R_L = 50 Ω, and n = 2, 3, 4. Fig. 5.9(b) shows the S-parameter characteristics and passband ripples with different image impedance of Z_1. The equal ripples and S-parameter characteristics are maintained although the termination and image impedances are different. Therefore, the changing image impedance of coupled line is not effected on the filter response. The simulation is done using R_S = 80 Ω, R_L = 50 Ω, n = 4, and Z_1 = 30, 50, 70 Ω. Fig. 5.9(c) shows S-parameter and passband ripples with different of r. Although r is very high, the passband characteristic is still maintained as can seem in Fig. 5.9(c). The *FBW* is exactly obtained 5%. However, the stopband attenuation is more increased when r is very high compare with the same n. The calculated values of the Chebyshev response are shown in Table 5.3.

TABLE 5.3 CALCULATED VALUES OF COUPLED LINE BANDPASS FILTER WITH CHEBYSHEV RESPONSE

f_c = 2.6 GHz, *FBW* = 5%, L_{Ar} = 0.0434 dB						n
Z_{0e}/Z_{0o} (Ω)	R_S = 20 Ω, R_L = 50 Ω, Z_1 = 50 Ω					
	62.33/41.86	56.89/44.61	73.05/38.73			2
	60.84/42.52	54.16/46.43	54.37/46.28	69.77/39.43		3
	60.34/42.75	53.66/46.81	52.89/47.4	53.83/46.68	68.71/39.7	4
	R_S = 80 Ω, RL = 50 Ω, n = 4					Z_1 (Ω)
	52.4/22.5	32.43/27.91	31.74/28.44	32.35/27.96	45.9/22.91	30
	75.75/38.28	53.92/46.61	52.89/47.4	53.83/46.67	68.71/39.7	50
	98.64/54.97	75.39/65.32	74.06/66.36	75.28/65.41	91.01/57.17	70
	R_S = 10 Ω, R_L = 500 Ω, Z_1 = 60 Ω					n
	67.04/54.31	64.09/56.4	63.48/56.88	65.77/55.16	186.41/62.19	4
	R_S = 50 Ω, R_L = 50 Ω, Z_1 = 60 Ω					
	79.91/48.37	64.56/56.04	63.48/56.88	64.56/56.04	79.91/48.37	
	R_S = 30 Ω, R_L = 90 Ω, Z_1 = 60 Ω					
	74.31/50.44	64.45/56.13	63.48/56.88	64.68/55.95	89.55/46.15	

Similarly, the circuit parameters of parallel coupled line BPF with Butterworth response is also obtained by using (5.23)-(5.25). The specification are chosen the same as Chebyshev response. Fig. 5.10 shows the *S*-parameters of BPF with Butterworth response. Similar to Chebyshev responses, the stopband attenuation characteristics become steeper as *n* increases as can seem in Fig. 5.10(a). Moreover,

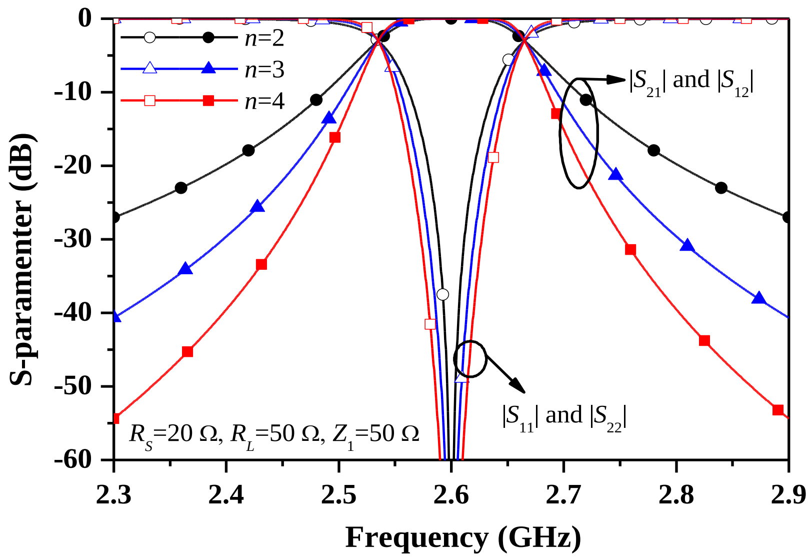

(a)

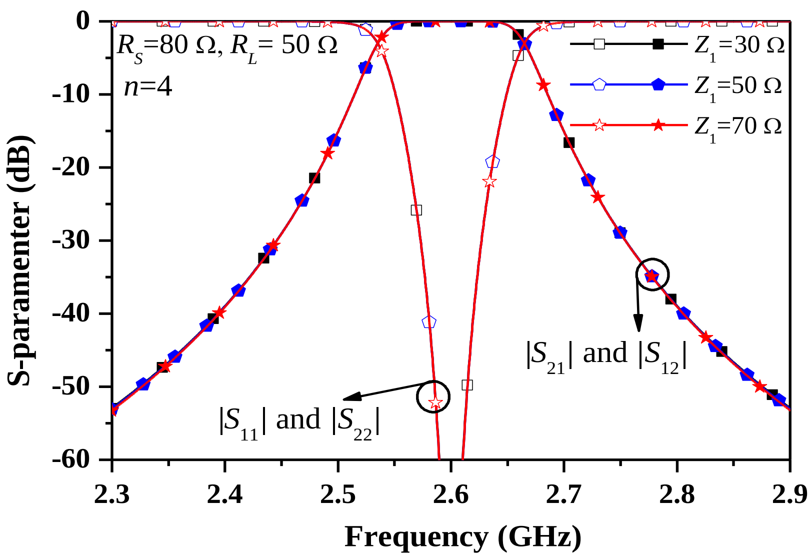

(b)

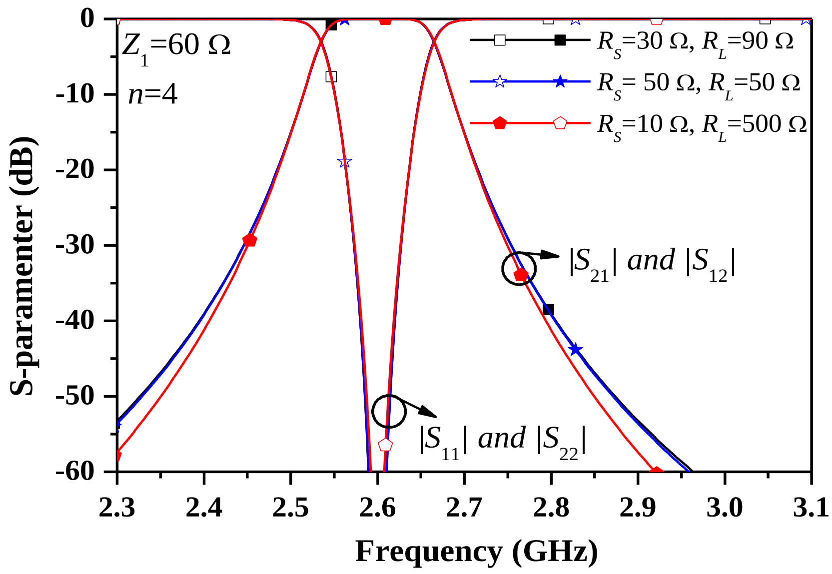

(c)

Fig. 5.10. *S*-parameters of Butterworth coupled line BPF with different (a) n, (b) Z_1, and (c) r.

the bandwidth of return loss is narrower as n decreases. Fig. 5.10(b) shown the *S*-parameter characteristics with different Z_1. Although, the image impedance of coupled line is changed, the filter response is not effected. Fig. 5.10(c) shows the *S*-parameter characteristics with different r. As can see, the filter response and *FBW* of 3 dB cutoff frequencies is maintained about 5% even though different r. Also the stopband attenuation is more increased when r is very high compared with the same n. The calculated variables values of the Butterworth response BPF are shown in Table 5.4.

TABLE 5.4 CALCULATED VALUES OF COUPLED LINE BANDPASS FILTER WITH BUTTERWORTH RESPONSE

f_c = 2.6 GHz, FBW = 5%						n
Z_{0e}/Z_{0o} (Ω)	R_S = 20 Ω, R_L = 50 Ω, Z_1 = 50 Ω					
	58.29/43.8	52.84/47.44	64.56/40.99			2
	59.97/42.93	52.81/47.47	52.93/47.38	67.94/39.91		3
	61.48/42.23	53.33/47.06	52.21/47.96	53.52/46.91	71.15/39.11	4
	R_S = 80 Ω, R_L = 50 Ω, n = 4					Z_1 (Ω)
	56.01/22.59	32.26/28.04	31.33/28.78	32.17/28.1	48.19/22.67	30
	79.43/37.85	53.62/46.84	52.21/47.96	53.52/46.91	71.15/39.11	50
	102.46/54.18	74.96/65.65	73.1/67.15	74.84/65.75	93.58/56.33	70
	R_S = 10 Ω, R_L = 500 Ω, Z_1 = 60 Ω					n
	67.67/53.91	63.68/56.72	62.66/57.56	65.66/55.24	221.62/75.74	4
	R_S = 50 Ω, R_L = 50 Ω, Z_1 = 60 Ω					
	82.42/47.65	64.18/56.33	62.66/57.56	64.18/56.33	82.42/47.65	
	R_S = 30 Ω, R_L = 90 Ω, Z_1 = 60 Ω					
	75.95/49.76	64.06/56.42	62.66/57.56	64.32/56.22	93.71/45.89	

The cases of low and high r are chosen from Table 5.3 and 5.4 to figure out the coupling coefficient variations of coupled lines according to image impedances. Fig. 5.11(a) shows the variation of coupling coefficients in case of n = 2, FBW = 5%, and L_{Ar} = 0.0434 dB with Chebyshev and Butterworth responses. C_1, C_2, and C_3 are the coupling coefficients of first, second, and third coupled lines, respectively. Z_1 are varied from 30 Ω to 150 Ω. The coupling coefficients between coupled lines are decreased as Z_1 increases. The coupling coefficients of Butterworth response are looser than those of Chebysheve response. Similarly, Fig.

5.11(b) shows the variation of coupling coefficients according to Z_1 in case of n = 4, FBW = 5%, L_{Ar} = 0.0434 dB, R_S = 10 Ω, and R_L = 500 Ω. In this case, the Chebyshev response has looser coupling characteristics when Z_1 is increased.

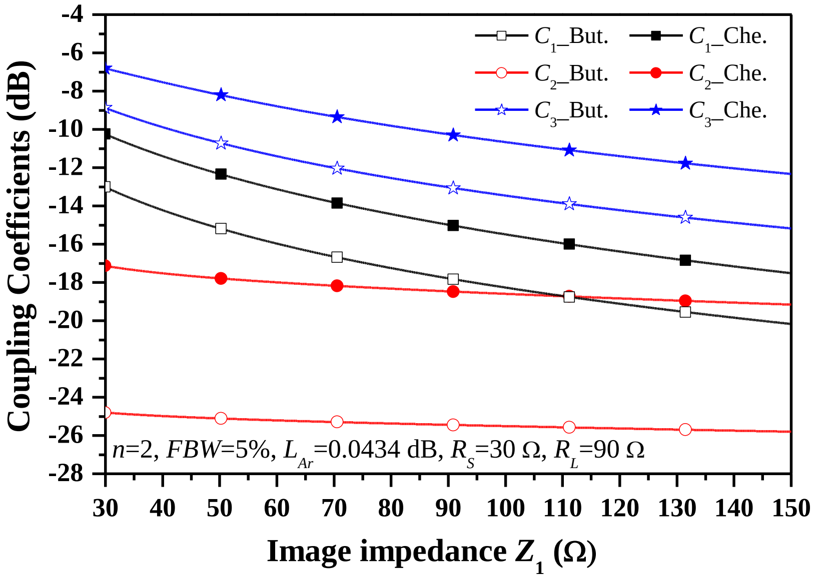

(a)

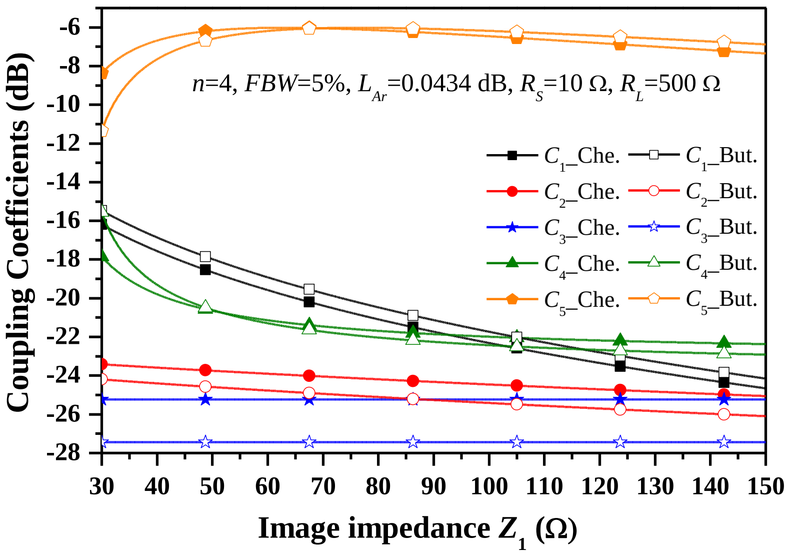

(b)

Fig. 5.11. Variation of coupling coefficients according to image impedance Z_1 for (a) n = 2 and (b) n = 4.

However, the coupling coefficient of last coupled line is increased when Z_1 are varied from 30 to 65 Ω and decreased when Z_1 are varied from 65 to 150 Ω. The coupling coefficients of intermediate coupled lines are constant when Z_1 vary from 30 to 150 Ω. As r is high, the coupling coefficients of the coupled line is tight. Therefore, the image impedance of coupled line can be used to control coupling coefficient of coupled line without effecting the passband response. Thus, the proposed design equations of the coupled line BPF can be used to design BPF with any arbitrary termination and image impedances. The higher Z_1 is preferable for looser coupling of coupled lines.

5.2 Filter Implementation

For the experimental validation, the arbitrary termination impedance BPFs were designed, simulated, and fabricated at an operating center frequency of f_0 = 2.6 GHz. The designed filters are specified as R_S = 20 Ω, 80 Ω, R_L = 50 Ω, FBW = 5%, and L_{Ar} = 0.0434 dB (S_{11} = -20 dB in the passband). The calculated elements values for Chebyshev and Butterworth are already shown in Table 5.3 and 5.4, respectively.

The proposed circuits were fabricated on a substrate RT/Duroid 5880 with a dielectric constant (ε_r) of 2.2 and thickness (h) of 31 mils. The electromagnetic (EM) simulation was performed using ANSYS HFSS.

5.2.1 Three stages Coupled Line BPF

The first BPF was designed with Chebyshev response with R_S = 20 Ω and R_L =

50 Ω. Fig. 5.12 shows the layout and photograph of fabricated filter 1. The physical dimensions of filter 1 are shown in Table 5.5 after final optimization. The simulated and measured *S*-parameters of the designed filter with narrow and broad band characteristics are shown in Fig. 5.13. The measured results are agreed well with those obtained from the simulations. The measured insertion and input/output return losses are better than 1.4 dB and 19 dB within the passband frequency range of 2.527 GHz to 2.667 GHz (*FBW* = 5.3 %), respectively.

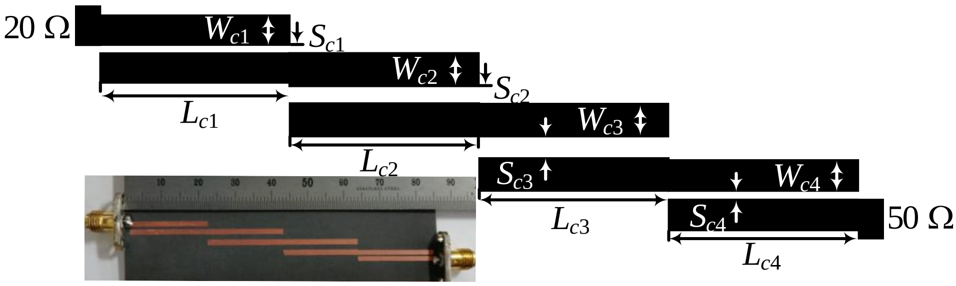

Fig. 5.12. Layout and photograph of fabricated bandpass filter 1.

TABLE 5.5 PHYSICAL DIMENSIONS OF FILTER 1. (UNIT: mm)

W_{c1}=1.55	W_{c2}=1.63	W_{c3}=1.6	W_{c4}=1.4
S_{c1}=0.65	S_{c2}=1.4	S_{c3}=1.38	S_{c4}=0.35
L_{c1}=21	L_{c2}=21	L_{c3}=20.75	L_{c4}=21.15

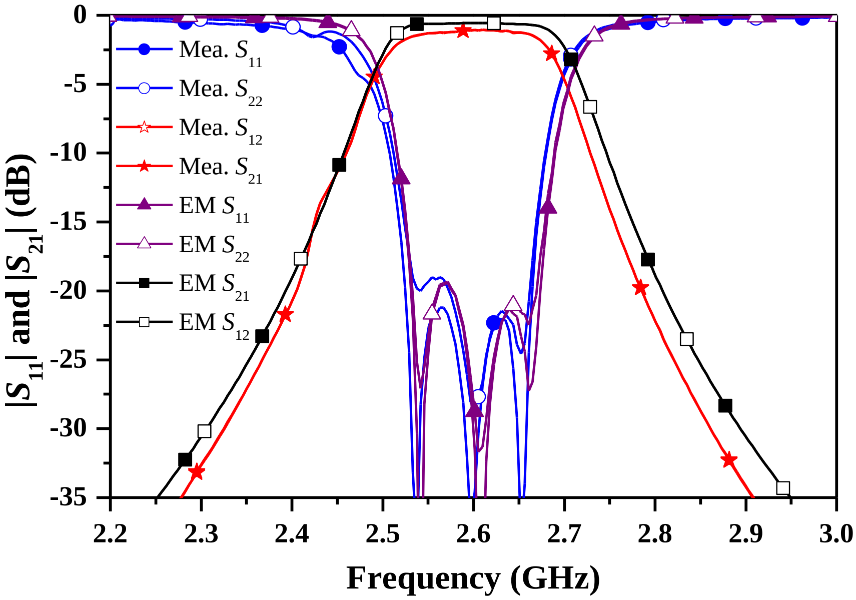

(a)

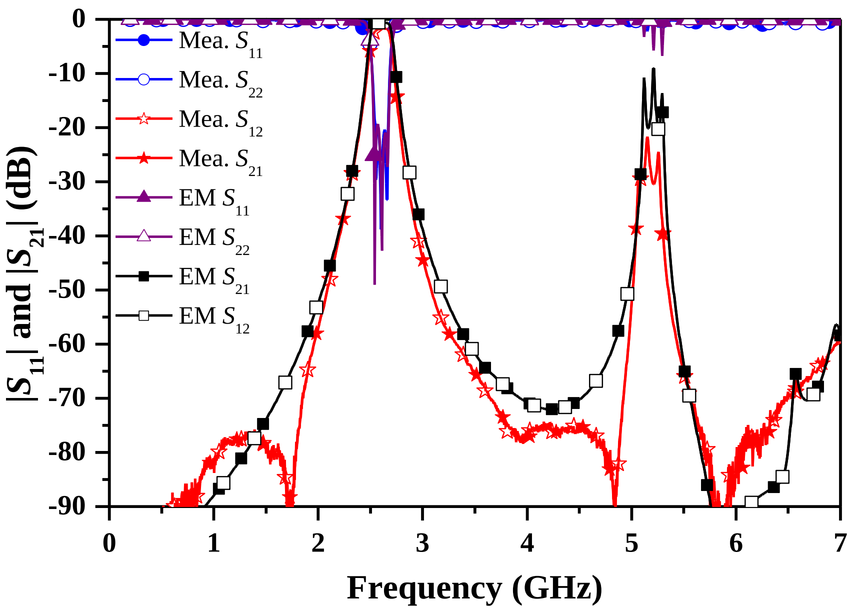

(b)

Fig. 5.13. Simulation and measurement results of arbitrary termination impedance bandpass filter 1 with (a) narrow and (b) broad bands.

5.2.2 Four stages Coupled Line BPF

The second filter was designed using Butterworth response with R_S = 80 Ω and R_L = 50 Ω. Fig. 5.14 shows the layout and photograph of fabricated filter. The final dimensions after EM simulation optimization are shown in Table 5.6. The simulated and measured *S*-parameters of the designed filter 2 with narrow and broadband characteristics are shown in Fig. 5.15. The measured results are well agreed with those obtained from the simulations. The measured results indicate that insertion and input/output return losses are better than 2 dB and 30 dB within the passband frequency 2.58 GHz to 2.63 GHz, respectively. The second filter provides a higher insertion loss than the first filter because of higher *n*. However, it provided steeper attenuation characteristics than the first filter. The limited return loss in passband may be due to limited *Q* of resonator or unequal even- and odd-mode phase velocities of the microstrip coupled stages [44].

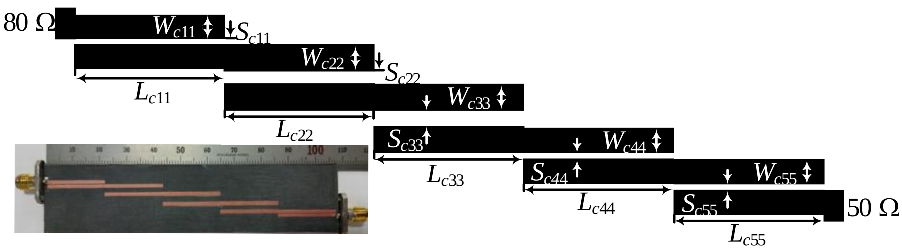

Fig. 5.14. Layout and photograph of fabricated bandpass filter 2.

TABLE 5.6 PHYSICAL DIMENSIONS OF FABRICATED BANDPASS FILTER 2. (unit : mm)

W_{c11}=1.02	W_{c22}=1.31	W_{c33}=1.3	W_{c44}=1.2	W_{c55}=1.13
S_{c11}=0.28	S_{c22}=1.7	S_{c33}=2.4	S_{c44}=1.8	S_{c55}=0.4
L_{c11}=21.1	L_{c22}=21	L_{c33}=21	L_{c44}=21.05	L_{c55}=21.2

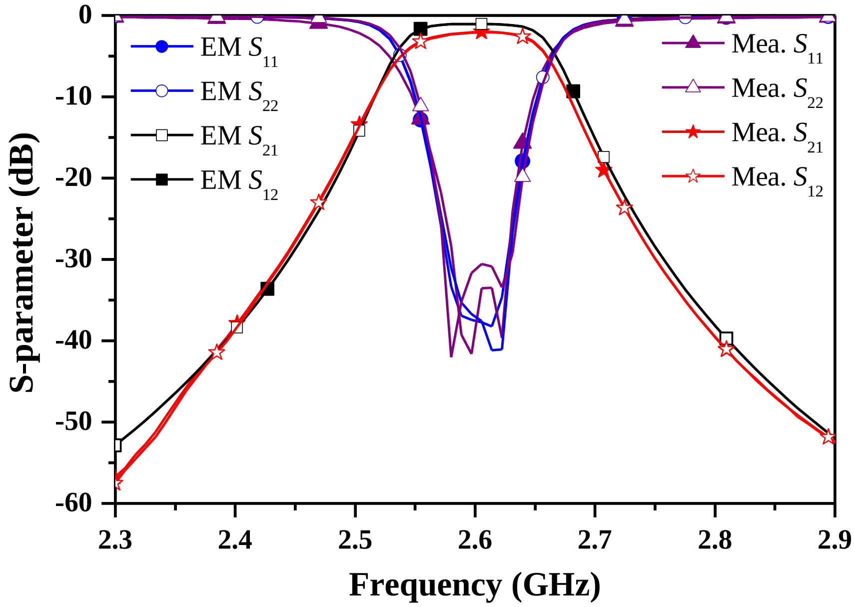

(a)

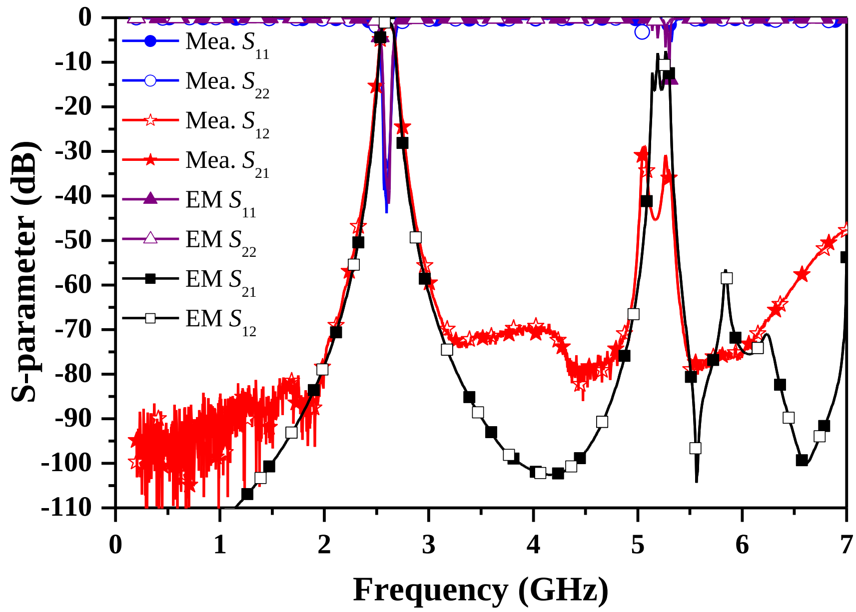

(b)

Fig. 5.15. Simulation and measurement results of arbitrary termination impedance bandpass filter 2 with (a) narrow and (b) broad bands.

The performance comparisons of the parallel coupled line BPFs and impedance transformers are summarized in Table 5.7. The structure of the proposed BPF is same with [15], however new design equations are derived for more general and accurate values. The new derived equations are more advantageous for higher order filters and higher termination impedance ratios. Also, the image impedance of coupled line might be chosen arbitrary for design convenience.

TABLE 5.7 PERFORMANCE COMPARISON WITH PREVIOUS WORKS RELATED TO PARALLEL COUPLED LINES BANDPASS FILTER

Ref.	f_0 (GHz)	Ter. Imp.	No. of stages	Coupling coef. (dB)	Design Equations	Impedance ratio	*FBW*
[2]	1.85	50	*i*	arbitrary	Analysis	NA	narrow
[9]	2	arbitrary	1	arbitrary	Analysis	low	narrow
[10]	2.6	arbitrary	1	arbitrary	Analysis	medium	narrow
[13]	2.6	arbitrary	2	arbitrary	Analysis	high	narrow
[15]	3	arbitrary	*i*	NA	Optimizing	low	wide
This work	**2.6**	**arbitrary**	***i***	**arbitrary**	**Analysis**	**high**	**narrow**

i=2 to n+1, Ter. Imp.: termination impedance of coupled lines

5.3 Summary and Discussion

The parallel coupled line bandpass filters with arbitrary termination and image impedances have been proposed and demonstrated in this paper. The design equations for the proposed filter have been derived based on the coupled line filter theory. In order to show the validity of the proposed design equations, two design examples of coupled line BPF with Chebyshev and Butterworth responses have been fabricated and measured. The simulation and measurement results are well agreed with the analysis. The new derived equations will be advantage in many applications such as power divider, matching network, and power amplifier design. Furthermore, the new design equations can provide more accurately and faster design.

CHAPTER 6

DISTRIBUTED UNEQUAL TERMINATION COUPLED LINE STEPPED IMPEDANCE RESONATOR BANDPASS FILTER

In this chapter, the general design equations of arbitrary termination impedance stepped impedance resonator (SIR) BPFs are analyzed and implement on a microstrip line. The new design equations are able to calculate with *n*-resonators, arbitrary termination impedance, arbitrary image impedance of coupled line, and controllable spurious frequencies. The coupling coefficients of coupled lines can be controlled by the image impedance (Z_2) of coupled line.

6.1 Theory and Design Equations

Basically, the conventional parallel coupled line bandpass filter (BPF) is composed of a half-wavelength resonators, where the coupling length is generally chosen as $\lambda/4$. However, the stepped impedance resonator (SIR) filter does not have the coupling length limited to $\lambda/4$. The total electrical length of the SIR is depended on ratio of characteristic impedance of stepped resonator. Fig. 6.1(a) shows the basic configuration of a parallel-coupled line BPF with SIR. Fig. 6.1(b) shows the schematic of proposed unequal termination impedance parallel coupled line SIR BPF. The proposed structure is composed by adding transmission line (TL) with characteristic impedance of Z_2 and electrical length of ($\pi/2$-θ_2) to the input and output ports. The electrical length of the coupled line and additional TL are used to cancel the imaginary part of input admittance of Y_{1S} and Y_{1L} as shown in

Fig. 6.2. Thus, the input admittance of Y_{1S} and Y_{1L} are always remained a real conductance. The proposed structure is able to design with equal or unequal termination impedance with arbitrary image admittance (Y_2). Fig. 6.2 (a) shows the equivalent circuit of Fig. 6.1(a). Since electrical length of θ_2 is less than λ/4 so the input admittance of Y_{1S} and Y_{1L} are always complex impedance in case G_S and $G_L \neq Y_2$. Therefore, the image admittance of coupled line (Y_2) must be chosen equal to the termination conductance in order to avoid mismatch. Fig. 6.2 (b) shows the equivalent circuit of proposed circuit of Fig. 6.1(b). Here, the total electrical length of TL at the input and output ports are always remained π/2 (λ/4). Therefore, the image admittance of the coupled line can be chosen equal or unequal to G_S and G_L.

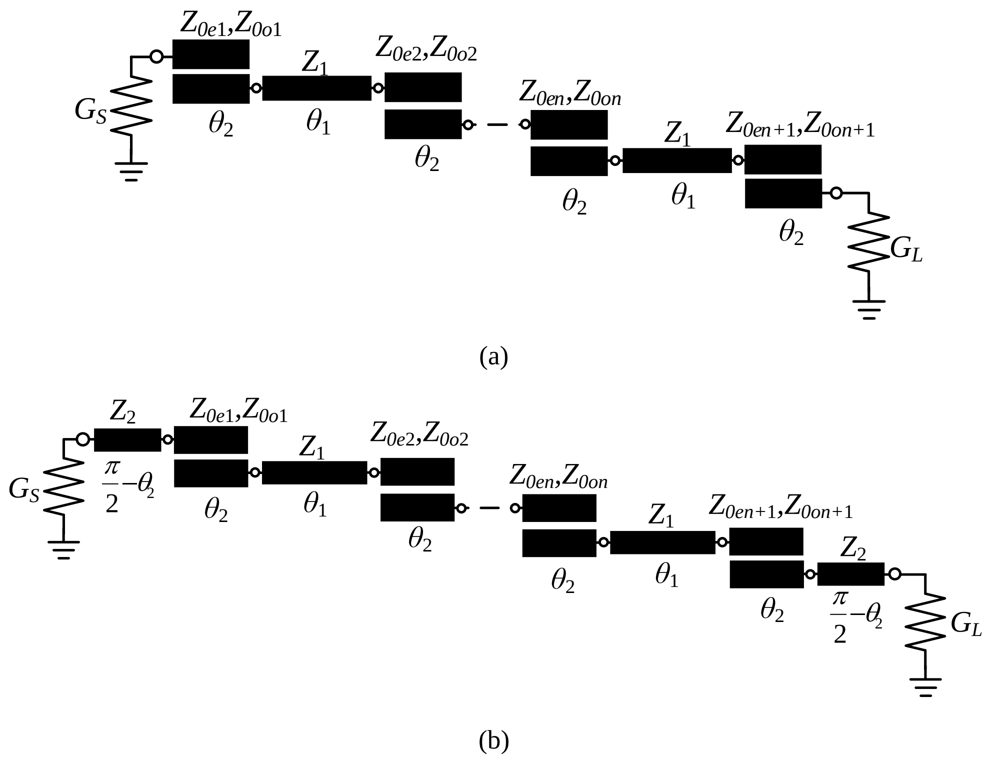

Fig. 6.1. Coupled line bandpass filter with stepped impedance resonators: (a) conventional and (b) proposed structure.

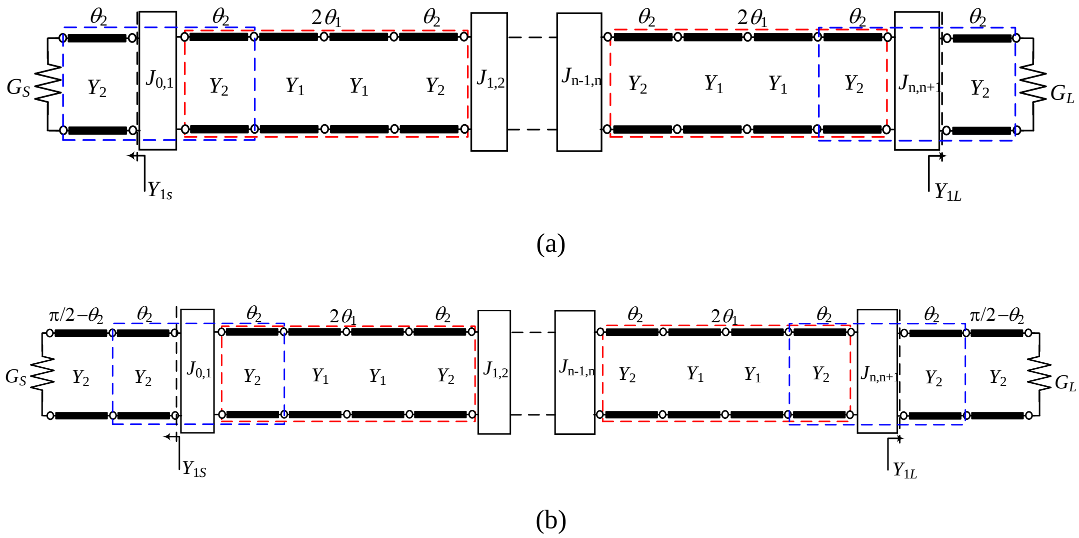

Fig. 6.2. Equivalent circuits of parallel coupled line stepped impedance resonators: (a) conventional circuit and (b) proposed circuit.

From the equivalent circuit of Fig. 6.2 (b), the simplicity of input admittance Y_{1S} looking into the source is obtained as (6.1).

$$Y_{1S} = Y_2 A_S \tag{6.1a}$$

where

$$A_S = \frac{Y_2}{G_S} \tag{6.1b}$$

Since $Y_2 = 1/Z_2$ is the image impedance of coupled line, the input admittance of Y_{1L} looking into the load is obtained as (6.2).

$$Y_{1L} = Y_2 A_L \tag{6.2a}$$

where

$$A_L = \frac{Y_2}{G_L} \tag{6.2b}$$

And G_S and G_L are the termination of source and load conductance, respectively.

Because of the input admittance Y_{1S} and $Y_{1\mathrm{L}}$ are pure real conductance so the general J-inverter equivalent circuit of Fig. 6.2 (b) can be expressed as shown in Fig. 6.3, where B_i (I = 1, 2, ⋯, n) are the susceptance of equivalent SIRs. As can seem in Fig. 6.3, the first and last J-inverter are effected with the image admittance Y_2 and conductance of G_S and G_L, respectively.

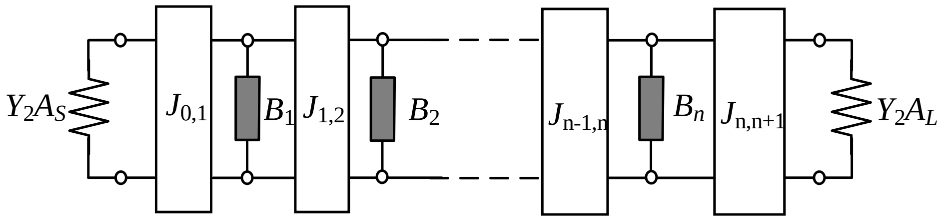

Fig. 6.3. Equivalent circuit Fig. 6.2 (b) of proposed SIR BPF.

6.1.1 Stepped Impedance Resonator

Now let consider the resonator structure of SIR. Fig. 6.4 shows a resonator structures of SIR. The SIR is symmetrical at (p-p') plan and has two different characteristic admittances of Y_1 ($1/Z_1$) and Y_2 ($1/Z_2$). The characteristics admittance of Y_1 and Y_2 can be chosen as $Y_1 < Y_2$ or vice versa. The admittance of the resonator from the open end [45], Y_{in4}, is given as

$$Y_{in1} = jY_2 \tan\theta_2$$

$$Y_{in2} = Y_1 \frac{Y_{in1} + jY_1 \tan 2\theta_1}{Y_1 + jY_{in1} \tan 2\theta_1} = jY_1 \frac{\tan\theta_2 + K \tan 2\theta_1}{K - \tan\theta_2 \tan 2\theta_1}$$

$$Y_{in4} = Y_2 \frac{Y_{in3} + jY_2 \tan\theta_2}{Y_2 + jY_{in3} \tan\theta_2} = jY_2 \frac{K \dfrac{\tan\theta_2 + K \tan 2\theta_1}{K - \tan\theta_2 \tan 2\theta_1} + \tan\theta_2}{1 - K \dfrac{\tan\theta_2 + K \tan 2\theta_1}{K - \tan\theta_2 \tan 2\theta_1} \tan\theta_2}$$

$$= jY_2 \frac{2K \tan\theta_2 + \left(K^2 - \tan^2\theta_2\right)\tan 2\theta_1}{K\left(1 - \tan^2\theta_2\right) - \left(K^2 + 1\right)\tan\theta_2 \tan 2\theta_1}, \ \tan 2\theta_1 = \frac{2\tan\theta_1}{1 - \tan^2\theta_1} \quad (6.3a)$$

$$= jY_2 \frac{2\left[K \tan\theta_2\left(1 - \tan^2\theta_1\right) + \left(K^2 - \tan^2\theta_2\right)\tan\theta_1\right]}{K\left(1 - \tan^2\theta_2\right)\left(1 - \tan^2\theta_1\right) - 2\left(1 + K^2\right)\tan\theta_1 \tan\theta_2}$$

$$= jY_2 \frac{2\left(K \tan\theta_1 + \tan\theta_2\right)\left(K - \tan\theta_2 \tan\theta_1\right)}{K\left(1 - \tan^2\theta_2\right)\left(1 - \tan^2\theta_1\right) - 2\left(1 + K^2\right)\tan\theta_1 \tan\theta_2}$$

where

$$K = \frac{Y_1}{Y_2} = \frac{Z_2}{Z_1}. \quad (6.3b)$$

Since K is the ratio of two characteristic admittance, the resonance condition can be obtained by giving Y_{in1} equal to zero. So, the resonance frequency can be found from (6.3) as

$$K - \tan\theta_1 \tan\theta_2 = 0 \quad (6.4)$$

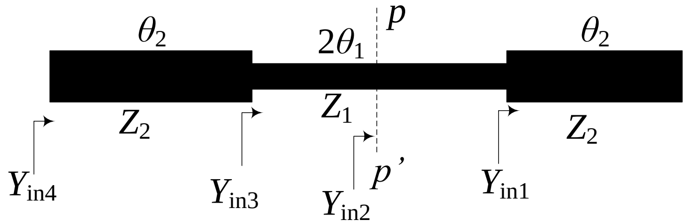

Fig. 6.4. Configuration of a stepped impedance resonator.

In case of $\theta_1 = \theta_2 = \theta_0$, resonant frequencies can be determined from (6.4) as mentioned in [45].

$$\theta(f_0) = \tan^{-1}\left(\sqrt{K}\right) \tag{6.5a}$$

$$\theta(f_1) = \frac{\pi}{2} \tag{6.5b}$$

$$\theta(f_2) = \pi - \tan^{-1}\sqrt{K} \tag{6.5c}$$

$$\theta(f_3) = \pi \tag{6.5d}$$

Thus, from (6.5) the ratio of the spurious resonant frequencies to the fundamental frequency can be determined as (6.6),

$$\frac{\theta(f_1)}{\theta(f_0)} = \frac{\pi}{2\tan^{-1}\sqrt{K}} \tag{6.6a}$$

$$\frac{\theta(f_2)}{\theta(f_0)} = \frac{\pi}{\tan^{-1}\sqrt{K}} - 1 \tag{6.6b}$$

$$\frac{\theta(f_3)}{\theta(f_0)} = \frac{\pi}{\tan^{-1}\sqrt{K}}\,. \tag{6.6c}$$

From (6.6), the relation of normalized spurious resonant frequencies can be determined by K and plotted in Fig. 6.5. The spurious resonant frequencies are changed according to impedance ratio of SIR as shown in Fig. 6.5. As can seem in Fig. 6.5, the higher-order of spurious resonant frequencies are moved far away from the fundamental frequency especially f_3 and f_4 as K decrease. Moreover, the spurious are moved close to the fundamental frequency as K increases. The harmonics frequencies are equally spaced each other only K = 1.

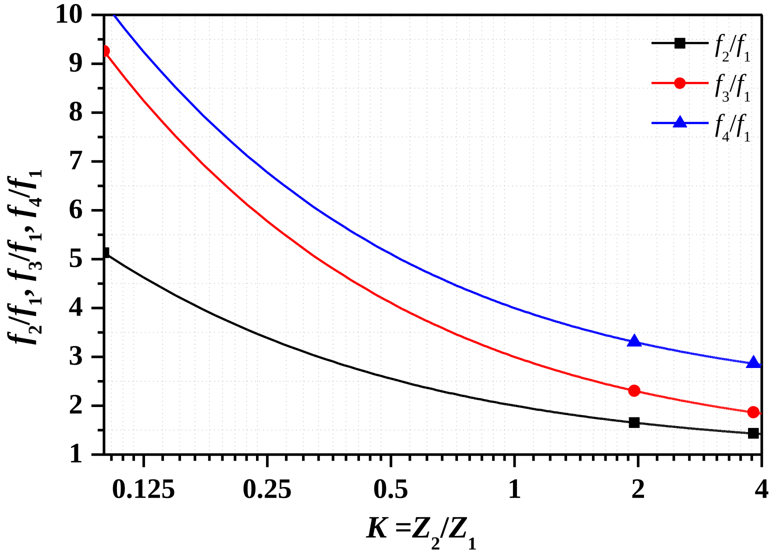

Fig. 6.5. Spurious resonant frequencies according to impedance ratio of SIR.

Fig. 6.6 shows the variation of characteristic impedances of Z_1 and Z_2, and total electrical length (θ_T) of SIR according to K. As seem in Fig. 6.6, the length of resonators are longer than half-wavelength with K > 1 and less than half-wavelength with K < 1. To get K < 1, the characteristic impedance of Z_1 is increased higher with the increase of Z_2. However, the Z_1 is decreased with K > 1. Suppose K = 0.5 and the characteristic impedance of Z_2 are varied from 20 to 70 Ω, the Z_1 are required 40 Ω to 140 Ω, respectively, as shown in Fig. 6.6. Thus, the tradeoff between Z_2 and K is required for the practical implementation. In the conventional of parallel-coupled line BPF with SIR, the characteristic impedance of Z_2 is chosen only equal to the termination impedance in order to get a matching.

However, Z_2 of the proposed network can be chosen arbitrary by adding length of $\pi/4$ - θ_2 to the input and output ports. The additional TL might be increased circuit size, however, it can be provided a convenient for connection the input and output ports.

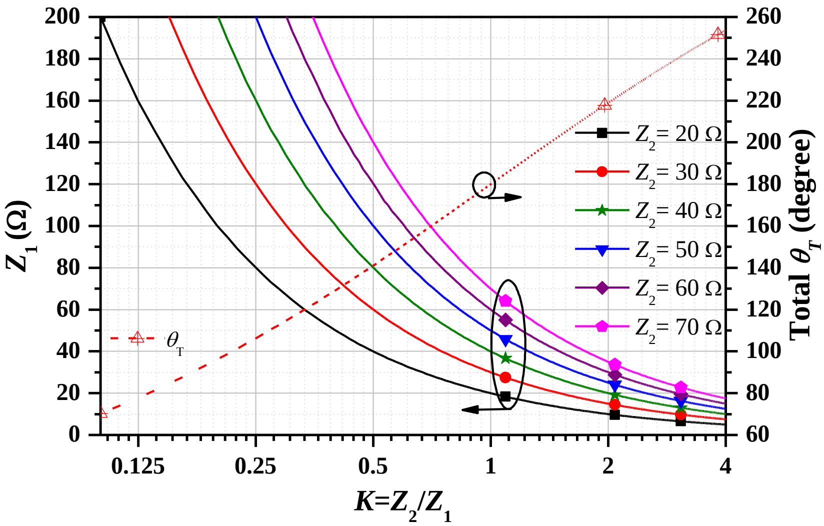

Fig. 6.6. Variation of Z_1 and total electrical length of SIR according to impedance ration of SIR and Z_2.

6.1.2 Slope Parameter and *J*-inverter of SIR

To design SIR BPFs, the slope parameter is usually used to characterize the resonance properties of resonators. From (6.5), the admittance slope parameter of SIR can be defined as

$$b = \frac{\omega_0}{2} \frac{dB}{d\omega}\bigg|_{\omega=\omega_0} = \frac{\theta_0}{2} \frac{dB}{d\theta}\bigg|_{\theta=\theta_0} . \tag{6.7}$$

From (6.3a), the slope parameter of SIR is found as (6.8) and the slope parameter of SIR is varied according to Y_2.

$$b = 2\theta_0 Y_2 \tag{6.8}$$

Therefore, the general *J*-inverter of arbitrary termination impedance and image admittance (Y_2) of parallel coupled line SIR BPF are derived as

$$J_{0,1} = Y_2 \sqrt{\frac{2A_S \theta_0 FBW}{g_0 g_1}} \tag{6.9a}$$

$$J_{i,i+1} = 2Y_2 \theta_0 FBW \sqrt{\frac{1}{g_i g_{i+1}}}, \quad i = 1, 2, \cdots, n \tag{6.9b}$$

$$J_{n,n+1} = Y_2 \sqrt{\frac{2A_L \theta_0 FBW}{g_n g_{n+1}}}\ . \tag{6.9c}$$

The derived design equations of multiple stage SIRs BPF with arbitrary termination impedance and image impedance can be directly adapted to design a practical filter. From the derived equations, it has been shown that the first and last *J*-inverter are much strongly effected on termination impedance and image impedance. Thus, the image impedance is very useful in the design of SIR BPFs with unequal termination impedances. As a result, the design specification can be extended.

The coupled line section can be transformed to the *J*-inverter with TL at both ends [32], as shown in Fig. 6.7. The equivalent relations between a coupled line circuit and the *J*-inverter circuit with TL are used to derive the even- and odd-mode characteristic impedances of coupled line. The relative formulas between coupled line and the J-inverter in Fig. 6.7 can be derived from the $ABCD$ matrix. For more general, the even- and odd-mode impedances can be written as (6.10) with a various of electrical length.

$$\left(Z_{0e}\right)_{i+1}\Big|_{i=0\text{ to }n} = Z_2 \frac{1+J_{i,i+1}Z_2\csc\theta + J_{i,i+1}^2 Z_2^2}{1-J_{i,i+1}^2 Z_2^2\cot^2\theta} \tag{6.10a}$$

$$\left(Z_{0o}\right)_{i+1}\Big|_{i=0\text{ to }n} = Z_2 \frac{1-J_{i,i+1}Z_2\csc\theta + J_{i,i+1}^2 Z_2^2}{1-J_{i,i+1}^2 Z_2^2\cot^2\theta}\,. \tag{6.10b}$$

From (6.10), the coupling coefficients (C) of coupled lines are determined as

$$C_{i+1}\Big|_{i=0\text{ to }n} = \frac{\left(Z_{0e}\right)_{i+1} - \left(Z_{0o}\right)_{i+1}}{\left(Z_{0e}\right)_{i+1} + \left(Z_{0o}\right)_{i+1}}\,. \tag{6.11}$$

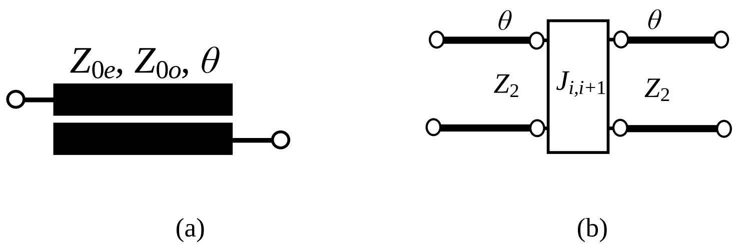

Fig. 6.7. (a) parallel coupled-line with two open terminations and (b) equivalent circuit has a J-inverter with two transmission line sections.

In order to demonstrate the analysis, SIR parallel coupled line BPF with arbitrary termination and image impedances were designed and simulated. The design formulas of (6.9) and (6.10) for an n-resonator are used to calculated the even- and odd-mode characteristic impedances of coupled line (see appendix E). The element values g_1, g_2, ···, g_n of the prototype low-pass filter (see appendix C), which may be calculated for either Butterworth or Chebyshev responses [35]. The design examples are done with n = 2, 3, and 4 and FBW = 5% for Butterworth and Chebyshev responses (ripple = 0.0434 dB). The passband bandwidths of Chebyshev and Butterworth responses are determined from the passband edge frequencies and 3-dB cutoff frequencies [35], respectively.

Fig. 6.8 (a) shows the variation of coupling coefficients and Z_1 in case of n = 4, FBW = 5%, R_S = 20 Ω, R_L = 50 Ω, and K = 0.7 with Chebyshev and Butterworth responses. C_i (i = 1, 2, ⋯, n) are the coupling coefficients of the coupled lines.

As can seem in Fig. 6.8(a), the first and last coupled line are required stronger coupling than the intermediate coupled line. As Z_2 increase from 5 to 100 Ω, the coupling of first and last coupled lines are become looser, however, the Z_1 is increased from 7.14 to 142.85 Ω. Also, the intermediate coupled line are constant with Z_2 increasing. Moreover, the couplings of coupled line of the Butterworth response are looser than the Chebyshev response. Fig. 6.8(b) shows the variation of coupling coefficients and Z_1 in case of n = 4, FBW = 5%, R_S = 15 Ω, R_L = 90 Ω, and K = 1.5. In this case, the coupling coefficient of the first and last coupled lines are looser than Fig. 6.8(a). As Z_2 increase from 5 to 150, the Z_1 is increased from 3.33 to 100 Ω, while the intermediate coupling of coupled lines are constant.

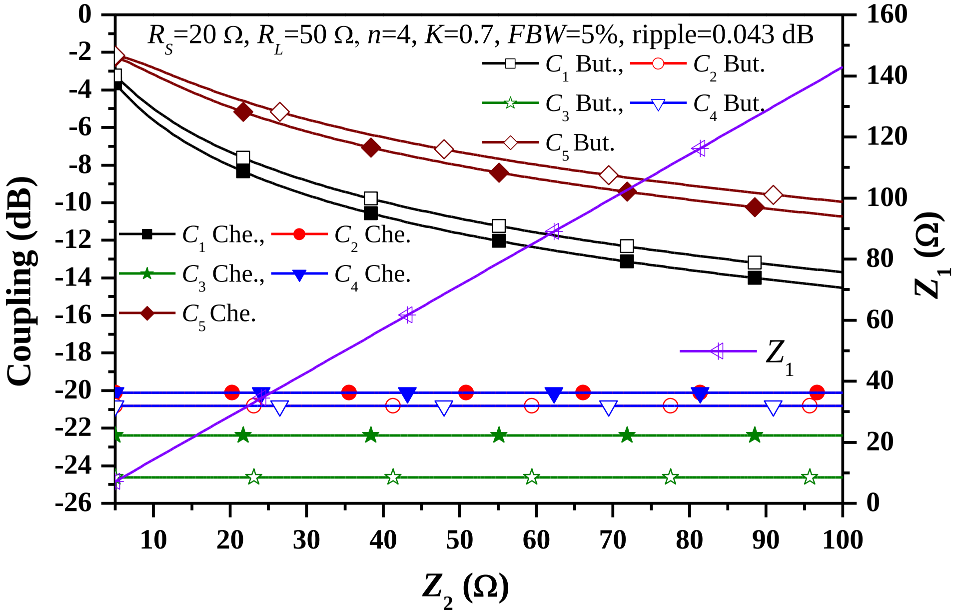

(a)

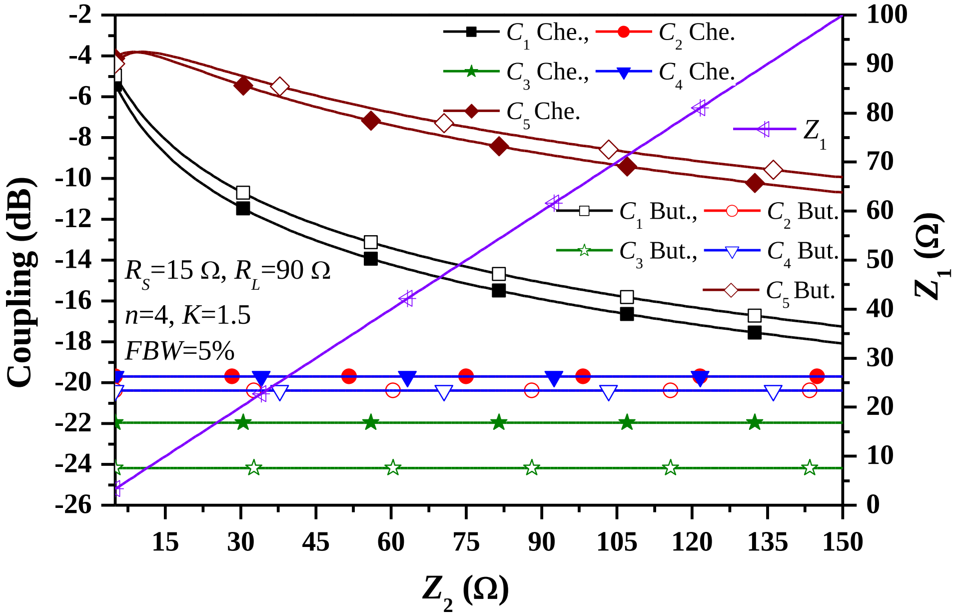

(b)

Fig. 6.8. Variation of coupling coefficients according to image impedance Z_2 for Chebyshev and Butterworth responses with (a) R_S=20, R_L=50, K=0.7 and (b) R_S=15, R_L=90, K=1.5.

Fig. 6.9(a) shows *S*-parameter characteristics of parallel coupled line SIR BPF for Chebyshev response with different of *n*. As seem in the figure, the stopband attenuation characteristics become steeper as *n* increases. Also, the second

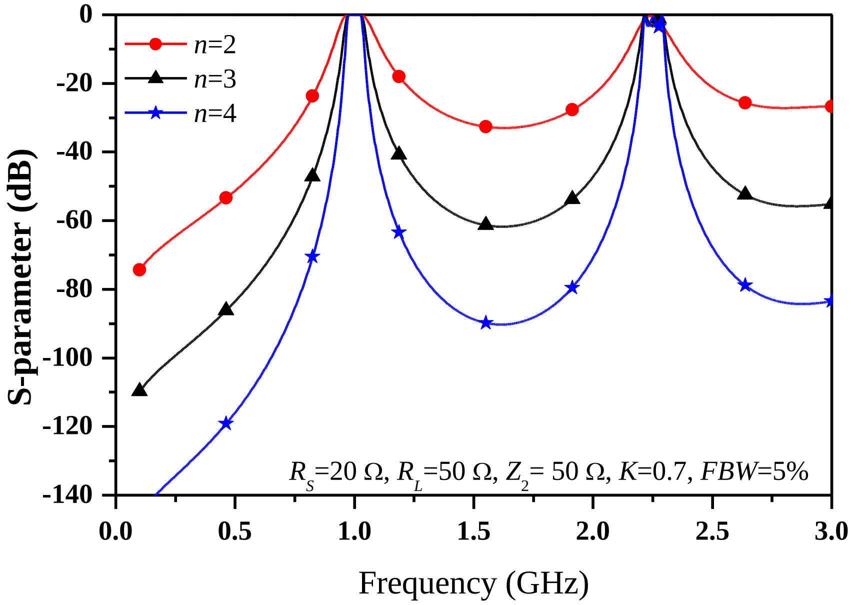

(a)

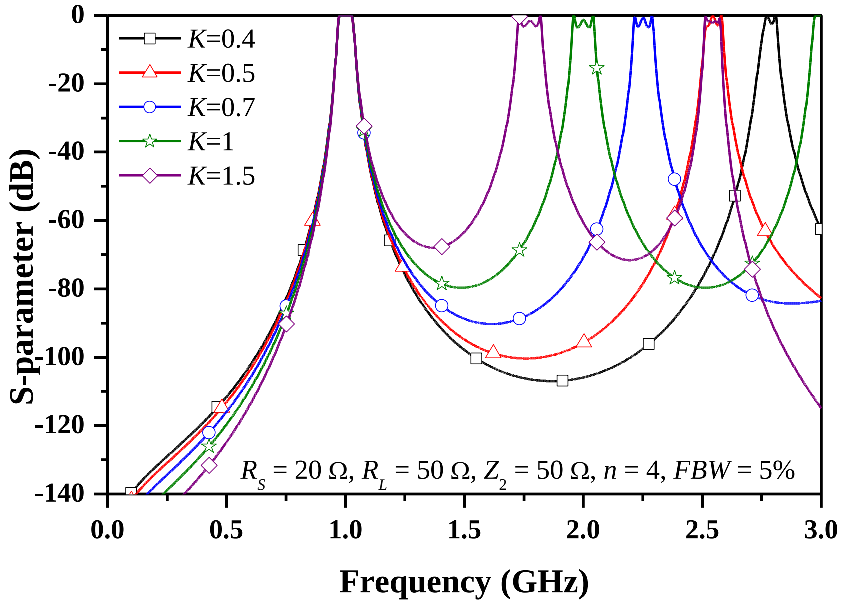

(b)

Fig. 6.9. *S*-parameter characteristics of Chebyshev response with different (a) *n* and (b) *K*.

harmonics frequency is located at 2.25 f_0 with chosen K of 0.7. The simulation is done using R_S = 20 Ω, R_L = 50 Ω, Z_2 = 50 Ω, and n varied from 2 to 4. Fig. 6.9(b) shows the S-parameter characteristics with a different of K. Base on the above analysis, the spurious frequencies are moved far away from passband of 1.77 f_0 to 2.8 f_0 with K decrease from 1.5 to 0.4. The bandwidth of the passband is still maintained the same although spurious frequencies resonant bandwidth are narrow. The simulation is done using R_S = 20 Ω, R_L =50 Ω, n = 4, Z_2 = 50 Ω, and K varies from 0.4 to 1.5. The calculated all variable values of the simulation in Fig. 6.9 are shown in Table 6.1.

TABLE 6.1 CALCULATED VALUES OF CHEBYSHEV RESPONSE COUPLED LINE SIR BPF WITH DIFFERENT OF n AND K

f_0 = 1 GHz, FBW = 5%, R_S = 20 Ω, R_L = 50 Ω, L_{Ar} = 0.0434 dB						n	
Z_{0e}/Z_{0o} (Ω)	Z_2 = 50 Ω, K = 0.7						
	72.34/38.45	60.83/42.47	94.52/35.31			2	
	68.93/39.39	56.26/44.99	56.26/44.99	86.42/36.02		3	
	67.85/39.72	55.46/45.52	54.1/46.48	55.46/45.52	83.98/36.31	4	
	n = 4					K	θ (°)
	69.98/39.02	55.29/45.63	53.98/46.57	55.29/45.63	89.54/35.37	0.4	32.3
	69.03/39.33	55.36/45.59	54.02/46.53	55.36/45.59	87.01/35.77	0.5	35.3
	67.85/39.72	55.46/45.52	54.1/46.47	55.46/45.52	83.98/36.31	0.7	39.9
	66.91/40.06	55.59/45.43	54.2/46.4	55.59/45.43	81.59/36.79	1	45
	66.15/40.34	55.77/45.31	54.33/46.31	55.77/45.31	79.68/37.21	1.5	50.8

Fig. 6.10(a) shows the S-parameter characteristics of SIR parallel coupled line BPF with different of Z_2 by fixing K = 0.7 and n = 4. In this case, the passband characteristic is constant with different Z_2. However, the stopband characteristics of

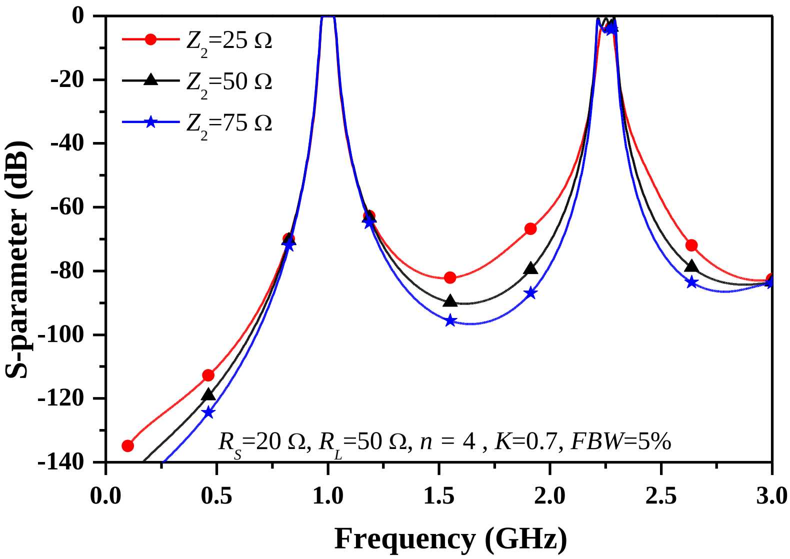

(a)

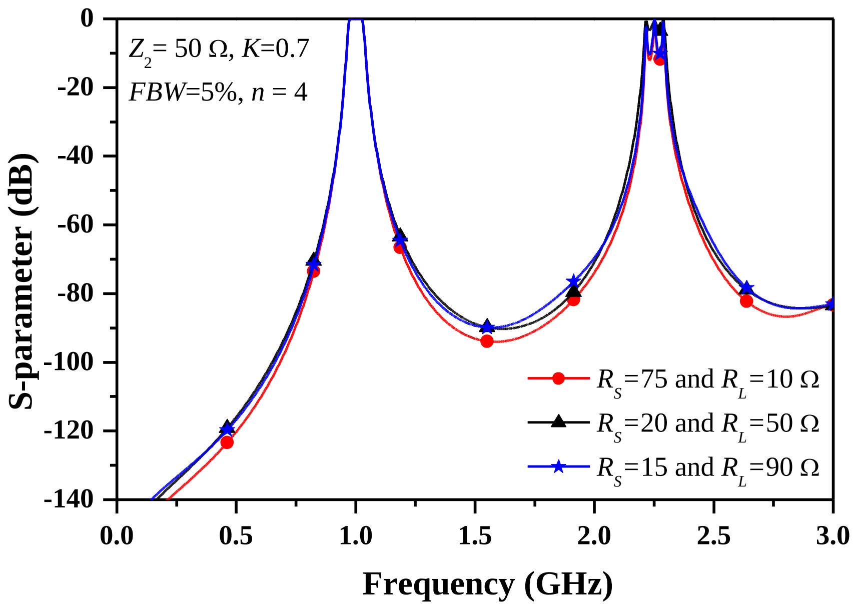

(b)

Fig. 6.10. *S*-parameter characteristics of Chebyshev response with different (a) Z_2 and (b) termination impedances.

the low and higher bands are improved with a high Z_2. Thus, higher Z_2 is preferable for high stopped band attenuation, but it can cause the realization difficulty of high Z_1. The simulation is done using R_S = 20 Ω, R_L = 50 Ω, n = 4, K = 0.7, and Z_2

varies from 25 to 75 Ω. Similarly, Fig. 6.10 (b) shows the *S*-parameter characteristics with different termination impedance. The termination impedances are chosen randomly. As can seem in Fig. 6.10(b), the stopped band characteristics are different according to termination impedance. As the ratio of termination impedances is higher, the stopband characteristic is slightly more attenuated. However, the characteristics near to the passband are similar. Thus, the changing termination impedance is not effected to the operating band characteristics. The simulation is done using Z_2 = 50 Ω, n = 4, K = 0.7, and randomly termination impedances. The calculated values of the Chebyshev response in Fig. 6.10 are shown in Table 6.2.

TABLE 6.2 CALCULATED VALUES OF CHEBYSHEV RESPONSE COUPLED LINE SIR BPF WITH DIFFERENT OF Z_2 AND TERMINATION IMPEDANCE

f_0 = 1 GHz, FBW = 5%, n = 4, K = 0.7 L_{Ar} = 0.0434 dB						Z_2
Z_{0e}/Z_{0o} (Ω)	R_S = 20 Ω, R_L = 50 Ω					
	39.37/18.55	27.73/22.76	27.05/23.24	27.73/22.79	55.66/17.38	25
	67.85/39.72	55.46/45.52	54.1/46.48	55.46/45.52	83.98/36.31	50
	95.7/61.76	83.19/68.28	81.15/69.71	83.19/68.28	112.83/56.69	75
	Z_2 = 50					R_S/R_L (Ω)
	97.23/35.15	55.46/45.52	54.1/46.48	55.46/45.52	61.58/42.12	75/10
	67.85/39.72	55.46/45.52	54.1/46.48	55.46/45.52	83.98/36.31	20/50
	64.85/40.76	55.46/45.52	54.1/46.47	55.46/45.52	105.54/34.84	15/90

The following cases are considered the Butterworth response. Similar to the Chebyshev response, *S*-parameter of SIR parallel coupled line BPF with Butterworth responses are shown in Fig. 6.11(a) with different n. The stopband attenuation is steeper as n increase. However, the bandwidth of passband is narrower than Chebyshev response as seen in Fig. 6.11(a). The simulation is done using R_S = 20 Ω, R_L = 50 Ω, K = 0.7, Z_2 = 50 Ω, and n varies from 2 to 4. Also, Fig. 6.11(b) shows the moving of spurious frequency from the passband with K increase. The calculated values of the Butterworth response in Fig. 6.11 are tabulated in Table 6.3.

TABLE 6.3 CALCULATED VALUES OF BUTTERWORTH RESPONSE COUPLED LINE SIR BPF WITH DIFFERENT n AND K

<table>
<tr><td colspan="6">f_0 = 1 GHz, FBW = 5%, R_S = 20 Ω, R_L = 50 Ω</td><td colspan="2" rowspan="2">n</td></tr>
<tr><td rowspan="10">Z_{0e}/Z_{0o} (Ω)</td><td colspan="5">Z_2 = 50 Ω, K = 0.7</td></tr>
<tr><td>63.72/41.21</td><td>54.15/46.44</td><td>75.04/37.83</td><td></td><td></td><td colspan="2">2</td></tr>
<tr><td>67.07/39.98</td><td>54.15/46.44</td><td>54.15/46.44</td><td>82.23/36.55</td><td></td><td colspan="2">3</td></tr>
<tr><td>70.35/38.98</td><td>55.01/45.83</td><td>53.12/47.23</td><td>55.01/45.83</td><td>89.73/35.68</td><td colspan="2">4</td></tr>
<tr><td colspan="5">n = 4</td><td>K</td><td>θ (°)</td></tr>
<tr><td>72.9/38.23</td><td>54.86/45.93</td><td>53.02/47.3</td><td>54.86/45.93</td><td>96.93/34.68</td><td>0.4</td><td>32.3</td></tr>
<tr><td>71.76/38.56</td><td>54.91/45.89</td><td>53.06/47.27</td><td>54.91/45.89</td><td>93.64/35.11</td><td>0.5</td><td>35.3</td></tr>
<tr><td>70.35/38.98</td><td>55.01/45.83</td><td>53.12/47.23</td><td>55.01/45.83</td><td>89.73/35.68</td><td>0.7</td><td>39.9</td></tr>
<tr><td>69.22/39.34</td><td>55.13/45.75</td><td>53.19/47.17</td><td>55.13/45.75</td><td>86.68/36.19</td><td>1</td><td>45</td></tr>
<tr><td>68.31/39.65</td><td>55.29/45.64</td><td>53.29/47.09</td><td>55.29/45.64</td><td>84.25/36.65</td><td>1.5</td><td>50.8</td></tr>
</table>

Similarly, Fig. 6.12 (a) shows the S-parameter characteristics of SIR coupled line BPF with different Z_2. Also, the stopped band attenuation is more attenuated with the higher Z_2. Fig. 6.12(b) shows the S-parameter characteristics with different termination impedances. As the ratio of termination is higher, the stopband characteristic is slightly more attenuated. The calculated values of the Butterworth response with different of Z_2 and termination impedance are shown in Table 6.4.

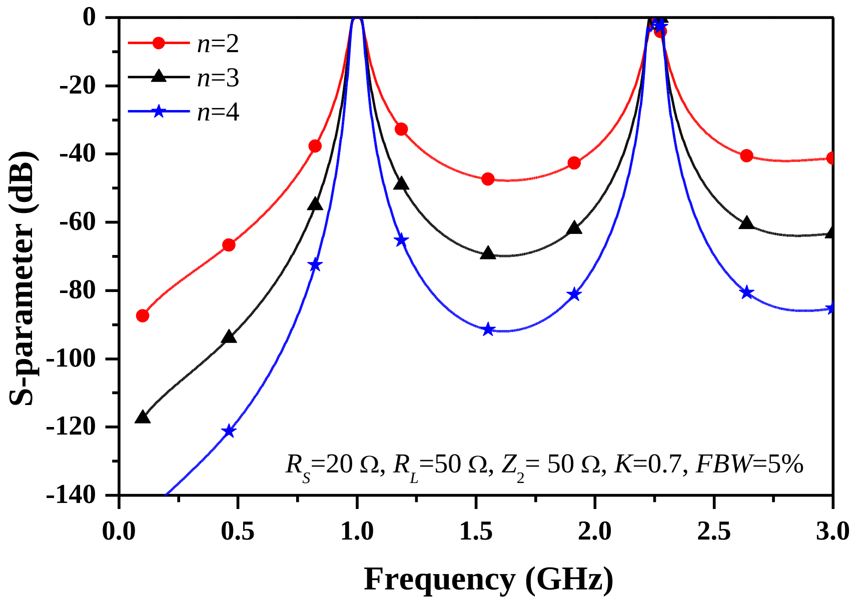

(a)

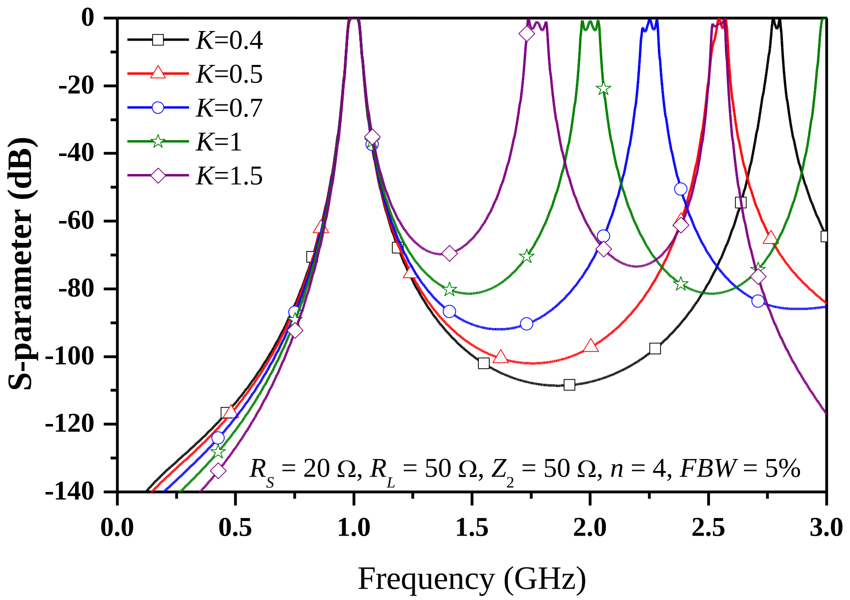

(b)

Fig. 6.11. *S*-parameters characteristic of Butterworth response with different (a) *n* and (b) *K*.

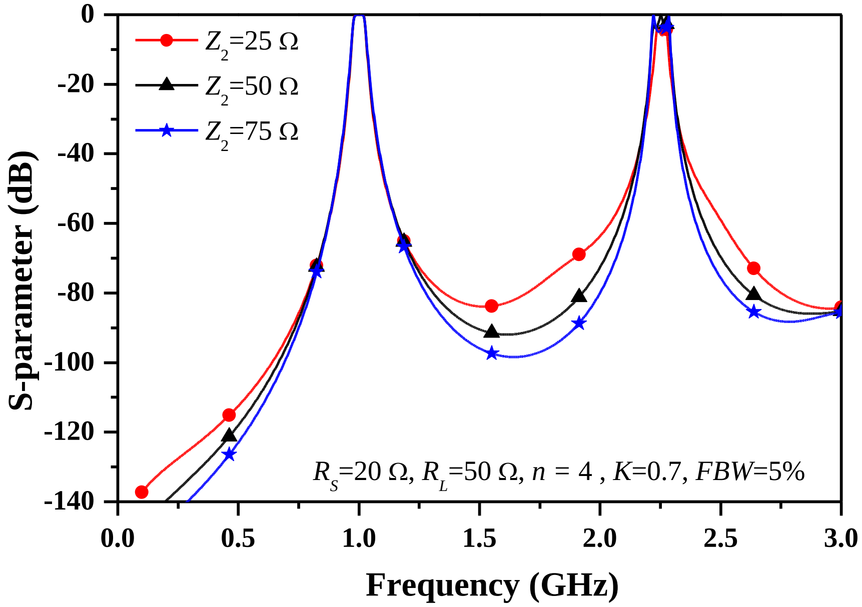

(a)

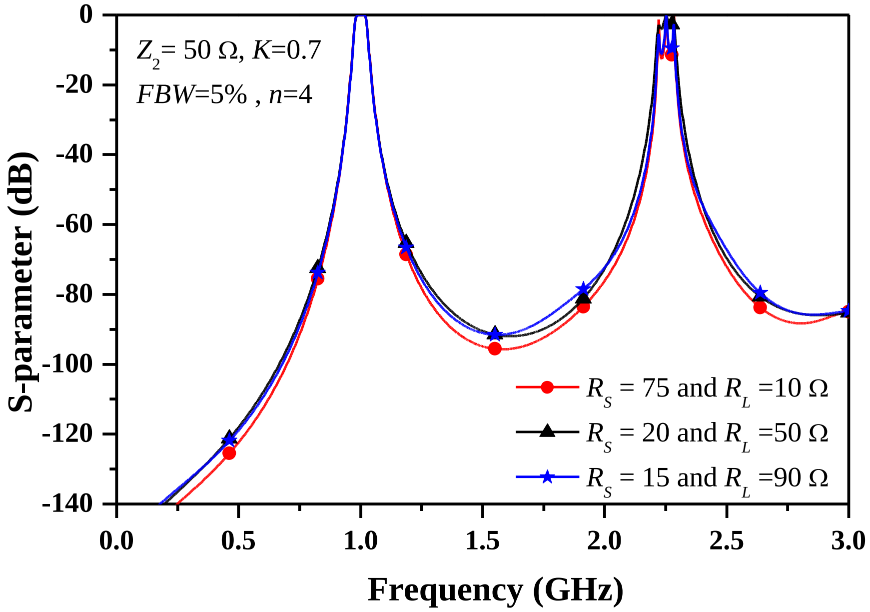

(b)

Fig. 6.12. *S*-parameters characteristics of Butterworth response with different of (a) Z_2 and (b) termination impedances.

TABLE 6.4 CALCULATED VALUES OF BUTTERWORTH RESPONSE COUPLED LINE SIR BPF WITH DIFFERENT Z_2 AND TERMINATION IMPEDANCE

f_0 = 1 GHz, FBW = 5%, n = 4, K = 0.7						Z_2
Z_{0e}/Z_{0o} (Ω)	R_S =20 Ω, R_L = 50 Ω					
	41.67/18.2	27.5/22.96	26.56/23.61	27.5/22.91	62.4/17.47	25
	70.35/38.98	55.01/45.83	53.12/47.23	55.01/45.83	89.73/35.68	50
	98.44/60.72	82.51/68.75	79.67/70.84	82.51/68.74	118.63/55.58	75
	Z_2 = 50					R_S/R_L (Ω)
	106.37/34.83	55.01/45.83	53.12/47.23	55.01/45.83	63.06/41.47	75/10
	70.35/38.98	55.01/45.83	53.12/47.23	55.01/45.83	89.73/35.68	20/50
	66.85/40.05	55.01/45.83	53.12/47.23	55.01/45.83	117.16/34.79	15/90

6.2 Simulation and Measurement

Based on the above analysis, a microstrip line SIR parallel-coupled line BPFs with arbitrary termination impedances are designed and implemented on substrate of RT/Duriod 5880 with a dielectric constant (ε_r) of 2.2 and thickness (h) of 31 mil. In order to design a proposed BPF, three filters are designed at the operating frequency of 2.6 GHz with termination impedances (R_S, R_L), Z_2, K, n, and FBW. Then, the design variables can be calculated using (6.9)-(6.11) (see appendix E). From (6.9)-(6.11), the elements values are calculated and tabulated in Table 6.5. The electromagnetic (EM) simulation was performed using Ansys HFSS.

TABLE 6.5 CALCULATED VALUES OF PROPOSED BPF WITH DIFFERENT OF n AND TERMINATION IMPEDANCE

f_0 = 2.6 GHz, FBW = 5%						
Z_{0e}/Z_{0o} (Ω)	R_S = 20 Ω, R_L = 50 Ω, Z_2 = 60 , K = 0.5, n = 2, L_{Ar} = 0.0434 dB				θ	1st filter
	85.33/46.48	72.75/51.08	110.43/42.3		35.26	
	R_S = 50 Ω, R_L = 100 Ω, Z_2 = 90 , K = 1.5, n = 3, L_{Ar} = 0.0434 dB				θ	2nd filter
	128.64/69.78	101.78/80.67	101.78/80.67	152.83/65.73	48.75	
	R_S = 90 Ω, R_L = 50 Ω, Z_2 = 70 , K = 0.5, n = 3				θ	3rd filter
	130.26/49.22	75.69/65.1	75.69/65.1	107.99/52.25	35.26	

6.2.1 Two stages Chebyshev response

The first BPF was designed with Chebyshev response with ripple = 0.043 dB, R_S = 20 Ω, R_L = 50 Ω, Z_2 = 60 Ω, K = 0.5, n = 2, and FBW = 5%. Fig. 6.13 shows the layout and photograph of fabricated filter. According to the above substrate, the final dimensions after EM simulation optimization are shown in Table 6.6. The total circuit size of proposed BPF is 34 mm × 23 mm.

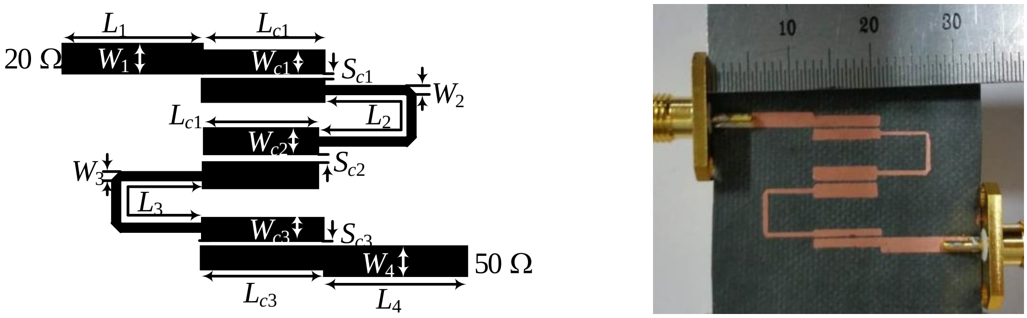

(a) (b)

Fig. 6.13. Two stage SIR BPF: (a) layout and (b) photograph of fabricated circuit.

TABLE 6.6 PHYSICAL DIMENSIONS OF FABRICATED TWO STAGES SIR BPF WITH CHEBYSHEV RESPONSE. (unit: mm)

W_1=W_4=1.8	W_{c1}=1.36	W_2=W_3=0.4	L_{c2}=8.05	L_{c3}=8.6
L_1=L_4=12.8	S_{c1}=0.23	W_{c2}=1.65	W_{c3}=1	
L_{c1}=8.49	L_2=L_3=17.1	S_{c2}=0.5	S_{c3}=0.102	

The EM simulated and measured *S*-parameters are compared in Fig. 6.14. The measured results are agreed well with the simulations. The first spurious resonance occurs at the 2.5 time above the center frequency. The measured insertion loss is 0.63 dB at the lower band edge of 2.54 GHz, 0.55 dB at center frequency of 2.6 GHz, and 0.65 dB at the upper band edge of 2.66 GHz. Also, the input and output return loss within the whole passband (*FBW* = 4.6%) are better than 20 dB. Moreover, the lower and upper stopband rejections of 20 dB is obtained from DC to 2.35 GHz and 3.1 to 5.74 GHz, respectively.

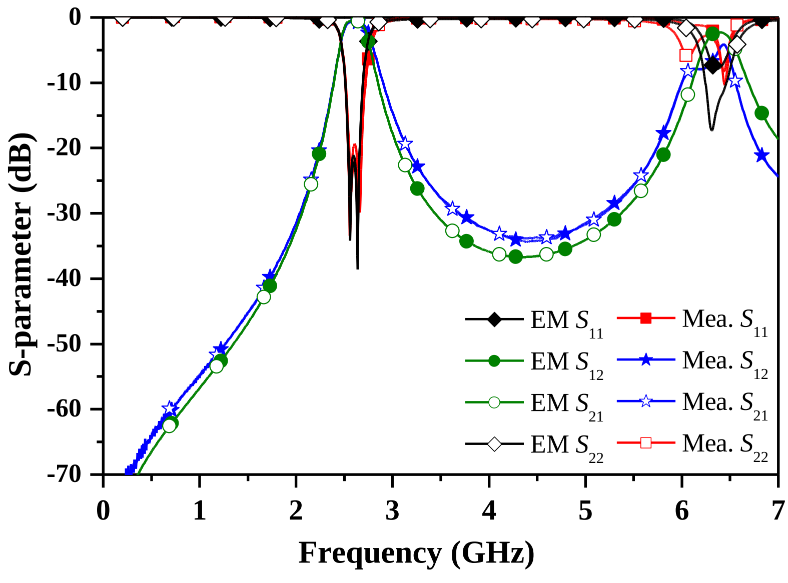

Fig. 6.14. Simulation and measurement results of two stage SIR BPF with Chebyshev response.

6.2.2 Three stages Chebyshev response

The second BPF was designed with Chebyshev response with ripple = 0.043 dB, R_S = 50 Ω, R_L = 100 Ω, Z_2 = 90 Ω, K =1.5, n = 3, and FBW = 5%. Fig. 6.15 shows the layout and photograph of fabricated filter. The final dimensions after EM simulation optimization are shown in Table 6.7. The total circuit size of proposed BPF is 30 mm × 57 mm.

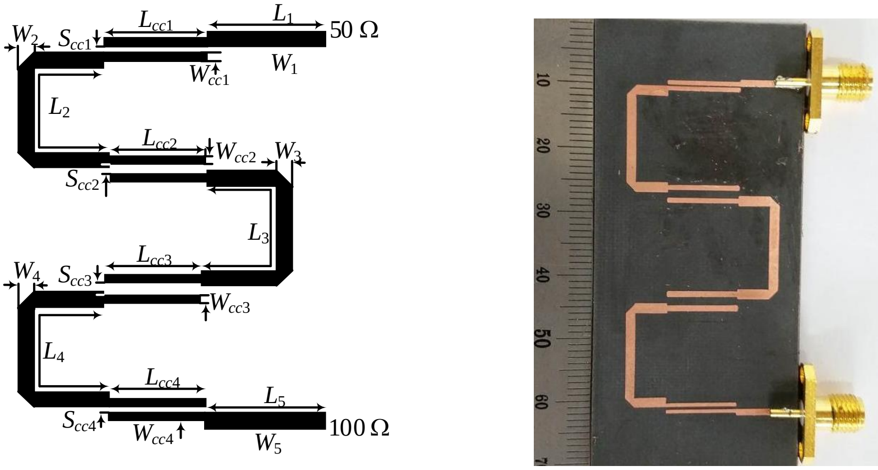

(a) (b)

Fig. 6.15. Three stages SIR BPF (a) layout and (b) photograph of fabricated circuit.

TABLE 6.7 PHYSICAL DIMENSIONS OF FABRICATED THREE STAGES SIR BPF WITH CHEBYSHEV RESPONSE. (unit: mm)

W_1=W_5=0.9	W_{cc1}=0.5	L_{cc2}=11.2	L_{cc3}=11.28	W_{cc3}=0.59	S_{cc4}=0.27
L_1=L_5=9.95	S_{cc1}=0.5	S_{cc2}=1.47	S_{cc3}=1.45	L_{cc4}=11.4	W_{cc4}=0.55
L_{cc1}=11.2	W_{cc2}=0.8	W_2=W_3=W_4=1.45		L_2=L_3=L_4=23.5	

The EM simulated and measured S-parameters are compared in Fig. 6.16. The measured results are agreed well with the simulations. Because of K = 1.5, the first spurious resonance occurs at the 1.8 time above the passband center frequency. The measured insertion loss is 1.75 dB at the lower band edge of 2.54 GHz, 1.6 dB at center frequency of 2.6 GHz, and 1.76 dB at the upper band edge of 2.64 GHz. Also, the input and output return loss better than -18 dB are obtained from 2.54 to 2.64 GHz. With n = 3, the stopband characteristics are obtained higher selectivity and wide stopband attenuation.

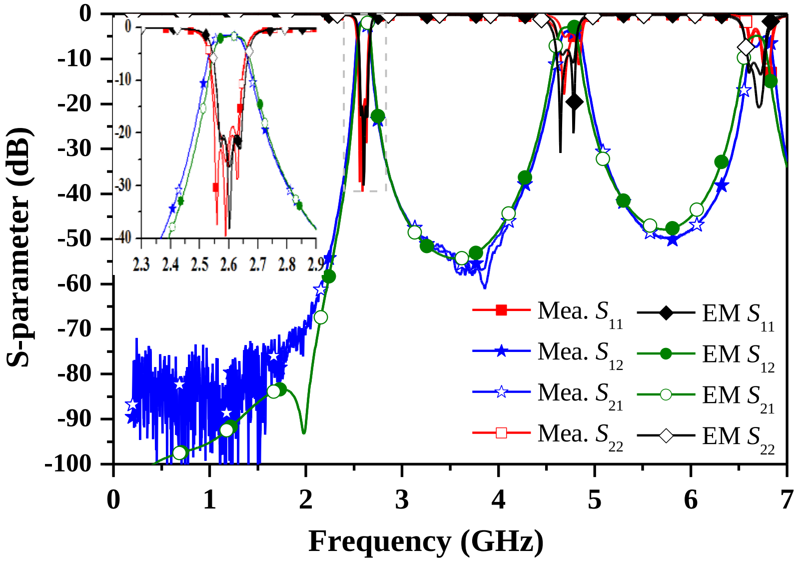

Fig. 6.16. Simulation and measurement results of three stages SIR BPF with Chebyshev response.

6.2.3 Three stages Butterworth response

The third BPF was designed with R_S = 90 Ω, R_L = 50 Ω, Z_2 = 70 Ω, K = 0.5, n = 3, FBW = 5%, and Butterworth response. Fig. 6.17 shows the layout and photograph of fabricated filter. The final dimensions after EM simulation optimization are shown in Table 6.8. The total circuit size of proposed BPF is 23 mm × 50 mm.

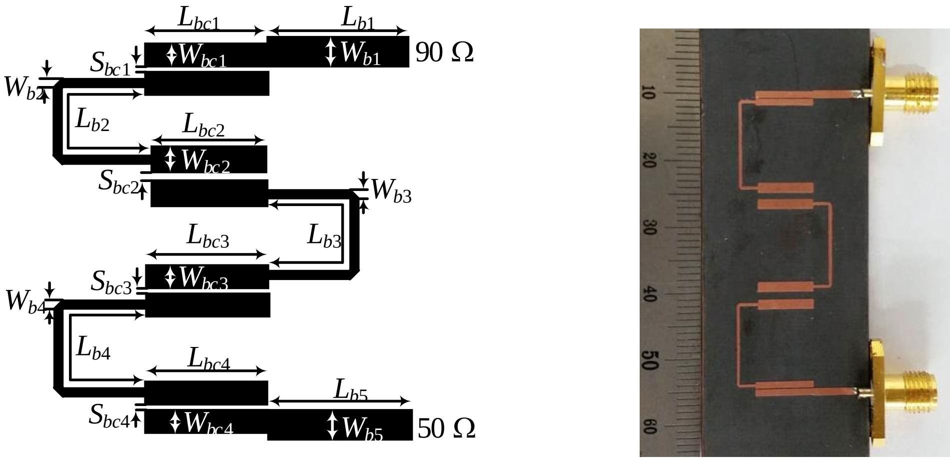

(a) (b)

Fig. 6.17. Three stages SIR BPF (a) layout and (b) photograph of fabricated circuit.

TABLE 6.8 PHYSICAL DIMENSIONS OF FABRICATED THREE STAGES SIR BPF WITH BUTTERWORTH RESPONSE. (unit: mm)

W_{b1}=W_{b4}=1	W_{bc1}=0.9	L_{bc2}=8.37	L_{bc3}=8.33	W_{bc3}=1.33	L_{bc4}=8.62
L_{b1}=L_{b4}=8.44	S_{bc1}=0.2	S_{bc2}=1.3	S_{bc3}=1.1	S_{bc4}=0.21	W_{bc4}=0.89
L_{bc1}=8.8	W_{bc2}=1.33	W_{b2}=W_{b3}=W_{b3}=0.27		L_{b2}=L_{b3}=L_{b3}=17.39	

The EM simulated and measured *S*-parameters are compared in Fig. 6.18. The measured results are agreed well with the simulations. The first spurious resonance occurs at 6.4 GHz (2.46 times) above the passband center frequency. The measured insertion and return loss at center frequency of 2.6 GHz are 1.7 dB and 31.9 dB, respectively. The *FBW* of the cut-off frequencies are 5% extend from 2.546 to 2.66 GHz. The stopband rejection of 50 dB is obtained from DC to 2.2 GHz of the low band and 3.1 to 5.7 GHz of the upper band.

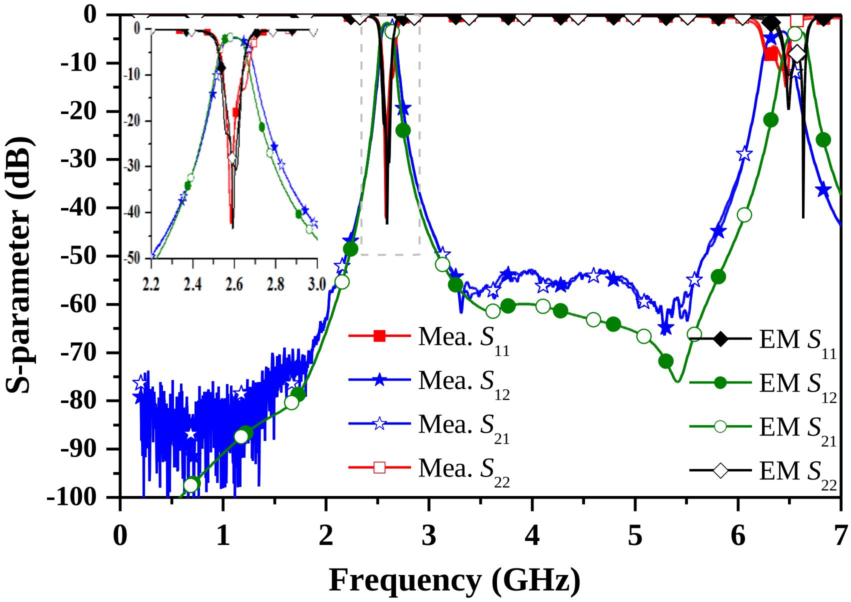

Fig. 6.18. Simulation and measurement results of three stages SIR BPF with Butterworth response.

6.3 Summary and Discussion

The stepped impedance resonator parallel coupled line BPFs with arbitrary termination and image impedances have been proposed and demonstrated in this chapter. The design equations for the proposed filter have been derived based on multi-stages coupled line filter theory. In order to show the validity of the proposed design equations, three design examples of coupled line SIR BPF with Chebyshev and Butterworth responses have been fabricated and measured. The simulation and measurement results are well agreed with the analysis. The new derived equations will be advantage in many applications such as power divider, matching network, and power amplifier design. Furthermore, the new design equations can provide more accurately and faster design.

CHAPTER 7

CONCLUSION AND FUTURE WORKS

This chapter presents the conclusion of this dissertation and some future research directions of unequal termination impedance bandpass filters with a high selectivity characteristics.

7.1 Conclusion

The dissertation presents design and synthesis of general coupled line unequal termination impedance BPF. Within six chapters, one of them was achieved with the original contribution that presented in journals and conference proceedings. The works are listed in the "publication" section in this dissertation.

In chapter 2, the general theory of two-ports network was presented. The described theories are frequently used to analyze the RF/microwave BPFs.

In chapter 3, the design of impedance transformer with ultra-high transforming ration were presented based on two cascade coupled lines. The analytical design equations are derived with different matching regions. By choosing the properly matched region, two transmission poles in the passband and a frequency selective transmission characteristics are obtained.

The chapter 4 presented the arbitrary termination impedance BPF using lumped elements. The design equations were derived from the prototype of the conventional low-pass filters.

Chapter 5 presented the new analysis of unequal termination impedance parallel coupled line BPF. The new design formulas are able to design parallel coupled line BPF with *n*-resonator, real-to-real arbitrary termination impedance, and arbitrary image impedance by using low-pass prototype elements value. The BPF with Chebyshev and Butterworth responses were designed, simulated, and fabricated at the operating center frequency of f_0 = 2.6 GHz.

In chapter 6, a new analysis BPF using parallel coupled stepped impedance resonators was presented. The new design equations were able to calculated with *n*-resonators, arbitrary termination impedance, arbitrary image impedance of coupled line, and control spurious frequencies. Three design examples of SIR coupled line BPF with Chebyshev and Butterworth responses have been fabricated and measured. The new derived equations are more advantage in many applications such as power divider, matching network, and power amplifier. These new analyses are significant impact on the modern wireless communication systems.

7.2 Direction to Future Research

The methodology and structure presented in this dissertation could be applied to design the higher stage filters with unequal termination impedance. Further, the design method presented in chapter 6 of this dissertation is much significant on controllable spurious frequency of unequal termination impedance BPF. Moreover, a high selectivity characteristic can be obtained by increasing number of stages. However, a circuit size and insertion loss were enlarged and high when the number of stages increase. Therefore, a size reduction, low insertion loss, and high selectivity are important in the view of design cost and performance. Thus, a miniaturized structure and high performance technology could be considered for this purpose.

The dual-band and multi-band filter with unequal termination impedance is one of research topics. So the resonators would be modified and designed with multi-mode resonators. A dual-band of unequal termination impedance BPF can directly matched the input/output termination impedance of an amplifier with dual-band operation without matching network.

REFERENCES

[1] S. B. Cohn, "Parallel-coupled transmission-line resonator filters," *IEEE Trans. Microwave Theory Tech.*, vol. 6, no. 4, pp. 223-231, Apr. 1958.

[2] D. Ahn, C. Kim, M. Chung, D. Lee, D. Lew, and H. Hong, "The design of parallel coupled line filter with arbitrary image impedance," *IEEE International Microwave Symposium Digest*, pp. 909-912, 1998.

[3] J. Park, J. Yun, and D. Ahn, "A design of the novel coupled-line bandpass filter using defected ground structure with wide stopband performance," *IEEE Trans. Microwave Theory Tech.*, vol. 50, no. 9, pp. 2037-2043, Sep. 2002.

[4] P. Cheong, S. Fok, and K. Tam, "Miniaturized parallel coupled-line bandpass filter with spurious-response suppression," *IEEE Trans. Microwave Theory Tech.*, vol. 53, no. 5, pp. 1810-1816, May 2005.

[5] K. Chin, Y. Chiou, and J. Kuo, "New synthesis of parallel-coupled line bandpass filter with Chebyshev responses," *IEEE Trans. Microwave Theory Tech.*, vol. 56, no. 7, pp. 1516-1523, Jul. 2008.

[6] R. Levy, "Synthesis of mixed lumped and distributed impedance-transforming filters," *IEEE Trans. Microwave Theory Tech.*, vol. 20, no. 3, pp. 223-233, Mar. 1972.

[7] P. Kim, G. Chaudhary, and Y. Jeong, "Wideband impedance transformer with out-of-band suppression characteristics," *Microwave Optic. Techno. Lett.*, vol. 56, no. 11, pp. 2612-2616, Nov. 2014.

[8] H. Nguyen, K. Ang, and G. Ng, "Design of coupled three-line impedance transformers," *IEEE Microwave Wireless Compon. Lett.*, vol. 24, no. 2, pp. 84-86, Feb. 2014.

[9] H. Ahn and T. Itoh, "Impedance-transforming symmetric and asymmetric DC blocks," *IEEE Trans. Microwave Theory Tech.*, vol. 58, no. 9, pp. 2463-2474, Sep. 2010.

[10] P. Kim, G. Chaudhary, and Y. Jeong, "Enhancement impedance transforming ratios of coupled line impedance transformer with wide out-of-band suppression characteristics," *Microwave Optic. Techno. Lett.*, vol. 57, no. 7, pp. 1600-1603, Jul. 2015.

[11] P. Kim, J. Jeong, G. Chaudhary, and Y. Jeong, "A design of unequal termination impedance power divider with filtering and out-of-band suppression characteristics," *Proceedings of the 45th European Microwave Conf.*, pp. 123-126, Sep. 2015.

[12] J. Jeong, P. Kim, and Y. Jeong, "High efficiency power amplifier with frequency band selective matching networks," *Microwave Optic. Techno. Lett.*, vol. 57, no. 9, pp. 2031-2034, Sep. 2015.

[13] P. Kim, G. Chaudhary, and Y. Jeong, "Ultra-high transforming ratio coupled line impedance transformer with bandpass response," *IEEE Microwave Wireless Compon. Lett.*, vol. 25, no. 7, pp. 445-447, Jul. 2015.

[14] Q. Wu, and L. Zhu, "Short-ended coupled-line impedance transformers with ultrahigh transforming ration and bandpass selectivity suitable for large load

impedances," *IEEE Trans. Compon. Packag. Manuf. Tech.*, vol. 6, no. 5, pp. -767-774, May 2016.

[15] H. Oraizi, M. Moradian, and K. Hirasawa, "Design and optimization of microstrip parallel-coupled line bandpass filters incorporating impedance matching," *IEICE Trans. Commun.*, vol. E89-B, no. 11, pp. 2982-2988, Nov. 2006.

[16] K. Chen and D. Peroulis, "Design of broadband highly efficient harmonic tuned power amplifier using in-band continuous Class-F^{-1}/F mode transferring," *IEEE Trans. Microwave Theory Tech.*, vol. 60, no. 12, pp. 4107-4116, Dec. 2012.

[17] M. Yang, J. Xia, Y. Guo, and A. Zhu, "Highly efficient broadband continuous inverse class-F power amplifier design using modified elliptic low-pass filtering matching network," *IEEE Trans. Microwave Theory Tech.*, vol. 64, no. 5, pp. 1515-1525, May. 2016.

[18] K. Chen and D. Peroulis "Design of highly efficient broadband class-E power amplifier using synthesized low-pass matching networks," *IEEE Trans. Microwave Theory Tech.*, vol. 59, no. 12, pp. 3162-3173, Dec. 2011.

[19] G. L. Matthaei, "Tables of Chebyshev impedance-transformation networks of low-pass filter form," *IEEE Proceedings*, vol. 52, no. 8, pp. 939–963, Aug. 1964.

[20] K. Chen, X. Liu, W. Chappell, and D. Peroulis, "Co-design of power amplifier and narrowband filter using high-Q evanescent-mode cavity resonator as the

output matching network," *IEEE International Microwave Symposium Digest*, pp. 1-4, 2011.

[21] K. Chen, J. Lee, W. Chappell, and D. Peroulis, "Co-design of highly efficient power amplifier and high-Q output bandpass filter," *IEEE Trans. Microwave Theory Tech.*, vol. 61, no. 11, pp. 3940-3950, Nov. 2013.

[22] K. Chen, T. Lee, and D. Peroulis, "Co-design of multi-band high-efficient power amplifier and three-pole high-Q tunable filter," *IEEE Microwave Wireless Compon. Lett.*, vol. 23, no. 12, pp. 647-649, Dec. 2013.

[23] C. Ge, X. Zhu, X. Jiang, and X. Xu, "A general synthesis approach of coupling matrix with arbitrary reference impedances," *IEEE Microwave Wireless Compon. Lett.*, vol. 25, no. 6, pp. 349-351, Jun. 2015.

[24] M. Makimoto and S. Yamashita, "Bandpass filter using parallel coupled stripline stepped impedance resonators," *IEEE Trans. Microwave Theory Tech.*, vol. MTT-28, no. 12, pp. 1413-1417, Dec. 1980.

[25] A. Worapishet, K. Srisathit, and W. Surakampontorn, "Stepped-impedance coupled resonators for implementation of parallel coupled microstrip filter with spurious band suppression," *IEEE Trans. Microwave Theory Tech.*, vol. 60, no. 6, pp. 1540-1548, Jun. 2012.

[26] K. U-yen, E. J. Wollack, T. Doiron, J. Papapolymerou, and J. Laskar, "The design of a compact, wide spurious-suppression bandwidth bandpass filter using stepped impedance resonators," 35th *European Microwave Conf.*, pp. 3-7, Oct. 2005.

[27] M. Makimoto and S. Yamashita, “Bandpass filters using parallel coupled strip-line stepped impedance resonators,” *IEEE MTT-S International Microwave Symposium Digest*, pp.141-143, 1980.

[28] Y. Chiou, J. Kuo, and E. Cheng, “Broadband quasi-Chebyshev bandpass filters with multimode stepped-impedance resonators (SIRs),” *IEEE Trans. Microwave Theory Tech*., vol. 54, no. 8, pp. 3352-3358, Aug. 2006.

[29] M. Makimoto and S. Yamashita, “Compact bandpass filters using stepped impedance resonators,” *IEEE Proceedings*, vol. 67, no. 1, pp. 16-19, Jan. 1979.

[30] M. Makimoto and S. Yamashita, “correction to compact bandpass filters using stepped impedance resonators,” *IEEE Proceedings*, vol. 67, no. 11, pp. 1568-1568, Nov. 1979.

[31] J. Kuo and E. Shih, “Microstip stepped impedance resonator bandpass filter with an extended optimal rejection bandwidth,” *IEEE Trans. Microwave Theory Tech*., vol. 51, no. 5, pp. 1554-1559, May 2003.

[32] D. M. Pozar, *Microwave Engineering*, 4th ed., John Wiley & Sons, New York, 2012.

[33] L. Zhu, S. Sun, and R. Li, *Microwave bandpass filters for wideband communications*, John Wiley & Sons, 2012.

[34] J. Hong, *Microstrip filters for RF/Microwave applications*, 2nd ed., John Wiley & Sons, New Jersey, 2011.

[35] G. L. Matthaei, L. Young, and E. M. T. Jones, *Microwave Filter, Impedance-Matching Networks, and Coupling Structures*. New York, NY, USA: McGraw-Hill, 1964.

[36] H. Ahn, *Asymmetric Passive Components in Microwave Integrated Circuits*. John Wiley & Sons, Inc., 2006.

[37] G. Gonzalez, *Microwave Transistor Amplifiers Analysis and Design*, 2nd edition, Prentice-Hall, Inc., 1997.

[38] P. Jarry and J. Beneat, *Advanced design techniques and realizations of microwave and RF filters*, John Wiley & Sons, 2008.

[39] E. G. Cristal and S. Frankel, "Hairpin-line and hybrid hairpin-line/half-wave parallel-coupled-line filters," *IEEE Trans. Microwave Theory Tech.*, vol. 20, no. 11, pp. 719-728, Nov. 1972.

[40] T. Lee, J. Lee, and D. Peroulis, "Dynamic bandpass filter shape and interference cancellation control utilizing bandpass-bandstop filter cascade," *IEEE Trans. Microwave Theory Tech.*, vol. 63, no. 8, pp. 2526-2539, Aug. 2015.

[41] D. Swanson and G. Macchiarella, "Microwave filter design by synthesis and optimization," *IEEE Microwave Magazine*, vol. 8, no. 2, pp. 55–69, Apr. 2007.

[42] E. Cristal, "Tables of maximally flat impedance-transformation networks of low-pass filter form," *IEEE Trans. Microwave Theory Tech.*, vol. 13, no. 5, pp. 693-695, Sep. 1965.

[43] G. L. Matthaei, "Design of parallel-coupled resonator filters," *IEEE Microwave Magazine*, vol. 8, no. 5, pp. 78-87, Oct. 2007.

[44] K. Chin and J. Kuo, "Insertion loss function synthesis of maximally flat parallel-coupled line bandpass filters," *IEEE Trans. Microwave Theory Tech.*, vol. 53, no. 10, pp. 3161-3168, Oct. 2005.

[45] M. Makimoto and S. Yamashita, *Microwave Resonators and Filters for Wireless Communication*, Springer-Verlag Berlin Heidelberg 2001.

요약

일반적으로 기존의 전력증폭기와 여파기는 50 Ω 의 임피던스를 기준하여 독립적으로 설계 된다. 따라서 전력증폭기와 여파기의 임피던스 정합을 위한 추가적인 정합회로가 필요하고, 이 정합회로의 추가적인 삽입손실은 전력증폭기의 출력과 효율저하를 일으킨다. 따라서 전력증폭기 정합회로 및 여파기는 삽입손실을 최소화 하는 방안을 고려해야 한다.

본 논문은 비대칭 종단 임피던스를 갖는 대역통과 여파기의 설계 방법을 제시한다. 또한 스퓨리어스 주파수를 조정하기 위해 새로운 병렬 결합선로 다단 임피던스 공진기 합성법을 제시한다. 제안하는 여파기는 저역통과 프로토타입의 소자값을 이용해 다단 또는 임의의 이미지 임피던스로 변환시킬 수 있으며, Chebyshev 또는 Butterworth 여파기의 응답 특성을 구현할 수도 있다. 또한 새롭게 제시된 구조를 현대의 통신시스템에서 응용하기 위한 수식들도 제시된다. 제안하는 여파기는 전력증폭기의 비용 및 크기를줄이고, 기존의 정합회로와 여파기의 삽입손실을 줄이기 위해 입/출력 측에 사용될 수 있다.

키워드 : 대역 통과 여파기, 다단 임피던스 공진기, 병렬 결합선로, 영상 임피던스, 종단 임피던스.

APPENDIX A: MatLab Coding

```
%%% Impedance Transformer filter (ZS>ZL)
clc;   clear all;
%% Insert variable
f=linspace(0.1,2.9,16001);  % Vary the frequencies
f0=1;                       % Center frequency
theta=0.5*pi*f/f0;              % Theta depending on varying
frequencies
ZS=input('input load impedance ZS=');
ZL=input('input load impedance ZL=');
r=ZS/ZL
Z0oe1=input('input load impedance Z0o=');  % Setting value of Z0o
of both coupled line
%% Find Z0e2
S11_dB1=input('Input load Magnetude S11 (dB)=');
S11_L=10^(-S11_dB1/20);
w=input('1=over-,2=under-,3=perpectly-matching:');
for x=w
    if x==1
        %% For over-matching
        M=sqrt((1-S11_L)/(r*(1+S11_L)));
        A=M^2+M; B=Z0oe1*(2-M^2-3*M); C=(3*M-M^2-4)*Z0oe1^2-
(M+1)*4*r*ZL^2; D=(Z0oe1^3*(2-M+M^2))+(4*r*ZL^2*Z0oe1*(M-3));
        Z0e_1=[A B C D]; Z0e1=roots(Z0e_1);
%         Z0ee1=Z0e1(2)
        Z0ee1=max(Z0e1)
        Z0ee2=Z0ee1*M+Z0oe1*(1-M)
    end
    if x==2
            %% For under-matching
            N=sqrt(1/r*(1+S11_L)/(1-S11_L)); % equation (10)
            An=N^2+N; Bn=Z0oe1*(2-N^2-3*N); Cn=(3*N-N^2-4)*Z0oe1^2-
(N+1)*4*r*ZL^2; Dn=(Z0oe1^3*(2-N+N^2))+(4*r*ZL^2*Z0oe1*(N-3));
            Z0e1_u1=[An Bn Cn Dn]; Z0e1_u=roots(Z0e1_u1);
```

```
%            Z0ee1=Z0e1_u(2)
            Z0ee1=max(Z0e1_u)
            Z0ee2=Z0ee1*N+Z0oe1*(1-N)
    end
    if x==3
            %% For perfeclty-matching
            Ap=(1/r)+(1/sqrt(r)); Bp=Z0oe1*(2-1/r-3/sqrt(r));
Cp=(3/sqrt(r)-1/r-4)*Z0oe1^2-(((1/sqrt(r))+1)*4*r*ZL^2);
            Dp=(Z0oe1^3*(2-
1/sqrt(r)+1/r))+(4*r*ZL^2*Z0oe1*(1/sqrt(r)-3));
            Z0e1_u1=[Ap Bp Cp Dp]; Z0e1_u=roots(Z0e1_u1);
%            Z0ee1=Z0e1_u(2)
            Z0ee1=max(Z0e1_u)
            Z0ee2=Z0ee1/sqrt(r)+Z0oe1*(1-1/sqrt(r))
    end
end
%% Substitute
Zm1=Z0ee1-Z0oe1; Zp1=Z0ee1+Z0oe1;
Zm2=Z0ee2-Z0oe1; Zp2=Z0ee2+Z0oe1;
%% find transmission zero frequency and bandwidth
f1=(2/pi)*acos(sqrt((Zm1^2-(r*Zm2^2))/((Zp1+Zp2)*(Zp1-(r*Zp2)))))
f2=2-(2/pi)*acos(sqrt((Zm1^2-(r*Zm2^2))/((Zp1+Zp2)*(Zp1-(r*Zp2)))))
Z0e1=Z0ee1;  Z0e2=Z0ee2;
C1_dB=20*log10((Z0e1-Z0oe1)/(Z0e1+Z0oe1))
C2_dB=20*log10((Z0e2-Z0oe1)/(Z0e2+Z0oe1))
 FBW=(f2-f1)/f0*100
% odd-mode equations
for a=1:length(theta)
    Z11=-j*(Zp1/2)*cot(theta(a));
    Z33=Z11;    Z44=Z11;    Z14=-j*(Zp1/2)*csc(theta(a));
    Z41=Z14;    Z13=-j*(Zm1/2)*csc(theta(a));     Z31=Z13;
    Z43=-j*(Zm1/2)*cot(theta(a));    Z34=Z43;
%% even-mode equation
    Aet=((Zp2+Zp1)*Zp1*(cos(theta(a)))^2-Zm1^2)/(Zm1*Zm2);
```

```
    Bet=j*cos(theta(a))*(((Zp1*Zm2^2)+(Zm1^2*Zp2)-
(Zp2+Zp1)*Zp1*Zp2*(cos(theta(a)))^2)/(2*Zm1*Zm2*sin(theta(a))));
    Cet=j*((2*sin(theta(a))*cos(theta(a)))*(Zp2+Zp1))/(Zm1*Zm2);
    Det=((Zp1+Zp2)*Zp2*(cos(theta(a)))^2-Zm2^2)/(Zm1*Zm2);
%% S-parameter of the full circuit
    S11e=(Aet*ZL+Bet-Cet*r*ZL^2-
(Det*r*ZL))/(Aet*ZL+Bet+Cet*r*ZL^2+(Det*r*ZL));
    S11e_dB(a)=20*log10(abs(S11e));
    S21e=((2*ZL*sqrt(r))/(Aet*ZL+Bet+Cet*r*ZL^2+(Det*r*ZL)));
    S21e_dB(a)=20*log10(abs(S21e));
    S21=S21e/sqrt(2);
    S21_dB(a)=20*log10(abs(S21));
    S22e=((-Aet*ZL)+Bet-
(Cet*r*ZL^2)+(Det*r*ZL))/(Aet*ZL+Bet+Cet*r*ZL^2+(Det*r*ZL));
    S22e_dB(a)=20*log10(abs(S22e));
end
% plot
plot(f, S11e_dB,f, S22e_dB, f, S21e_dB,'linewidth', 3);
axis([0.1 2.9*f0 -60 0])    % limited display
legend('S_1_1_e','S_2_2_e','S_2_1_e');
ylabel('|S_i_j| (dB)','fontsize',16);
xlabel('Normalized frequency (f/f_0)','fontsize',16);
grid on;
```

APPENDIX B : MatLab Coding for Unequal Termination Impedance Lumped Elements Coupled Resonator BPF

```
%% Chapter 3
clc;    clear all; format long
disp('*LUMPED ELEMENTS COUPLED RESONATOR BANDPASS FILTER*')
disp('*         PROGRAMER: PHIRUN KIM          *')
%% Calculating Value
g0=1;      f0=1*1e9;
RS=input('Input Source Impedance RS(ohm)       =');
XS=input('Input Source admittance XS(ohm)       =');
RL=input('Input Load Impedance RL(ohm)         =');
XL=input('Input Source admittance XL(ohm)       =');
FBW=0.05;%input('Input fractional bandwidth FBW(%)     =');
GA=1/RS;       GB=1/RL;       W0=2*pi*f0;
%% Calculate the shifting frequencies
f1=f0*(sqrt(1+(XS*FBW/(RS*2*g(1)))^2)+(FBW*XS/(2*RS*g(1))))
W1=2*pi*f1;
f2=f0*(sqrt(1+(XL*FBW/(RL*2*g(n)))^2)+(FBW*XL/(2*RL*g(n))))
W2=2*pi*f2;
%% Setting Inductance of resonators
Lr1=4*1e-9;     Lr2=4*1e-9;     Lr3=Lr2;
%% Calculate Capacitance of resonator
Cr(1)=1/(Lr1*W1^2);
for k=2:n-1
    Cr(k)=1/(Lr2*W0^2);
end
Cr(n)=1/(Lr2*W2^2);
%% Calculate J-inverter
J(1)=sqrt((GA*W1*Cr(1)*FBW)/(g0*g(1)));
J(2)=FBW*sqrt((Cr(1)*W1*Cr(2)*W0)/(g(1)*g(2)));
for k=3:n-1
     J(k)=W0*FBW*sqrt(Cr(k-1)*Cr(k)/(g(k-1)*g(k)));  %Calculate J2,3
end
```

```
J(n)=FBW*sqrt((Cr(n-1)*W0*Cr(n)*W2)/(g(n-1)*g(n)));
J(n+1)=sqrt((GB*W2*Cr(n)*FBW)/(g(n)*g(n+1)));
%% Calculated Series Capacitance
CS(1)=J(1)/(W0*((sqrt(1-(J(1)*RS)^2))+(XS*J(1))));
for k=2:n
    CS(k)=J(k)/W0;
end
CS(n+1)=J(n+1)/(W0*((sqrt(1-(J(n+1)*RL)^2))+(XL*J(n+1))));
%% Calculated the additional Capacitor
C01e=((CS(1)*(1-(W0*CS(1)*XS)))/((RS^2*(W0*CS(1))^2)+(1-
W0*CS(1)*XS)^2))-((J(1)^2*XS)/W0);
Cne=((CS(n+1)*(1-(W0*CS(n+1)*XL)))/((RL^2*(W0*CS(n+1))^2)+(1-
(W0*CS(n+1)*XL))^2))-(((J(n+1))^2*XL)/W0);
%% Calculated Capacitance of Shunt Resonators
C(1)=Cr(1)-C01e-CS(2);
for k=2:n-1
    C(k)=Cr(k)-CS(k)-CS(k+1);
end
C(n)=Cr(n)-CS(n)-Cne;
%% Disply values
CS(n);     C(n)   ;
disp('Resonator Capacitance(pF)'); disp(CS*1e12);
disp('Series Capacitor value(pF)'); disp(C*1e12);
```

APPENDIX C: MatLab Coding for LPF Prototype Value

```
%% coding to find value of g0, g1, g2 ... to gn
RLo=input('input the passband Return loss S11(dB)='); % |S11|
Lar=-10*log10(1-10^(0.1*RLo));  %Passband Ripple
H=input('Chebyshev (1) and Butterworth (2)=');
n=input('Insert number of stang n=');  % input number of stages
for W=H
    if W==1
        beta=log(coth(Lar/17.37));       Gamma=sinh(beta/2/n);
%% Calculated value of lowpass prototype
for k=1:n
    a(k)=sin((2*k-1)*pi/2/n);    b(k)=Gamma^2+(sin(k*pi/n))^2;
end
for k=1:n+1
    if k==1
        g(k)=2*a(k)/Gamma;
    elseif k==n+1
        if mod(n,2)==0
            g(k)=(coth(beta/4))^2;
        else
            g(k)=1;
        end
    else
        g(k)=4*a(k-1)*a(k)/b(k-1)/g(k-1);
    end
end
    end
    if W==2
    %% Calculated value of Butterworth
    for k=1:n
        g(k)=2*sin((((2*k)-1)*pi)/(2*n));       g(n+1)=1;
    end
    end
end
```

APPENDIX D : MatLab Coding for Unequal Termination Impedance Parallel Coupled Line BPF

```
clc;   clear all; format long
disp('*UNEQUAL TERMINATION PARALLEL COUPLED LINE BANDPASS FILTER*')
disp('*        PROGRAMER: PHIRUN KIM         *')
RS=input('Input Source Impedance RS(ohm)      =');
RL=input('Input Load Impedance RL(ohm)        =');
FBW=input('Input the fractional bandwidth FBW=');
Z0=input('Input the Image impedance of coupled line Z0=');
g0=1;     GS=1/RS;    Y0=1/Z0;   GL=1/RL;
AS=Y0/GS;  AL=Y0/GL;
%% Calculate J-inverter
for x=n
   if x==2
      m1=AS*(pi/2)*FBW;      m2=(g0*g(1))-((pi/4)*FBW*(AS-
(1/AS)));
      J(1)=Y0*sqrt(m1/m2);       % Calculate J0,1
      J(3)=Y0*sqrt((AL*(pi/2)*FBW)/((g(2)*g(3))-((pi*FBW/4)*(AL-
(1/AL)))));   % Calculate J2,3
      J(2)=FBW*Y0*(pi/2)*sqrt(((((J(1)^2/(2*Y0^2))*(1-
(1/AS^2)))+1)*(((J(3)^2/(2*Y0^2))*(1-
(1/AL^2)))+1))/(g(1)*g(2)));  % Calculate J1,2
   else
      m1=AS*(pi/2)*FBW;      m2=(g0*g(1))-((pi/4)*FBW*(AS-
(1/AS)));
      J(1)=Y0*sqrt(m1/m2);       % Calculate J0,1
      m3=(((J(1)^2/(2*Y0^2))*(1-(1/AS^2)))+1);
      J(2)=((FBW*pi*Y0)/2)*sqrt(m3/(g(1)*g(2)));  % Calculate J1,2
      J(n+1)=Y0*sqrt((AL*(pi/2)*FBW)/((g(n)*g(n+1))-
((pi*FBW/4)*(AL-(1/AL)))));   % Calculate Jn,n+1
      J(n)=((pi*Y0*FBW)/2)*sqrt((((J(n+1)^2/(2*Y0^2))*(1-
(1/AL^2)))+1)/(g(n-1)*g(n)));  % Calculate Jn-1,n
for k=3:n-1
```

```
        J(k)=((pi*Y0*FBW)/2)*sqrt(1/(g(k-1)*g(k)));
end
    end
end
%% Calculate Even- and odd-mode impedance
for k=1:n+1
    Z0e(k)=Z0*(1+(J(k)*Z0)+(J(k)*Z0)^2);
    Z0o(k)=Z0*(1-(J(k)*Z0)+(J(k)*Z0)^2);
end
A=[g
    J
    Z0e
    Z0o];
disp(A)
```

APPENDIX E : MatLab Coding for Unequal Termination Impedance Parallel Coupled Line SIR BPF

```
clc;    clear all;   format long
disp('*UNEQUAL TERMINATION PARALLEL COUPLED SIR BPF*')
disp('*        PROGRAMER: PHIRUN KIM         *')
%%
RS=input('Input Source Impedance RS(ohm)      =');
RL=input('Input Source Impedance RL(ohm)      =');
FBW=input('Input Source Impedance FBW(%)      =');
Z2=input('Input Source Impedance Z2(ohm)      =');
RZ=input('Input Impedance Ratio RZ=Z2/Z1      =');
g0=1;      GS=1/RS;     Y2=1/Z2;    GL=1/RL;
theta0=atan(sqrt(RZ));
Y1=Y2*RZ;     Z1=1/Y1;     L=theta0*(180/pi) % length of TL
AS=Y2/GS;    AL=Y2/GL;
%% Calculate J-inverter
for k=2:n
J(1)=Y2*sqrt((AS*2*theta0*FBW)/(g0*g(1)));       % Calculate J0,1
J(k)=(2*theta0*Y2*FBW)*sqrt(1/(g(k-1)*g(k)));
J(n+1)=Y2*sqrt((2*AL*theta0*FBW)/(g(n)*g(n+1))); % Calculate Jn,n+1
end
%% Calculate Even- and odd-mode impedance
for k=1:n+1
   Z0e(k)=(Z2*(1+(J(k)*Z2*csc(theta0))+(J(k)*Z2)^2))/(1-
(J(k)^2*Z2^2*cot(theta0)^2));
   Z0o(k)=(Z2*(1-(J(k)*Z2*csc(theta0))+(J(k)*Z2)^2))/(1-
(J(k)^2*Z2^2*cot(theta0)^2));
end
disp(J)
disp(Z0e)
disp(Z0o)
```

CURRICULUM VITAE

Phirun Kim

#7304, Division of Electronics and Information Engineering, Chonbuk National University, 567 Baeje-daero, Jeonju-si, Chollabuk-do, 561-756, Republic of Korea

Mobile Phone : +82-10-6868-2458

E-mail : fmphirun@gmail.com, fmphirun@jbnu.ac.kr

RESEARCH INTERESTS

RF passive/active circuits design such as **matching network, impedance transformer, balun, power divider, filters, and amplifier.**

EDUCATION

Ph.D., Electronic and Information Engineering, *Chonbuk National University, Korea* Academic Advisor : Professor Yongchae Jeong	2013-present
M.E., Electronic and Information Engineering, *Chonbuk National University, Korea* Academic Advisor : Professor Yongchae Jeong	2011-2013
B.E., Electronic Engineering, *National Polytechnic Institute of Cambodia, Phnom Penh, Cambodia*	2006-2011

AWARDS AND HONORS

Outstanding graduate student award In recognition of contribution to the principles of graduate research while in pursuit of the Doctoral degree in Division of Electronics and Information Engineering	2015
Electronics Award (sponsored by National Polytechnic Institute of Cambodia, Phnom Penh, Cambodia)	2009

REFERENCES

Yongchae Jeong, Ph.D

Professor, Academic Advisor (*Senior Member, IEEE*)

#7304, Division of Electronics and Information Engineering,

Chonbuk National University,

567 Baekje-daero, Jeonju-si, Chollabuk-do, 54896, Republic of Korea

Phone : +82-63-270-2458

Fax : +82-63-270-2394

E-mail : ycjeong@jbnu.ac.kr

Jongsik Lim, Ph.D

Professor, (*Senior Member, IEEE*)

Department of Electrical Engineering,

Soonchunhyang University,

22 SoonChunghyang-ro, Shinchang-myeon, Asan-si, Chungcheongnam-do, 31538, Republic of Korea

Phone : +82-41-530-1332

Fax : +82-41-530-1548

E-mail : jslim@sch.ac.kr

PUBLICATIONS

INTERNATIONAL PEER-REVIEWED JOURNALS

[1] Girdhari Chaudhary, **Phirun Kim**, Yongchae Jeong, and Jae-Hun Yoon, “Design of high efficiency RF-DC conversion circuit using novel termination networks for RF energy harvesting system,” *Microwave Optic. Techno. Lett.*, vol. 54, no. 10, pp. 1729-1732, Oct. 2012.

[2] **Phirun Kim**, Girdhari Chaudhary, and Yongchae Jeong, “A dual-band RF energy havesting using frequency limited dual-band impedance matching,” *Progress in Electromag. Research*, vol. 141, pp. 443-461, 2013.

[3] **Phirun Kim,** Girdhari Chaudhary, and Yongchae Jeong, “Analysis and Design of a Branch-line Balun with High-isolation Wideband Characteristics,” *Microwave Optic. Techno. Lett.*, vol. 57, no. 7, pp. 1228-1234, Sep 2014.

[4] **Phirun Kim**, Girdhari Chaudhary, and Yongchae Jeong, “Wideband impedance transformer with out-of-band suppression characteristics,” *Microwave Optic. Techno. Lett.*, vol. 56, no. 11, pp. 2612-2616, Nov. 2014.

[5] **Phirun Kim,** Girdhari Chaudhary, and Yongchae Jeong, “Ultra-high Transforming Ratio Coupled Line Impedance Transformer with Bandpass Response,” *IEEE Microwave Wireless Compon. Letter*, vol. 25, no. 7, pp. 445-447, July 2015.

[6] **Phirun Kim,** Girdhari Chaudhary, and Yongchae Jeong, “Enhancement Impedance Transforming Ratios of Coupled Line Impedance Transformer with Wide Out-of-band Suppression Characteristics,” *Microwave Optic. Techno. Lett.*, vol. 57, no. 7, pp. 1600-1603, May 2015.

[7] Junhyung Jeong, **Phirun Kim**, Yongchae Jeong, “High Efficiency Power Amplifier With Frequency Band Selective Matching Networks,” *Microwave Optic. Techno. Lett.*, vol. 57, no. 9, pp. 2031-2034, Sep. 2015.

[8] **Phirun Kim**, Girdhari Chaudhary, and Yongchae Jeong, “Unequal Termination Branch-Line Balun With High-Isolation Wideband Characteristics,” *Microwave Optic. Techno. Lett.*, vol. 58, no. 8, pp. 1775-1778, Aug. 2016.

[9] **Phirun Kim**, Girdhari Chaudhary, and Yongchae Jeong, “An Ultra-Wideband Bandpass Filter with High Return Loss and Controllable Notch Band,” *Microwave Optic. Techno. Lett.*, vol. 58, no. 12, pp. 2922-2926, Dec. 2016.

DOMESTIC JOURNALS

[1] Girdhari Chaudhary, Junhyung Jeong, **Phirun Kim**, Yongchae Jeong, “Negative Group Delay Circuit with Improved Signal Attenuation and Multiple Pole Characteristics,” *Journal of Electromagnetic Engineering and Science,* vol. 15, no. 2, pp. 76-81, Apr. 2015.

[2] **Phirun Kim**, Junsik Park, Junhyung Jeong, Seungho Jeong, Girdhari Chaudhary, and Yongchae Jeong, “High Selectivity Coupled Line Impedance

Transformer with Second Harmonic Suppression," *Journal of Electromagnetic Engineering and Science*, vol. 16, no. 1, pp. 13-18, Jan. 2016.

INTERNATIONAL CONFERENCE PRESENTATIONS

[1] Girdhari Chaudhary, **Phirun Kim**, Yongchae Jeong, Jongsik Lim and Jaehoon Lee, "Analysis and circuit modeling method for defected microstrip structure in planar transmission lines," *Proc. Asia-Pacific Microwave Conf.*, pp. 999-1002, 2011.

[2] Girdhari Chaudhary, **Phirun Kim**, Yongche Jeong, and Jongsik Lim, "Dual-mode bandpass filter with independently tunable center frequency and bandwidth," *IEEE Radio-frequency integration technology symposium*, pp. 56-58, Nov. 2012.

[3] **Phirun Kim**, Girdhari Chaudhary, Yongchae Jeong, and Jongsik Lim, "Dual-band Impedance Matching Network with Transmission Zeros Using Resonators," *Progress in Electromag. Research Sympos.*, pp. 627, Aug. 2013.

[4] Girdhari Chaudhary, **Phirun Kim**, Yongchae Jeong, and Jongsik Lim, "A Design of Multi-harmonics Load Network for Class-S Power Amplifier," *Progress in Electromag. Research Sympos.*, pp. 1636, Aug. 2013.

[5] Girdhari Chaudhary, Junhyung Jeong, **Phirun Kim**, Yongchae Jeong and Jongsik Lim, "Compact Negative Group Delay Circuit Using Defected Ground Structure," *Asia-Pacific Microwave Conf.*, pp. 22-24, Nov. 2013.

[6] Girdhari Chaudhary, **Phirun Kim**, Jaeyeon Kim, and Yongchae Jeong, "Coupled line negative group delay circuits with Very Low Signal Attenuation and Multiple-poles Characteristics," *European Microwave Conf.*, pp. 25-27, Oct. 2014.

[7] Jongsik Lim, Junhyung Jeong, **Phirun Kim**, Yongchae Jeong, Sang-Min Han, and Dal Ahn, "4-way Power Divider Using Common DGS and Stacked-substrate Structure," *Progress in Electromag. Research Sympos.*, pp. 934, Aug. 2014.

[8] **Phirun Kim**, Qi Wang, Girdhari Chaudhary, and Yongchae Jeong, "Freuency Selective Coupled Lines Impedance Transformer," *International Symposium on Information Technology Convergence*, vol. 3, no. 2, pp. 559-560, Oct. 2014.

[9] Junsik Park, Jaeyeon Kim, Seungwook Lee, **Phirun Kim**, and Yongchae Jeong, "CMOS RF Energy Harvesting Rectifier using Parasitic Capacitance Compensation Technique and Low-Pass Filter," *International SoC Design Conference*, Nov. 2014.

[10] Jaeyeon Kim, Junsik Park, Seungwook Lee, **Phirun Kim**, and Yongchae Jeong, "Fully Integrated Negative Group Delay Circuit Using CMOS Amplifier and Boding-wire," *International SoC Design Conference*, Nov. 2014.

[11] Girdhari Chaudhary, Junhyung Jeong, **Phirun Kim**, and Yongchae Jeong, "Transmission line Negative Group Delay Circuit with Multiple-poles

Characteristics," 2014 *Korea-Japan Microwave Workshop*, pp. 137-138, Dec. 2014.

[12] Girdhari Chaudhary, **Phirun Kim**, Junhyung Jeong, Yongchae Jeong, Jongsik Lim, "Dual-Band Negative Group Delay Circuit Using Defected Microstrip Structure," *IEEE Radio & Wireless Week*, pp. 129-131, Jan. 2015.

[13] **Phirun Kim**, Girdhari Chaudhary, Junsik Park, Yongchae Jeong, and Jongsik Lim, "High Frequency-Selectivity Impedance Transformer," *IEEE Radio & Wireless Week*, pp. 135-137, Jan. 2015.

[14] **Phirun Kim**, Junhyung Jeong, Girdhari Chaudhary, Yongchae Jeong, and Jongsik Lim, "Bandpass-to-allstop switchable filter with broadband harmonics suppression," *Progress in Electromag. Research Sympos.*, pp. 1755, Jul. 2015.

[15] Girdhari Chaudhary, Seungho Jeong, **Phirun Kim**, and Yongchae Jeong, "Coupled Line Power Divider with Multiple-pole Negative Group Delay Characteristics," *Progress in Electromag. Research Sympos.*, pp. 2033, Jul. 2015.

[16] **Phirun Kim**, Junhyung Jeong, Girdhari Chaudhary, and Yongchae Jeong, "A Design of Unequal Termination Impedance Power Divider with Filtering and Out-of-band Suppression Characteristics," *European Microwave Conf.*, pp. 123-126, Sep. 2015.

[17] Qi Wang, Junhyung Jeong, **Phirun Kim**, and Yongchae Jeong, “Analysis and Design of Conventional Wideband Branch Line Balun,” *International Symposium on Information Technology Convergence*, pp. 386-389, Oct. 2015.

[18] Girdhari Chaudhary, **Phirun Kim**, Junhyung Jeong, Yongchae Jeong, Jongsik Lim, “Power Divider with Tunable Positive and Negative Group Delays Using Parasitic Compensated PIN Diode,” 2016 *Radio and Wireless Symposium*, pp. 4-6, Jan. 2016.

[19] Girdhari Chaudhary, **Phirun Kim**, Junhyung Jeong, Yongchae Jeong, Jongsik Lim, “A Design of Negative Group Delay Power Divider: Coupling Matrix Approach with Finite Unloaded-Q Resonators,” 2016 *IEEE International Microwave Symposium*, May 2016.

[20] Seungho Jeong, Boram An, **Phirun Kim**, Yongchae Jeong, and Jongsik Lim, “A Design of Phase Shifter with Constant Insertion Loss,” *Progress in Electromag. Research Sympos.*, Aug. 2016.

[21] Girdhari Chaudhary, **Phirun Kim**, Junhyung Jeong, and Yongchae Jeong, “A Power Divider with Positive and Negative Group Delay Characteristics,” 2016 *URSI Asia-Pacific Radio Science Conf.*, pp. 1195-1197, Aug. 2016.

[22] **Phirun Kim**, Girdhari Chaudhary, and Yongchae Jeong, “A Compact Ultra-wideband Bandpass Filter with High Return Loss Characteristic,” *Asia-Pacific Microwave Conf.*, 2016.